ABSTRACT

SMITH-MOORE, CAROLINE MICHAEL. Development and Characterization of a Condensed Reverse Tricarboxylic Acid Cycle for Use in Plants. (Under the direction of Drs. Amy Grunden and Heike Sederoff).

The rate of increase in agricultural productivity has fallen below the increase in demand for agricultural products. In order to meet this demand, methods for increasing plant yield, biomass, and productivity are required. Biomass accumulation is limited in plants by the amount of carbon fixation that is able to occur. The enzyme responsible for CO_2 fixation in the Calvin-Benson cycle is ribulose-1,5-bisphosphate carboxylase/oxygenase (RuBisCO). Despite its prevalence in carbon fixation, RuBisCO is an inefficient enzyme with a slow catalytic rate. These limitations reduce the carbon fixation efficiency in plants, particularly C_3 plants which undergo photorespiration. A strategy to enhance carbon fixation in plants is the incorporation of microbially-derived carbon fixation cycles. Bacteria and archaea possess a variety of RuBisCO-independent carbon fixation pathways, which could be incorporated in the chloroplast to increase carbon fixation. In this work, a condensed version of the reverse tricarboxylic acid (rTCA) cycle was developed and evaluated.

The condensed rTCA (crTCA) cycle was originally designed to consist of five enzymatic steps. In the first step, succinate is converted to succinyl-CoA through the activity of the enzyme succinyl-CoA synthetase. The second step is the carboxylation of succinyl-CoA to produce 2-oxoglutarate. This reaction is catalyzed by 2-oxoglutarate:ferredoxin oxidoreductase and is the first carbon fixation step. The third step is the carboxylation of 2-oxoglutarate, producing oxalosuccinate. This reaction is catalyzed by 2-oxoglutarate carboxylase and is the second carbon fixation step. The fourth step is catalyzed by the enzyme oxalosuccinate reductase to produce isocitrate from oxalosuccinate. For the final step

isocitrate is hydrolyzed to produce glyoxylate and succinate by isocitrate lyase. The succinate continues to flux through the cycle again, while the gyloxylate exits. In this work carbon fixation by the crTCA cycle was demonstrated *in vitro* using ^{13}C-labeling assays and detection with LC-MS. Additional analysis demonstrated that the crTCA cycle was functional when the 2-oxoglutarate carboxylase was omitted, confirming that the cycle primarily functions with four steps instead of five. To evaluate the feasibility of utilizing the crTCA cycle in plants, the crTCA cycle enzymes were expressed individually in tobacco and found to be functional.

Development of the crTCA cycle required careful analysis of its component enzymes, particularly those responsible for carbon fixation. The 2-oxoglutarate:ferredoxin oxidoreductase from *Bacillus* sp. M3-13 was characterized biochemically and evaluated structurally using molecular modeling and molecular dynamic simulations. This enzyme was found to have an extremely high affinity for its substrates 2-oxoglutarate and Coenzyme A. Structural comparison between the *Bacillus* enzyme and a similar enzyme from *Sulfolobus tokodaii* with a different substrate specificity revealed many structural similarities in the binding pocket. It also revealed interesting differences in binding pocket residues and a role of dynamics in substrate selection.

Lastly, for efficient function of the crTCA cycle in plants, the supplementary proteins biotin protein ligase (BirA) and a 4Fe-4S ferredoxin (Fdx), would be required. In this work, transgenic *Arabidopsis thaliana* plants were created expressing *birA*, *fdx*, or both. The plants grew normally with no obvious morphological or growth phenotypes compared to the control. Plants expressing *birA* appeared to have moderate increases in biotinylation of the

chloroplastic acetyl-CoA carboxylase biotin carboxyl carrier protein 1. Methyl viologen plate assays were conducted for Fd expressing plants, but further assessment is needed.

The development and characterization of the crTCA cycle represents a significant advance in the creation of synthetic carbon fixation cycles. These studies provide the first demonstration of a four-step carbon fixation cycle and lay the groundwork for future optimization and implementation in plants.

Development and Characterization of a Condensed Reverse Tricarboxylic Acid Cycle for Use in Plants

by
Caroline Michael Smith-Moore

A dissertation submitted to the Graduate Faculty of
North Carolina State University
in partial fulfillment of the
requirements for the degree of
Doctor of Philosophy

Functional Genomics

Raleigh, North Carolina

2018

APPROVED BY:

_____
Dr. Amy M. Grunden
Co-Chair of Advisory Committee

_____
Dr. Heike W. Sederoff
Co-Chair of Advisory Committee

_____
Dr. Benjamin G. Bobay
External Member

_____
Dr. Imara Y. Perera

_____
Dr. Nathaniel G. Hentz

BIOGRAPHY

Caroline Smith-Moore was born in Jacksonville, North Carolina to Heidi Karr Baur and George Donald Smith. As a child, she was always fascinated by nature and curious about the world around her. She would frequently enlighten (annoy) her family with interesting facts she learned from watching the Discovery Channel or reading. Upon graduation from high school she chose to attend North Carolina State University to pursue a degree in microbiology, not knowing this fateful decision would lead her to a place she would call home for the next 14 years (and counting.)

During her undergraduate career she began doing research in Dr. Amy Grunden's lab. As the work progressed, she followed it to the lab of Dr. Wendy Boss. In the Boss lab, she got her first taste of working in plant science and the rigors of research. Under the guidance of Dr. Wendy Boss and Dr. Yang Ju Im, she conducted research on the use of an archaeal enzyme, superoxide reductase, to increase stress tolerance in *Arabidosis thaliana*. Caroline finished her B.S. in 2007, and entered into the Masters of Microbial Biotechnology program.

In this program she learned a great deal about the biotechnology industry. She continued doing research during this time in the lab of Dr. Imara Perera, and later obtained an internship at a small biotechnology company called Mycosynthetix. After achieving her first Master's degree in 2009, Caroline continued her education by completing a Masters of Business Administration program in 2010. While completing this program, she resumed her research under Dr. Wendy Boss, and after graduation obtained a research associate position with Dr. Imara Perera. This position led Caroline to new heights as the project she was fortunate enough to work on let her send her research to the International Space Station

aboard the last Space Shuttle flight, STS-135. It was truly an honor and a highlight of her career.

While in this position, Caroline was accosted at a Fresh Market by professors and convinced to enter a Ph.D. program. She entered into the Functional Genomics program and into the lab of Dr. Amy Grunden. If there is a running theme in her career path, it is that she is difficult to get rid of and frequently returns…like a staph infection. In Dr. Grunden's lab Caroline worked to develop a condensed, reverse TCA cycle to enhance carbon fixation in plants, and to evaluate and characterize its components. During this time she also married Andrew Scott Moore, and considers herself very lucky to get to spend her life with her best friend. They currently have two beautiful dogs, Ginger and Gracie. Who, despite an utter lack of training, are very good girls. Caroline is continuing her career as a Senior Scientist in cell line development at the Biomanufacturing Training and Education Center (BTEC) at N.C. State. She still enjoys nature and science, and still enlightens (annoys) her family with facts she now learns from her work.

ACKNOWLEDGEMENTS

First I would like to thank my advisor Dr. Amy Grunden for accepting me into her lab not once, but twice. I am extremely grateful for the opportunity to have worked with her on such exciting projects, and to have grown as a scientist with her guidance. I would also like to thank my graduate committee members: Drs. Heike Sederoff, Imara Perera, Benjamin Bobay, and Nat Hentz for their patience, advice, and support. Thank you Heike for your insight and endless pursuit of the tough questions. I would like to thank Imara for believing in me and fostering in me a love of research through the years we worked together. I first learned to be a scientist under your direction, and I'm not sure I would have pursued this path without you, thank you. I would also like to thank Ben for all of his help and his willingness to answer all of my 100 emails. Lastly, thank you Nat for taking a chance on a long shot, I'm sure than decision will pay off one of these days. I would also like to acknowledge Greg Buhrman for his guidance and help in attempting X-ray crystallography, and Kevin Blackburn for his help.

Earning a Ph.D., along with any other colossal task, takes more than one person. It takes the love, support, and friendship of many. That is the one thing I have found no shortage of in graduate school. I would like to thank the past and present members of the Grunden lab, specifically Dr. Denise Aslett, Hannah Wapshott, Dr. Karen O'Connell, Jake Dums (honorary member), Dr. Becky Kitchener, and Dr. Stephanie Mathews. Thank you Denise for being my partner in crime on the ARPA-E project, and for your friendship and support. Thank you Hannah for providing much needed comic relief and support during all of my stressful times. Thank you Karen for all of the enthralling conversations and your wisdom. I'm so glad our time in the lab overlapped. I also need to thank Jake Dums for his

conversation, spirit, and friendship. Participating in Get the Focus On with you and Becky was vital to my success and sanity. Becky, this year would have been unbearable without you. You are a phenomenal scientist, and I'm so honored to call you friend. Lastly, Stephanie, I cannot even pretend that there are words that could thank you enough. Thank you for being my sounding board, my collaborator, my voice of reason, my maid of honor, and my best friend. I also need to thank Eric Land for having amazing protocols, and always being will to share his knowledge with me. I would be remiss if I did not thank the Perfection Trap group. Lindsay, Kelly, Jessica, and Fran you are all amazing women and supported me when I needed it most.

To my family, thanks for being proud of me and supporting me, even when you didn't necessarily understand what I was doing or why. Your love and support has kept me grounded, and your sarcasm keeps me humble. I love you all very much. In particular, I would like to thank my mother and step father, Heidi and Walt Baur, for supporting me all of these years, and for encouraging me to pursue my passions with the knowledge that I always have a safety net if I need it. I would also like to thank my father, George Smith, for always reminding me to take it easy and to remember to take time for myself. I promise I will do that one day.

My last thank you is for Andrew. If you have ever lived with a scientist, particularly one enrolled in graduate school, you will know it is not for the faint of heart. The emotional roller coaster of engaging in research is very real and is not easy to leave in the lab. Andrew Moore has managed not only to live with me, but to love me through the duration of my graduate program, and if that is not deserving of a medal then I don't know what is. I

honestly could not have made it without your unwavering support and love. Also thanks to my dogs, for never failing to be excited no matter when I got home.

TABLE OF CONTENTS

LIST OF TABLES

LIST OF FIGURES

CHAPTER 1.

Bacteria and Archaea as a Source of Traits for Enhanced Plant Phenotypes

Caroline M. Smith-Moore and Amy M. Grunden

Abstract

Rising global demand for food and population increases are driving the need for improved crop productivity over the next 30 years. Plants have inherent metabolic limitations on productivity such as inefficiencies in carbon fixation and sensitivity to environmental conditions. Bacteria and archaea inhabit some of the most inhospitable environments on the planet and possess unique metabolic pathways and genes to cope with these conditions. Microbial genes involved in carbon fixation, abiotic stress tolerance, and nutrient acquisition have been utilized in plants to enhance plant phenotypes by increasing yield, photosynthesis, and abiotic stress tolerance. Transgenic plants expressing bacterial and archaeal genes will be discussed along with emerging strategies and tools to increase plant growth and yield.

1.1 Introduction

There is a dire need for continued improvement in crop productivity over the next 30 years. With the population slated to exceed 9 billion by 2050 and greater demand for meat products, it is predicted that an 85% increase in primary foodstuffs will be required (Long et al., 2015). This increase outpaces the current ability of agriculture to produce sufficient food to meet demand (Long et al., 2015). In addition to the crops needed to feed the expanding population, crops are required for producing sustainable biofuels and bioproducts to reduce the reliance on fossil fuels. To make this already challenging problem more difficult, the yield improvements need to be achieved without significant increases in land, water, or fertilizer use as these are all becoming limited and pose additional threats to the environment (Tilman et al., 2011).

While it is unlikely that any singular solution will solve this problem, genetic engineering will play a pivotal role in helping to meet this need. Promising sources for potential beneficial crop traits are bacteria and archaea. These organisms inhabit the widest array of environments on the planet and have the largest metabolic diversity compared to other lifeforms. In addition to the vast metabolic diversity, the use of microbial genes instead of those derived from plant sources could aid in evading plant regulatory networks (Tamoi et al., 2006). Genetic modification using microbial genes has the potential to generate crops with enhanced photosynthesis, abiotic stress tolerance, and nutrient use, all key factors in crop yield. Figure 1-1 highlights a number of targets used for the generation of transgenic plants with phenotypes relevant to increasing yield. Since the development of *Agrobacterium*-mediated transformation, the generation of transgenic plants expressing microbially-sourced genes has been a popular strategy to enhance plant phenotypes and

probe plant metabolism. Early work often sought to provide a bacterial/archaeal intervention for a specific stress or environmental condition. This includes the expression of numerous osmolytes (Goddijn et al., 1997; Hayashi et al., 1997; Holmström et al., 2000; Nakayama et al., 2000; Tarczynski et al., 1992) and antioxidant enzymes (Foyer et al., 1995; Gaber et al., 2006; Im et al., 2005; Shikanai et al., 1998), as well as enzymes involved in nutrient acquisition (Giannino et al., 2008; López-Arredondo and Herrera-Estrella, 2012). What began with the expression of single genes, has recently expanded into the expression of metabolic pathways and enzyme complexes (Ivleva et al., 2016; Kebeish et al., 2007; Lin et al., 2014a; Occhialini et al., 2016). An example of which is the expression of the glyoxylate shunt from *Escherichia coli* in *Arabidopsis* and *Camelina sativa* where it acts as a photorespiratory bypass (Dalal et al., 2015; Kebeish et al., 2007). Plants expressing this bacterial pathway have enhanced biomass and yield (Dalal et al., 2015; Kebeish et al., 2007). Table 1 summarizes the numerous transgenic plants created using microbial genes, which will be discussed in detail in this review.

This review will discuss bacterial and archaeal genes and pathways, which have been evaluated in plants. In particular, genes and pathways involved in CO_2 fixation, abiotic stress tolerance, and the acquisition of nitrogen and phosphate will be discussed as these are areas closely related to yield. Emerging strategies and future directions for enhancing crop productivity using microbial genes will be examined as well.

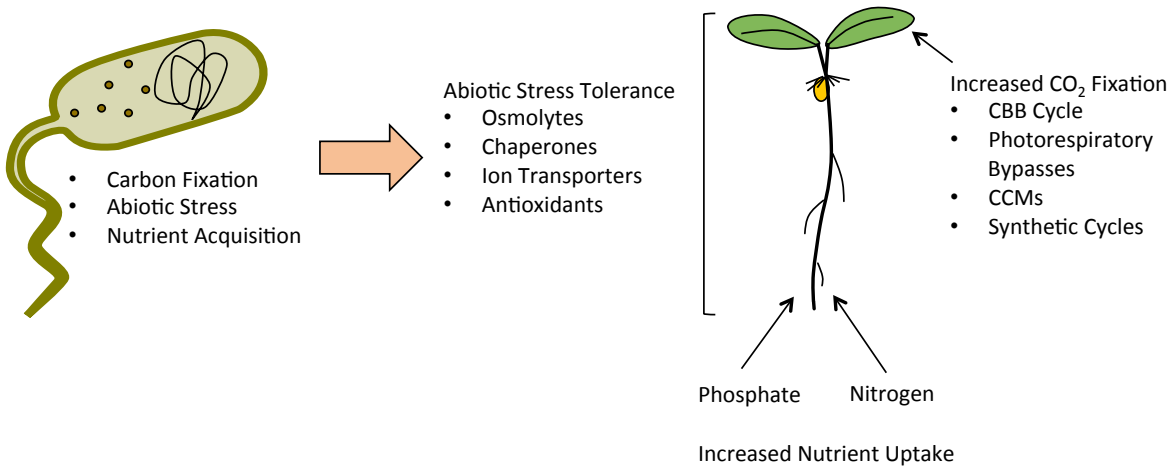

Figure 1-1. Microbial genes and pathways used to generate transgenic crops with phenotypes related to enhanced yield. These phenotypes are abiotic stress tolerance, increased CO_2 fixation, and increased nutrient uptake and efficient usage. Abiotic stress tolerance genes include genes involved in osmolyte biosynthesis, chaperones, ion transporters, antioxidant enzymes, and genes involved in non-enzymatic antioxidant biosynthesis. Genes for increased CO_2 fixation include those involved in the Calvin-Benson-Bassham (CBB) cycle, metabolic pathways for glycolate metabolism (photorepiratory bypasses), carbon concentrating mechanisms (CCMs), and microbial CO_2 fixation cycle genes. To increase nutrient uptake and use efficiency, genes involved in phosphate and nitrogen metabolism and uptake are of interest.

Table 1-1. Transgenic plants created using microbial genes and pathways.

Pathway	Gene(s)/Pathways	Source Organism	Plant	Phenotype	Reference
CBB cycle	*rbcL*	*Synechococcus* PCC6301	Tobacco	N/A; Functional Rubisco complexes were not formed	(Kanevski et al., 1999)
	rbcL	*Rhodospirillum rubrum*	Tobacco	Growth with supplemental CO_2; Delayed growth	(Whitney and Andrews, 2001)
	Multimeric Rubisco and Rubisco Chaperones	*Synechococcus elongatus* PCC7942	Tobacco	Growth with supplemental CO_2; Delayed growth	(Lin et al., 2014b; Occhialini et al., 2016)
	SBPase/FBPase	*Synechococcus elongatus* PCC7942	Tobacco, Rice, & Soybean	Increased carbon fixation and biomass	(Gong et al., 2015; Köhler et al., 2016; Miyagawa et al., 2001; Tamoi et al., 2006)
Photorespiratory Bypass	Glyoxylate Shunt (GDH, GCL, and TSR)	*Escherichia coli*	*Arabidopsis thaliana; Camelina sativa;* potato	Increased biomass, decreased photorespiration, and increased yield	(Dalal et al., 2015; Kebeish et al., 2007; Nolke et al., 2014)
	GCL, Hydroxypyruvate isomerase	*Escherichia coli*	Tobacco	Stunted growth with chlorosis and necrosis; Hydroxypyruvate isomerase not expressed	(Carvalho et al., 2011)
CCM	*bicA/sbtA*	*Synechococcus*	*Arabidopsis thaliana*; tobacco	N/A; Functional expression not achieved	(Pengelly et al., 2014; Rolland et al., 2016; Uehara et al., 2016)
	ictB	*Synechococcus PCC7942*	*Arabidopsis thaliana*; tobacco; rice; soybean	Increased CO_2 uptake, increased growth under drought; Increased biomass in soybean	(Gong et al., 2015; Hay et al., 2017; Lieman-Hurwitz et al., 2003)
	Carboxysome	*Synechococcus*	Tobacco	N/A; Proteins assembled into organized structures	(Lin et al., 2014a)
Synthetic CO_2 fixation cycles	crTCA Cycle	Many organisms, all microbial	*Camelina sativa*	N/A; Enzymes functional when expressed in plants	Unpublished data
	CETCH Cycle	Many organisms, not all microbial	N/A	N/A	(Schwander et al., 2016)

Table 1-1. (continued).

Pathway	Gene(s)/Pathways	Source Organism	Plant	Phenotype	Reference
Osmolytes	*betA*	*Escherichia coli*	Tobacco; maize; cotton; wheat	Increased tolerance to chilling, drought, and salt	(Duan et al., 2009; He et al., 2011; Holmström et al., 2000; Lv et al., 2007; Quan et al., 2004a, 2004b; Wei et al., 2011; Zhang et al., 2012)
	codA/cox	*Arthrobacter globiformis; Arthrobacter pascens*	*Arabidopsis thaliana; Brassica juncea;* persimmon; tomato; rice; potato	Increased tolerance to chilling, heat, salt, and drought	(Ahmad et al., 2010, 2008, Alia et al., 1999, 1998; Gao et al., 2000; Goel et al., 2011; Hayashi et al., 1998, 1997; Konstantinova et al., 2002; Li et al., 2011; Mohanty et al., 2002; Park et al., 2007, 2004; Prasad et al., 2000; Sakamoto et al., 1998; Sulpice et al., 2003)
	otsA/otsB	*Escherichia coli*	Tobacco; potato; rice	Increased tolerance to drought, salt, and cold stress	(Garg et al., 2002; Goddijn et al., 1997; Jang et al., 2003; Pellny et al., 2004; Pilon-Smits et al., 1998)
	mtlD	*Escherichia coli*	*Arabidopsis thaliana;* tobacco; eggplant; poplar; wheat; rice	Increased drought and salt tolerance	(Abebe et al., 2003; Hu et al., 2005; Karakas et al., 1997; Prabhavathi et al., 2002; Pujni et al., 2007; Tarczynski et al., 1992; Thomas et al., 1995)
	ectA, ectB, ectC	*Halomonas elongata* & *Marinococcus halophilus*	Tobacco; tomato	Increased salt tolerance	(Moghaieb et al., 2017, 2006; Nakayama et al., 2000; Rai et al., 2006)
	GgpPS	*Azotobacter vinelandii*	*Arabidopsis thaliana;* potato	Growth retardation at high level accumulation and increased salt stress tolerance at low level accumulation	(Klahn et al., 2009; Sievers et al., 2013)

Table 1-1. (continued).

Pathway	Gene(s)/Pathways	Source Organism	Plant	Phenotype	Reference
Chaperones	*cspA* & *cspB*	*Escherichia coli; Bacillus subtilis*	*Arabidopsis thaliana;* rice; maize	Increased tolerance to cold, heat, and drought stress	(Castiglioni et al., 2008)
	hsp70/dnaK	*Aphanothece halophytica*	Tobacco; rice	Increased tolerance to salt and heat; Increased biomass and yield	(Ono et al., 2001; Sugino et al., 1999; Uchida et al., 2008)
Ion Transporters	*nhaA*	*Escherichia coli*	Rice	Increased tolerance to salt and drought stress	(Wu et al., 2005)
Antioxidant Enzymes/ Compounds	*katE*	*Escherichia coli*	Tobacco; rice; tomato	Increased tolerance to salt and photooxidative stress	(Al-Taweel et al., 2007; Miyagawa et al., 2000; Mohamed et al., 2003; Moriwaki et al., 2008; Nagamiya et al., 2007; Shikanai et al., 1998)
	gpx	*Synechocystis* PCC6803	*Arabidopsis thaliana*	Increased tolerance for chilling, salt, drought, and H_2O_2	(Gaber et al., 2006)
	sor	*Pyrococcus furiosus*	*Arabidopsis thaliana*; NT1 tobacco cells; *Cornus canadensis* L.f.	Increased tolerance for heat, light, and methyl viologen stress	(Geng et al., 2016; Im et al., 2009, 2005)
	fdx	*Anabaena* sp. PCC7120	Tobacco	None	(Ceccoli et al., 2011)
	fld	*Anabaena* PCC7119	Tobacco; bent grass	Increased tolerance for methyl viologen, heat, drought, light, and UV; Resistance to iron starvation	(Blanco et al., 2011; Z. Li et al., 2016; Tognetti et al., 2007, 2006)
	gor	*Escherichia coli*	Tobacco; wheat; poplar	Increased tolerance to oxidative stress when expressed in the chloroplast	(Aono et al., 1993; Foyer et al., 1991, 1995; Le Martret et al., 2011; Melchiorre et al., 2009)
	gshII	*Escherichia coli*	Poplar; *Brassica juncea*	Resistance to heavy metals. Minimal increase in GSH content	(Foyer et al., 1995; Herschbach et al., 1998; Strohm et al., 1995; Yong Liang Zhu et al., 1999)

Table 1-1. (continued).

Pathway	Gene(s)/Pathways	Source Organism	Plant	Phenotype	Reference
Antioxidant Enzymes/ Compounds (Cont.)	*γ-ecs*	*Escherichia coli*	Poplar; tobacco; *Brassica juncea*	Increased phytochelatins, and enhanced heavy metal tolerance; Increased GSH amount	(Creissen et al., 1999; Herschbach et al., 1998; Noctor et al., 1998; Reisinger et al., 2008; Y L Zhu et al., 1999)
	gcl-gs	*Streptococcus thermophilus*	Tobacco	20-30 fold increase in GSH; Increased tolerance to oxidative stress and heavy metal	(Liedschulte et al., 2010)
Nitrogen Fixation	*asnA*	*Escherichia coli*	Lettuce; *Lotus corniculatus*; *Brassica napus*; tomato	Lettuce had increased leaf are and amino acid/protein content. Others had reduced growth	(Bellucci et al., 2004; Giannino et al., 2008; Martínez-Andújar et al., 2013; Seiffert et al., 2004; Sobolev et al., 2010)
	Nitrogenase genes	*Klebsiella pneumoniae*	Tobacco	N/A. Some genes produced active proteins *in planta*	(Allen et al., 2017; Ivleva et al., 2016)
Phosphate uptake	*ptxD*	*Pseudomonas stutzeri* WM88	*Arabidopsis thaliana*; tobacco	Plants capable of utilizing phosphite as a phosphorous source	(López-Arredondo and Herrera-Estrella, 2012)

1.2 Photosynthesis

Photosynthesis encompasses the oxygenic (light-harvesting) and anoxygenic (carbon fixing) reactions of plant metabolism. In oxygenic photosynthesis energy from light is received by the photosystems and converted to reducing equivalents and ATP, which are utilized during carbon fixation (anoxygenic photosynthesis) by the Calvin Benson-Bassham (CBB) cycle. The carbohydrates generated from the CBB cycle fuel plant metabolism, and generate plant biomass. The maximum theoretical amount of photosynthetically active light that plants can successfully convert into biomass is 9.4% for C_3 plants and 12.3% for C_4 plants (Zhu et al., 2010). Despite great strides in increasing yield during the "Green Revolution," crop conversion of light energy to plant biomass is far from the theoretical

maximum (Zhu et al., 2010). This is a particular problem for C_3 plants, which are even less efficient due to photorespiration, described below. Photosynthetic inefficiencies exist in both the oxygenic photosynthetic reactions and in the CBB cycle. While there are potential interventions utilizing microbial, particularly cyanobacterial, genes to increase oxygenic photosynthesis, none of these have been realized in a plant to date. One such example is the utilization of cyanobacterial chlorophylls *d* and *f* to expand the usable photosynthetic spectrum (Evans, 2013). However, improving carbon fixation through the employment of microbial pathways and genes is an expanding area of research, which will be the focus of this section.

1.2.1 Calvin Benson-Bassham Cycle Modifications

While the CBB cycle is the most widespread carbon fixation cycle, it suffers from several inefficiencies, and flux through the cycle is a limiting factor of biomass accumulation (Ducat and Silver, 2012). The primary restriction on CBB cycle flux is the carbon fixing enzyme ribulose-1,5-bisphosphate carboxylase/oxygenase (Rubisco). In the CBB cycle Rubisco catalyzes the carboxylation of ribulose-1,5-bisphosphate (RuBP) to form two molecules of 3-phosphoglycerate (3-PGA), which go on to regenerate RuBP or to begin carbohydrate synthesis. In addition to carboxylation, Rubisco can catalyze the oxygenation of RuBP in a pathway known as photorespiration, leading to a net loss of fixed carbon. Figure 1-2 shows the CBB cycle along with the pathway of photorespiration. Despite being the most abundant enzyme on the planet and responsible for 90% of inorganic carbon fixation, Rubisco is inefficient and slow (turnover frequency of 1-10 $CO_2\ s^{-1}$) (Erb and Zarzycki, 2018). Additionally, in order to catalyze its reactions Rubisco must first be activated by a

Rubisco activase (Erb and Zarzycki, 2018). All of these factors make Rubisco an attractive target for improvement to enhance photosynthetic carbon assimilation.

Many attempts have been made to engineer Rubisco for increased catalytic rate, increased specificity, or both (Bainbridge et al., 1995; Medrano et al., 1995; Whitney et al., 2011; Zhu & Spreitzer, 1996). However, only very minimal gains have been made using this method, as any gains in catalysis are tied to a decrease in CO_2 specificity (Tcherkez et al., 2006). The inefficiency of Rubisco is likely tied to its evolution in an environment with a lower concentration of O_2 than the current atmosphere and a divergence between higher catalysis seen in bacterial Rubisco and higher CO_2 specificity observed in plants (Shih et al., 2016). Another strategy for improving Rubisco function aside from protein engineering is replacement of plant Rubisco with a bacterial Rubisco with higher catalytic activity. This method could prove to be particularly effective with the implementation of additional carbon concentrating mechanisms. There are several technical challenges associated with this method considering that Rubisco is a complex, multimeric enzyme with its small subunit (rbcS) gene in the nuclear genome and its large subunit (rbcL) gene in the chloroplast genome (Whitney et al., 2011). This technical challenge hindered early attempts to generate a chimeric Rubisco in *Nicotiana tabacum* (tobacco) with the *Synechococcus* PCC6301 rbcL as functional complexes were not formed (Kanevski et al., 1999). An alternative strategy was attempted utilizing a homodimeric Rubisco composed of two rbcL subunits from *Rhodospirillum rubrum*. The *rbcL* gene was transformed into tobacco plastids through homologous replacement of the tobacco *rbcL*. These plants were capable of autotrophic growth when supplemented with CO_2, though they had significantly delayed growth (Whitney and Andrews, 2001). This growth phenotype is due to the greatly reduced CO_2

specificity of the *R. rubrum* Rubisco compared to the endogenous tobacco Rubisco (Whitney and Andrews, 2001). Recently, a multimeric Rubisco from *Synechococcus elongatus* PCC7942 was transformed into tobacco plastids to replace the tobacco *rbcL* (Lin et al., 2014b). Two cyanobacterial assembly factors were also transformed, but were later shown to be unnecessary for assembly (Occhialini et al., 2016). Plants expressing the *S. elongatus* PCC7942 Rubisco were capable of photoautotrophic growth with elevated CO_2, but displayed the same delayed growth as seen previously as the cyanobacterial Rubisco has lower CO_2 specificity (Lin et al., 2014b). Conversely, plants expressing the cyanobacterial Rubisco had higher CO_2 fixation rates per unit enzyme (Lin et al., 2014b). While the phenotypes observed for cyanobacterial Rubisco plants were not ideal, these studies serve as a proof of concept and could form the basis of promising strategy if combined with a carbon concentrating mechanism to enhance Rubisco carboxylation.

In addition to the limitations of Rubisco, there are also other potential enzymatic bottlenecks of the CBB cycle, specifically the sedoheptulose-1,7-bisphosphatase (SBPase) and fructose-1,6-bisphosphatase (FBPase) (Figure 1-2). Modeling studies have suggested that the amount of SBPase and FBPase are not optimal for photosynthesis at current atmospheric CO_2 levels and the problem will be amplified at the elevated CO_2 levels predicted for the future (Zhu et al., 2007). SBPase and FBPase exist at the branching point of the CBB cycle where metabolites either participate in the regeneration of RuBP to continue the CBB cycle or diverge off into starch synthesis (Miyagawa et al., 2001). While it has been shown that decreases in FBPase do not lead to significant changes in CO_2 assimilation, small decreases in SBPase lead to decreased photosynthesis and stunted growth, highlighting its importance (Harrison et al., 2001). This dynamic is further supported through evaluation of the

contribution of SBPase and FBPase through the creation of transgenic plants overexpressing these enzymes (Miyagawa et al., 2001; Tamoi et al., 2006). It was shown that SBPase overexpressing plants had increased carbon fixation and growth, whereas the FBPase overexpressing plants had elevated starch content, but no effects on growth or carbon fixation (Tamoi et al., 2006). Cyanobacteria possess an enzyme which is a combined SBPase/FBPase performing both activities at nearly equal rates (Miyagawa et al., 2001). The use of a cyanobacterial SBPase/FBPase is particularly expedient as the plant SBPase and FBPase are subject to strict redox regulation by the thioredoxin system, while the cyanobacterial versions are not (Tamoi et al., 2006). Transgenic tobacco expressing the *Synechococcus* PCC7942 SBPase/FBPase in the chloroplast had increased biomass, CO_2 fixation, and increased Rubisco activity (Miyagawa et al., 2001). Expression of SBPase/FBPase has also been examined in transgenic rice and soybean (Gong et al., 2015; Köhler et al., 2016). Both transgenic rice and soybean have increased photosynthesis, and transgenic soybean also had better seed yield for plants exposed to higher temperatures and increased CO_2 compared to their wild type control lines (Gong et al., 2015; Köhler et al., 2016). These studies suggest that the use of a cyanobacterial SBPase/FBPase is a promising strategy for enhancing flux through the CBB cycle to enhance plant biomass.

1.2.2 Photorespiration Bypass/Recycling

As mentioned previously, Rubisco is the enzyme responsible for carbon fixation in the CBB cycle. In addition to its carboxylation activity, Rubisco also catalyzes the oxygenation of RuBP to form one molecule of PGA and one molecule of 2-phosphoglycolate (P-Gly). The P-Gly is dephosphorylated in the chloroplast to glycolate, before being

transferred to the peroxisome where it is oxidized to glyoxylate. The glyoxylate is further converted to glycine in the peroxisome, which is transported to the mitochondria. In the mitochondria, two molecules of glycine are converted to serine with the production of CO_2, and NH_3. Serine will ultimately get converted to PGA and fed back into the CBB cycle. However, the CO_2 created in the production of serine is lost and leads to a net loss of fixed carbon and a decrease in photosynthetic efficiency. Figure 1-2 provides a schematic of photorespiration. The tendency of Rubisco to catalyze the oxygenation reaction depends on the concentration of CO_2 present. This is a particular problem in C_3 plants which lack a mechanism to concentrate carbon at the site of Rubisco. At the current atmospheric CO_2 concentration and a temperature of 25°C, C_3 plants lose nearly 30% of carbon fixed in photosynthesis to photorespiration (Zhu et al., 2010). This loss is increased at higher temperatures as the affinity of Rubisco for CO_2 decreases and oxygen is able to concentrate as plants close their stomata (Peterhansel and Maurino, 2011).

While the most obvious solution to this problem might be to knockout or knockdown the genes involved in photorespiration, this strategy leads to a conditionally lethal phenotype in which the plants require low O_2 or high CO_2 for survival (Ogren, 1984; Somerville, 2001). This is likely due to the buildup of photorespiratory intermediates which cannot be properly metabolized without the photorespiratory pathway (Peterhansel and Maurino, 2011). Another strategy which has shown significant promise is the use of metabolic pathways, photorespiratory bypasses, to redirect the P-gly produced by photorespiration in a way that minimizes carbon, nitrogen, and energy losses while preventing the buildup of photorespiratory intermediates (Xin et al., 2015).

Bacteria, including *E. coli*, contain a pathway that allows them to metabolize glycolate as a sole carbon source (Kebeish et al., 2007). The first enzyme involved is glycolate dehydrogenase (GDH), which oxidizes glycolate to glyoxylate. Two molecules of glyoxylate are then ligated together by glyoxylate carboligase (GCL) to produce tartric semialdehyde, with the release of one molecule of CO_2. Tartronic semialdehyde reductase (TSR) converts tartronic semialdehyde to glycerate, which feeds into metabolism (Figure 1-2) (Kebeish et al., 2007). This catabolic pathway was first utilized as a photorespiratory bypass in transgenic *Arabidopsis thaliana* (Kebeish et al., 2007). It was shown that the expression of all three enzymes in the chloroplast resulted in increased biomass of both the root and shoot material, reduced photorespiration, and overall increase in photosynthesis (Kebeish et al., 2007). It was also demonstrated that plants expressing the three subunits (DEF) of the GDH had increased biomass over wild type (Kebeish et al., 2007). Similar phenotypes were observed for *Camelina sativa* expressing the GDH, and the full photorespiratory bypass (Dalal et al., 2015). *Camelina* plants expressing either partial or full bypass also demonstrated increases in seed yield greater than 50% (Dalal et al., 2015). Similarly, potato plants expressing a fused polyprotein of *E. coli* GDH had increased tuber size and weight (Nolke et al., 2014). The increased photosynthesis and biomass phenotype seen in plants expressing *E.coli* GDH alone raises questions about the fate of glyoxylate in the chloroplast and suggests the existence of as yet undefined pathways for its metabolism (Dalal et al., 2015).

One other similar bacterial photorespiratory bypass has been evaluated, but found to be unsuccessful. In the bypass attempted by Carvalho, et al. *E. coli* GCL and hydroxypyruvate isomerase were targeted to the peroxisome of tobacco to metabolize

glyoxylate transported from photorespiration (Figure 1-2) (Carvalho et al., 2011). The hydroxypyruvate isomerase was responsible for the conversion of tartric semialdehyde to hydroxypyruvate but was not successfully expressed in the transformed tobacco plants (Carvalho et al., 2011). Plants expressing the GCL alone in the peroxisome had a chlorotic and necrotic phenotype with stunted growth in ambient air conditions (Carvalho et al., 2011). It remains unknown if expression hydroxypyruvate isomerase might alleviate this inhibited phenotype.

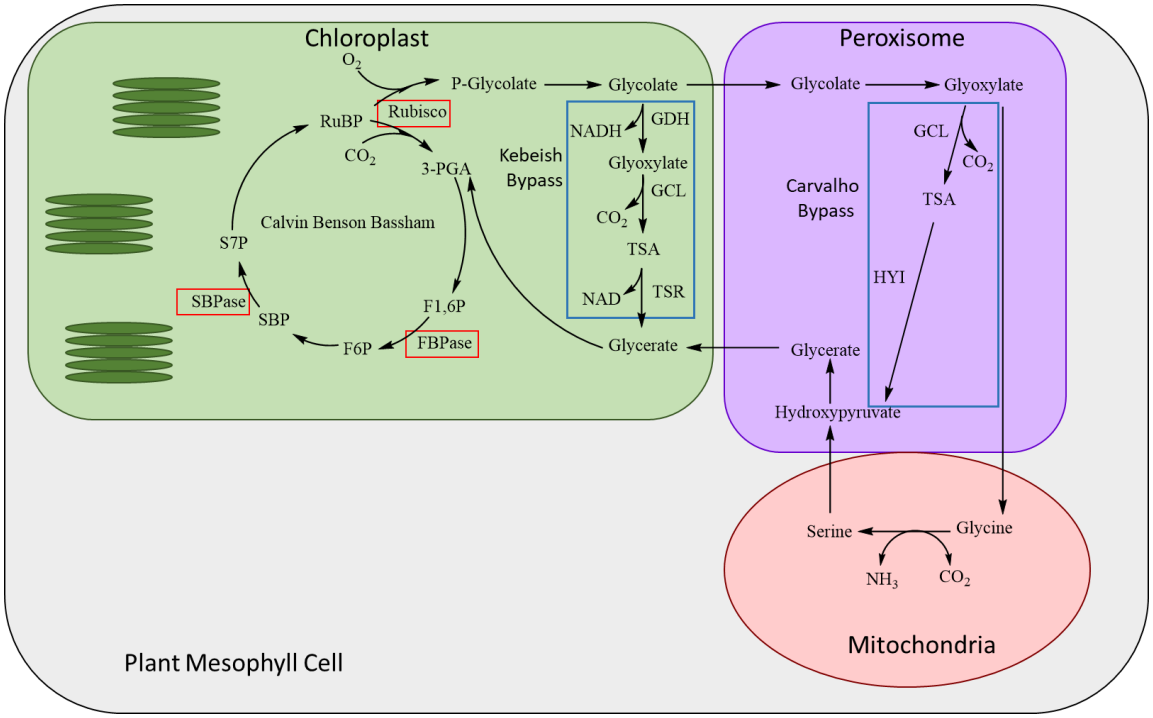

Figure 1-2. Targets for CBB modification and microbially-derived photorespiratory bypasses. Targets for CBB modification are indicated by red boxes and are abbreviated as follows: ribulose-1,5-bisphosphate (RuBP), 3-phosphoglycerate (3-PGA), fructose 1,6-bisphosphate (F1,6P), fructose 6-phosphate (F6P), sedoheptulose 1,7-bisphosphate (SBP), and sedoheptulose 7-phosphate (S7P). Photorespiratory bypasses are indicated by blue boxes and are abbreviated as follows: glycolate dehydrogenase (GDH), glyoxylate carboligase (GCL), tartronic semialdehyde (TSA), tartronic semialdehyde reductase (TSR), and hydroxypyruvate isomerase (HYI). (Kebeish et al., 2007; Carvalho et al., 2011)

1.2.3 Carbon Concentrating Mechanisms

To compensate for the promiscuous nature of Rubisco, C_4 plants, algae, and cyanobacteria have developed mechanisms to concentrate CO_2 at the site of Rubisco in order to increase its efficiency. The cyanobacterial carbon concentrating mechanism (CCM) is multifaceted involving both structural and enzymatic methods. In order to concentrate inorganic carbon intracellularly, cyanobacteria express a variety of bicarbonate and CO_2 transporters and accumulate inorganic carbon as bicarbonate in the cytoplasm. The intracellular bicarbonate is then transported into the carboxysome.

Carboxysomes are complex cellular micro-compartments composed of a proteinaceous shell and housing Rubisco and carbonic anhydrase (Long et al., 2016). Inside the carboxysome, bicarbonate is concentrated through the selective permeability of the carboxysome shell and is converted to CO_2 by carbonic anhydrase. This effectively concentrates CO_2 around Rubisco, limiting its oxygenation activity and driving the production of 3-PGA for the CBB cycle. Translating aspects of the cyanobacterial CCM to C_3 plants is currently an area of great interest. Modeling studies suggest that the expression of the three primary bicarbonate transporters could increase photosynthesis by 16%, and expression of only bicarbonate transporter A (BicA) could increase photosynthesis by 9% (McGrath and Long, 2014). While these incremental gains are promising, increases of 60% are predicted in leaves with functional carboxysomes lacking stromal carbonic anhydrase (McGrath and Long, 2014).

Expression of a cyanobacterial bicarbonate transporter is clearly the lower hanging fruit for implementation in plants. The cyanobacterial BicA and the sodium-dependent bicarbonate transporter A (SbtA) are excellent candidates as they are encoded by a single

gene (McGrath and Long, 2014). However, proper folding, targeting, and insertion of an integral membrane protein are not straightforward processes. The first attempt to express *bicA* from *Synechococcus* PCC7002 in tobacco chloroplasts utilized plastid transformation, and it was found that 75% of the BicA was localized to the thylakoid membrane and 25% in the chloroplast envelope (Pengelly et al., 2014). However, this expression led to no phenotypic differences or increase in CO_2 assimilation, suggesting that BicA was not active in the plants (Pengelly et al., 2014). There are many potential reasons for this including the lack of an unidentified activating mechanism present in cyanobacteria that is not produced in plants. Despite the lack of activity, it was shown that BicA could be expressed in plant chloroplasts. Additional work expressing BicA and SbtA in plants has focused on efficient targeting and localization, but expression of an active version of either transporter has not been achieved (Rolland et al., 2016; Uehara et al., 2016).

In addition to the known transporters, there are other genes associated with carbon accumulation, but without a known function. The *ictB* gene from *Synechococcus* PCC7942 was identified from a high CO_2 requiring mutant (Bonfil et al., 1998). This gene was originally hypothesized to be a bicarbonate transporter, but that theory has since been disproven (Bonfil et al., 1998; Price et al., 2011). The function of IctB is still unknown. The *ictB* gene was first transformed into *Arabidopsis* and tobacco and shown to increase CO_2 uptake, and under low humidity conditions, increase growth (Lieman-Hurwitz et al., 2003). Given the success of *ictB* expression in *Arabidopsis* and tobacco, the gene has also been expressed in rice and soybean (Gong et al., 2015; Hay et al., 2017). Increases in CO_2 uptake were observed in both rice and soybean, and increases in plant biomass were noted in soybean (Hay et al., 2017). The mechanism underlying the ability of this single

cyanobacterial gene to enhance photosynthesis is currently an open question. Further study on IctB function is needed to clarify its role and aid in determining its most effective expression and localization in plants.

A high risk/high reward strategy for incorporating the cyanobacterial CCM in plants is the expression and formation of the carboxysome in plant chloroplasts (McGrath and Long, 2014). While the presence of a functional carboxysome in plants would undoubtedly enhance CO_2 fixation, there are many difficult technical hurdles. Successful formation of a carboxysome in the chloroplast will likely require efficient plastid transformation of the carboxysome shell proteins and a functional carbonic anhydrase and Rubisco (McGrath and Long, 2014). In addition, both the carbonic anhydrase and Rubisco must be folded and activated appropriately to be encapsulated in the carboxysome shell and maintain activity. However, a few pieces of evidence suggest that this approach may not be as far-fetched as it seems. For instance, functional carboxysomes have been expressed in *E. coli* (Bonacci et al., 2012). Additionally, *Synechococcus* PCC7942 shell proteins were expressed transiently in tobacco using chloroplast signal peptides and were shown to assemble into organized structures in the chloroplast resembling microcompartments (Lin et al., 2014a). Finally, the ability to express functional cyanobacterial Rubisco in plant chloroplasts as described previously provides support for the eventual production of functional carboxysomes in plants. However, many challenges still exist including evaluation of the energy requirements for carboxysomal formation and function along with ensuring that the carboxysome receives sufficient bicarbonate (Rae et al., 2017).

1.2.4 Synthetic Carbon Fixation Cycles

While the CBB cycle is likely the most well-known CO_2 fixation cycle, it is far from the only cycle. Five other carbon fixation cycles have been identified in bacteria and archaea (Bar-Even et al., 2010). These cycles include the reverse tricarboxylic acid cycle (rTCA), the reductive acetyl-CoA pathway, the 3-hydroxypropionate cycle, the 3-hydroxypropionate/4-hydroxybutyrate cycle, and the dicarboxylate/4-hydroxybutyrate cycle. Synthetic biology approaches have made it possible to consider creating synthetic carbon fixation cycles utilizing any combination of enzymes, identified from the ever-growing list of characterized biological reactions, to augment or even replace the CBB cycle. Computational modeling of potential alternate pathways has identified several alternate CO_2 fixation pathways taking into account thermodynamic constraints (Bar-Even et al., 2010). The ability to use *in silico* modeling to complete an initial evaluation of these potential cycles is an invaluable tool, as evaluating these cycles experimentally poses many challenges (Ducat and Silver, 2012).

One of the possible cycles identified is a condensed version of the rTCA cycle, termed the crTCA cycle. This CO_2 fixation pathway consists of four/five enzymatic steps, excluding several of the strictly anaerobic enzymes of the more traditional rTCA. The first step of the crTCA cycle is catalyzed by succinyl-CoA synthetase (SCS), which converts succinate to succinyl-CoA with the hydrolysis of one ATP. In the second step the succinyl-CoA is carboxylated by 2-oxoglutarate ferredoxin oxidoreductase (KOR) to produce 2-oxoglutarate. The 2-oxoglutarate is further carboxylated by 2-oxoglutarate carboxylase (OGC) to oxalosuccinate or by isocitrate dehydrogenase (ICDH) to isocitrate, which are the 3 and 4 steps, respectively. In the final step, isocitrate is hydrolyzed by isocitrate lyase (ICL) into succinate and glyoxylate. The cycle was evaluated *in silico* and shown to be feasible in a

number of physiological conditions, but was ultimately discounted due to its requirement for an oxygen-sensitive enzyme and another enzyme only identified in a thermophile (Bar-Even et al., 2010). In plants the crTCA cycle would scavenge CO_2 and bicarbonate in the chloroplast, which would be converted to glyoxylate. The addition of the *E. coli* glycolate photorespiratory bypass would allow for the scavenged carbon to be assimilated back into the CBB cycle. However, production of glyoxylate in the chloroplast has previously been shown to have no negative effects on plant phenotypes (Dalal et al., 2015; Kebeish et al., 2007). Our lab has demonstrated the function of this cycle *in vitro* and shown functional expression of each of the cycle enzymes through transient tobacco expression. In addition to the *in vitro* characterization, all of the crTCA cycle enzymes have been expressed in the seed oil crop *Camelina sativa*. This is the first example of this cycle functioning *in vitro*, and the first example of a synthetic CO_2 fixation pathway expressed in plants.

Another CO_2 fixation pathway that has been identified and characterized *in vitro* is the crotonyl-coenzyme A/ethylmalonyl-CoA/hydroxybutyryl-CoA (CETCH) cycle (Schwander et al., 2016). This cycle consists of 13 integral enzymatic steps and 4 additional enzymes for regeneration of cofactors. This cycle goes a step beyond those hypothesized previously as it also incorporated enzyme active site optimization to drive the cycle kinetics (Schwander et al., 2016).

1.3 Abiotic Stress

Crop productivity depends on a variety of conditions coming together to allow for optimal growth and production. However, the truth is the majority of crops are not grown under optimal conditions in the field. Plants are subjected to a variety of suboptimal

conditions, culminating in abiotic stress. These stresses can include drought, temperature, salinity, soil contents (heavy metals, nutrient availability), light, etc. It has been suggested that abiotic stresses can reduce crop yield by over 50% (Atkinson and Urwin, 2012). Crop losses due to environmental stresses are predicted to increase in the future due to climate change (Mickelbart et al., 2015). The development of plants capable of coping with environmental stress is vital. Several microbial genes have been introduced into plants to increase stress tolerance including genes for the production of osmolytes, chaperones, ion transporters, and antioxidant enzymes.

1.3.1 Osmoprotectants

Compatible solutes or osmolytes are low molecular weight, water soluble compounds including sugars, amino acids, organic acids, polyamines, and lipids (Chen and Murata, 2011). Production of these osmoprotectants is a common way organisms mitigate the effects of various abiotic stresses. In plants, osmoprotectants are particularly effective against salt and drought stress (Chen and Murata, 2011). These molecules are thought to mitigate stress through stabilization of the membrane and cellular components, as well as scavenging reactive oxygen species (ROS) (Reguera et al., 2012).

Perhaps the most studied compatible solute is glycinebetaine (*N,N,N*-trimethylglycine, GB). This compound is naturally produced in both bacteria and plants, among other organisms. In plants the production of GB is induced by stress, and the concentration is correlated with the level of stress (Chen and Murata, 2011, 2002; Rhodes and Hanson, 1993). Despite the benefits of GB accumulation, many economically relevant crops are classified as GB non-accumulators such as rice, tobacco, and potato (Ahmad et al.,

2008; Quan et al., 2004b). GB biosynthesis in most organisms involves a two-step oxidation of choline. In plants the enzymes involved are choline monooxygenase for the first oxidation, and NAD^+-dependent betaine aldehyde dehydrogenase catalyzes the second oxidation (Chen and Murata, 2011, 2002). In bacteria such as *E. coli* the first oxidation is catalyzed by choline dehydrogenase, encoded by the gene *betA,* which is capable of performing the second oxidation as well (Holmström et al., 2000). This gene has been utilized to increase stress tolerance in tobacco (Holmström et al., 2000), *Zea mays* L. (maize) (Quan et al., 2004a, 2004b), *Gossypium hirsutum* (cotton) (Lv et al., 2007; Zhang et al., 2012), and *Triticum aestivum* L. (wheat) (He et al., 2011). Plants expressing *betA* had increased tolerance to chilling (Holmström et al., 2000; Quan et al., 2004a; Zhang et al., 2012), drought (He et al., 2011; Lv et al., 2007; Quan et al., 2004b), and salt (Holmström et al., 2000).

A different pathway for GB biosynthesis exists in the soil bacteria *Arthrobacter globiformis* and *A. pascens* (Chen and Murata, 2002). This pathway utilizes the enzyme choline oxidase (CodA from *A. globiformis* and Cox from *A. pascens*), which directly oxidizes choline to form GB (Chen and Murata, 2002; Ikuta et al., 1977). While both *cox* and *codA* have been used to generate transgenic GB accumulating plants, the *codA* gene has been the most extensively studied (Chen and Murata, 2011) and to date has been expressed in *Arabidopsis thaliana* (Alia et al., 1999, 1998, Hayashi et al., 1998, 1997; Sulpice et al., 2003), *Brassica juncea* (Indian mustard) (Prasad et al., 2000), *Diospyras kaki* (Japanese persimmon) (Gao et al., 2000), *Lycopersicon esculentum* (tomato)(Goel et al., 2011; Li et al., 2011; Park et al., 2007, 2004), *Oryza sativa* (rice) (Konstantinova et al., 2002; Mohanty et al., 2002; Sakamoto et al., 1998), and *Solanum tuberosum* (potato) (Ahmad et al., 2008). These transgenic plants exhibited broad stress tolerance in response to chilling, heat, salt, and

drought stress. Additionally, expression of the gene in the chloroplast results in the accumulation of GB in the chloroplast leading to increased stress tolerance. Because of this, the majority of these transgenic plants have been engineered for chloroplastic expression of the compatible solute synthesis genes (Park et al., 2007). In order to further build on the beneficial phenotypes seen in GB accumulating transgenic plants, *betA* and *codA* have also been used in gene stacking efforts with other stress tolerance genes (Ahmad et al., 2010; Duan et al., 2009; Wei et al., 2011). This is a promising method to further increase plant stress tolerance phenotypes beyond what is possible with a single gene.

Another compatible solute and osmoprotectant molecule, which has been used to enhance plant abiotic stress tolerance, is trehalose. Trehalose is a non-reducing disaccharide molecule present is a diverse array of organisms where it is used as an osmoprotectant for abiotic stress (Iordachescu and Imai, 2008). Among these organisms are anhydrobiotic organisms such as "resurrection plants," which are capable of surviving complete dehydration. In these organisms, trehalose helps the plants survive desiccation by stabilizing dehydrated proteins, lipid membranes, and other biological structures (Garg et al., 2002; Iordachescu and Imai, 2008). While trehalose is present in plants, it is typically present in low levels (Marco et al., 2015). The importance of trehalose in other biological systems to mitigate abiotic stress drove interest in the generation of transgenic crops, which could accumulate trehalose.

Trehalose is synthesized from UDP glucose by the enzymes trehalose phosphate synthase (TPS) and trehalose phosphate phosphatase (TPP) (Iordachescu and Imai, 2008). In *E. coli* these enzymes are encoded by the genes *otsA* and *otsB,* respectively. Early attempts to increase accumulation of trehalose involved the generation of transgenic plants expressing

otsA and/or *otsB* (Goddijn et al., 1997; Pilon-Smits et al., 1998). While these plants demonstrated drought tolerance, they also displayed undesirable pleiotropic effects including stunted growth (Goddijn et al., 1997; Pilon-Smits et al., 1998). To overcome this problem, fusion proteins of *otsA* and *otsB* were generated to limit any accumulation of the trehalose-6-phosphate intermediate (Garg et al., 2002; Jang et al., 2003). Transgenic rice plants expressing the *otsA-ostB* fusion are resistant to drought, salt, and cold stress without any undesirable changes to their phenotype (Garg et al., 2002; Jang et al., 2003). Despite the presence of significant phenotypes, the accumulation of trehalose in transgenic plants was low and did not correlate well with level of tolerance (Iordachescu and Imai, 2008). This suggests an indirect role for trehalose in stress tolerance, such a ROS scavenging or increasing photosynthetic capacity (Garg et al., 2002; Iordachescu and Imai, 2008; Pellny et al., 2004).

The sugar alcohol mannitol is another compatible solute and osmoprotectant in plants and other organisms (Marco et al., 2015). In plants, particularly celery, mannitol concentrations are increased in response to salt stress (Abebe et al., 2003). To increase mannitol concentrations, the manniol-1-phosphate dehydrogenase (*mtlD*) gene from *E. coli* was used to transform tobacco (Karakas et al., 1997; Tarczynski et al., 1992), *Arabidopsis thaliana* (Thomas et al., 1995), *Solanum melongena* L. (eggplant) (Prabhavathi et al., 2002), *Populus tomentosa* (poplar) (Hu et al., 2005), wheat (Abebe et al., 2003), and rice (Pujni et al., 2007). In all instances, plants expressing *mtlD* demonstrated tolerance to drought and salt stresses.

While heterologous expression of microbial genes augmented the production of these compatible solutes, prokaryotes are also capable of producing compatible solutes that are not

produced by plants or not common in plants, such as ectoine and glucosylglycerol (Klahn et al., 2009; Nakayama et al., 2000). Ectoine is a compatible solute common in halophillic bacteria and is synthesized from L-aspartate β-semialdehyde in three steps catalyzed by the enzymes L-2,4-diaminobutyric acid aminotransferase (*ectB*), L-2,4-diaminobutyric acid acetyl transferase (*ectA*), and L-ectoine synthase (*ectC*) (Nakayama et al., 2000; Rai et al., 2006). Expression of *Halomonas elongata* and *Marinococcus halophilus* ectoine biosynthetic pathway genes (*ectA, ectB,* and *ectC*) has been demonstrated in tobacco (Moghaieb et al., 2006; Nakayama et al., 2000; Rai et al., 2006) and tomato (Moghaieb et al., 2017). Plants and plant cells producing ectoine are resistant to salt stress (Moghaieb et al., 2017, 2006; Nakayama et al., 2000; Rai et al., 2006) and are able to preserve photosynthetic function when challenged with salt stress (Moghaieb et al., 2017, 2006; Rai et al., 2006). Additionally, it was found that ectoine specifically accumulated in the roots where it enhanced water uptake (Moghaieb et al., 2017, 2006).

Glucosylglycerol (GG) is the primary compatible solute utilized by moderately halotolerant cyanobacteria (Klahn et al., 2009; Sievers et al., 2013). GG is synthesized via a two-step process where GG-phosphate is produced by GG-phosphate synthase from glycerol-3-phosphate and ADP-glucose. The GG-phosphate is then dephosphorylated by GG-phosphate phosphatase (Klahn et al., 2009; Sievers et al., 2013). Some heterotrophic bacteria, such as *Azotobacter vinelandii*, possess an enzyme which performs both steps of the GG biosynthesis called GG-phosphate phosphatase/synthase (GgpPS) (Klahn et al., 2009; Sievers et al., 2013). GgpPS has been heterologously expressed in *Arabidopsis thaliana* (Klahn et al., 2009) and potato (Sievers et al., 2013). In *Arabidopsis* it was found that the production of

high levels of GG in the plant hindered growth, whereas low levels of production provided protection against salt stress (Klahn et al., 2009).

In addition to the described compatible solutes, there are many others that could be exploited to enhance plant stress tolerance. Prokaryotes possess an impressive diversity of compatible solutes, many of which are not natively produced by plants (Empadinhas and da Costa, 2008). Compatible solutes utilized by halophillic, thermophillic, or other extreme environment living bacteria and archaea might prove to be particularly useful for mitigating these stresses in plants.

1.3.2 Chaperones

As plants and other organisms encounter stress, metabolic processes become increasingly difficult requiring the production of chaperones and other proteins to assist in maintaining homeostasis (López-Arredondo et al., 2015). RNA chaperones are abundant in all organisms, and function in keeping RNA in an accessible form for biological activity (Castiglioni et al., 2008). In response to cold shock, bacteria express cold shock proteins (CSPs), which contain a cold shock domain (CSD). This domain binds to DNA or RNA with little selectivity or specificity, and aids in stress adaptation through a post-transcriptional method (Castiglioni et al., 2008).

To evaluate the capability of bacterial CSPs to enhance stress tolerance in plants, the cold shock proteins CspA from *E. coli* and CspB from *Bacillus subtilis* were used to generate transgenic *Arabidopsis thaliana*, rice, and maize (Castiglioni et al., 2008). Plants constitutively expressing CspA or CspB demonstrated broad abiotic stress tolerance (cold, heat, and drought). In addition to greenhouse-controlled trials, yield enhancements were also

demonstrated in maize grown in the field under water deficit conditions (Castiglioni et al., 2008). Maize hybrids expressing CspB received regulatory approval and are being sold under the name Droughtgard®.

Protein denaturation and mis-folding is another common result of stress (Jacob et al., 2017). In order to maintain homeostasis, particularly in response to heat stress, both prokaryotes and eukaryotes produce heat shock proteins (HSPs) (Jacob et al., 2017). HSPs are chaperones which act to resolve misfolded proteins and protein aggregates and restore native conformation (Uchida et al., 2008). Plants and microbes express a number of HSPs in response to stress. One such protein is Hsp70, also known as DnaK in bacteria. Hsp70/DnaK binds to misfolded proteins, and with the help of Hsp60, refolds them (Uchida et al., 2008). A DnaK chaperone with high refolding activity was identified from the halotolerant cyanobacterium, *Aphanothece halophytica* (Hibino et al., 1999). To evaluate the ability of DnaK chaperones to improve stress tolerance in plants, the *A. halophytica dnaK* gene was expressed in tobacco (Ono et al., 2001; Sugino et al., 1999). Tobacco plants expressing DnaK were found to be both salt (Sugino et al., 1999) and heat tolerant (Ono et al., 2001). In a continuation of this work, DnaK expressing tobacco and rice plants were evaluated for improvements in yield (Uchida et al., 2008). Tobacco and rice plants exhibited increases in biomass and seed yield, particularly in response to heat or salt stress compared to wild type (Uchida et al., 2008). Given the favorable phenotypes observed to date, expression of bacterial chaperones in plants represents a promising strategy for crop improvement.

1.3.3 Ion Transporters

The ions Na^+ and H^+ are vital for cellular function. Fluctuations in their concentration can have deleterious effects on cellular survival. In plants, drought and salt stress often lead to an imbalance in Na^+ and H^+, leading to osmotic stress (Ahuja et al., 2010). Na^+/H^+ antiporters are responsible for the transport of Na^+ and Li^+ in exchange for H^+ to maintain homeostasis (Wu et al., 2005). Overexpression of Na^+/H^+ antiporters has been shown to increase salt tolerance, likely through the sequestration of Na^+. While this effect has been primarily evaluated using the *Arabidopsis thaliana* NHXI, it has also been shown using *E. coli* nhaA (Wu et al., 2005). Transgenic rice plants were generated to constitutively express EC-nhaA, though it was found that the amount of EC-nhaA produced was responsive to salt concentration and decreased at high concentrations (>200mM) (Wu et al., 2005). Despite these alterations in expression, these transgenic lines demonstrated increased tolerance to both salt and drought, and increased yield under these conditions, suggesting the use of EC-nhaA as a promising trait for stress tolerance (Wu et al., 2005).

1.3.4 Antioxidant Enzymes/Compounds

Reactive oxygen species (ROS), such as hydrogen peroxide (H_2O_2), singlet oxygen ($^1O_2$), superoxide anion (O_2^-), and hydroxyl radical (OH^-), are generated through normal metabolism in aerobic organisms (Halliwell, 2006). It is widely accepted that ROS play an important role in plant signaling (Suzuki et al., 2012). However, under adverse conditions ROS, specifically O_2^-, can build up in the cell and lead to cell death through damage of cellular macromolecules (i.e. lipid peroxidation, oxidation of metalloproteins, DNA strand breaks) (Gill and Tuteja, 2010; Suzuki et al., 2012). Plants possess a variety of antioxidant

enzymes (superoxide dismutase, catalase, ascorbate peroxidase, etc.) and non-enzymatic antioxidants (glutathione, ascorbic acid, etc.) to mitigate the effect of ROS production, but persistent stress conditions can overcome these systems leading to tissue damage and death (Gill and Tuteja, 2010).

Many antioxidant systems and enzymes are shared across domains. These homologous enzymes while sharing the same function may possess different affinities or rates of activity making them attractive potential transgenes. An example of this is the *E. coli* catalase (*katE*). Catalase is a heme-containing enzyme, which catalyzes the conversion H_2O_2 into H_2O and O_2 (Gill and Tuteja, 2010). Catalase is ubiquitous in plants, and is vital for ROS detoxification. The *E. coli* catalase was utilized in plants to enhance stress tolerance above what is achievable with endogenous catalase. It was chosen for this purpose as it has a higher affinity for H_2O_2 than the plant catalase and would not be regulated by the plant (Mohamed et al., 2003; Moriwaki et al., 2008; Shikanai et al., 1998). This strategy has been employed in tobacco (Al-Taweel et al., 2007; Miyagawa et al., 2000; Shikanai et al., 1998), rice (Moriwaki et al., 2008; Nagamiya et al., 2007), and tomato (Mohamed et al., 2003). Plants expressing *katE* show resistance to salt and photooxidative stress. As the chloroplast is the primary site of ROS generation in plant cells, localization of KatE to the chloroplast provided protection of the photosynthetic machinery including photosystem II subunit D1 from photooxidative damage (Al-Taweel et al., 2007; Miyagawa et al., 2000; Mohamed et al., 2003; Shikanai et al., 1998).

In addition to catalase, plants and other organisms express an array of peroxidases, which also scavenge H_2O_2. While ascorbate peroxidase, peroxiredoxin, and others are more well known in plants, glutathione peroxidase (GPX) is a vital antioxidant enzyme in animals

and other organisms (Gaber et al., 2006; Noctor et al., 2012). Plant GPXs are less active than their mammalian counterparts because they contain a cysteine in their active site in place of the selenocysteine present in mammalian GPX (Bela et al., 2015). These enzymes play a vital role in detoxifying lipid hydroperoxides and protection of membranes from lipid peroxidation (Gaber et al., 2006). The cyanobacterium *Synechocystis* PCC6803 possesses GPX-like enzymes that not only detoxify lipid and fatty acid hydroperoxides but do so without the use of GSH (Gaber et al., 2006). Transgenic *Arabidopsis* plants were made that express the *Synechocystis* PCC6803 GPX. These plants were found to have broad stress tolerance, including to chilling, salt, drought, and H_2O_2 exposure (Gaber et al., 2006). This stress tolerance was found in combination with a decrease in lipid peroxidation under all stress conditions (Gaber et al., 2006). These results suggest a route for protection or mitigation of one of the most damaging effects of ROS in the cell and potentially a pathway for repair of damaged membranes.

Superoxide reductase (SOR) is an antioxidant enzyme found primarily in anaerobic bacteria and archaea that reduces O_2^- to H_2O_2 (Grunden et al., 2005; Jenney et al., 1999). This enzyme is well adapted for use in anaerobic organisms as it reduces superoxide without producing additional O_2. This unique feature is also beneficial in a plant system as the production of additional molecular oxygen could lead to the generation of more ROS. Additionally, SOR has a higher affinity for O_2^- than SOD, which allows it to detoxify ROS more effectively. SOR from the thermophilic archaea, *Pyrococcus furiousus*, was expressed constitutively in the cytosol in NT1 tobacco cells, *Arabidopsis thaliana*, and *Cornus canadensis* L. f. (ornamental dogwood) (Geng et al., 2016; Im et al., 2009, 2005). Plants expressing SOR demonstrated increased heat, light, and methyl viologen tolerance compared

to non-expressing plants. Further research is needed to determine if other stresses could be mitigated through SOR production. Additionally, expression of SOR in the chloroplast could further enhance plant stress tolerance as a significant proportion of ROS are generated in the chloroplast.

Ferredoxins are small, iron-sulfur proteins responsible for electron transfer in a wide variety of metabolic reactions. Ferredoxin is critically important in the chloroplast as the primary method of electron transfer for electrons produced during the light reactions of photosynthesis (Zurbriggen et al., 2008). Once reduced by photosystem I, ferredoxin shuttles electrons to ferredoxin $NADP^+$ reductase (FNR) for the production of NADPH, utilized in the CBB cycle. In addition to shuttling electrons to FNR, chloroplast ferredoxin plays a role in nitrate assimilation, amino acid metabolism, lipid metabolism, and a number of other metabolic processes, as well as activating ferredoxin-thioredoxin reductase (FTR) which has an important regulatory role for the CBB cycle and other enzymes (Zurbriggen et al., 2008). In response to various environmental conditions and stresses, ferredoxin participates in cyclic electron flow and the water-water cycle to prevent over-reduction which can lead to the generation of ROS (Miyake, 2010). Importantly, in the water-water cycle, ferredoxin is responsible for the regeneration of reduced ascorbate. Ferredoxin-deficient plants have a variety of negative phenotypes including hindered growth, photosynthetic deficiencies, and increased sensitivity to oxidative stress (Blanco et al., 2011; Ceccoli et al., 2011). Despite its vital role in chloroplast metabolism and maintaining redox balance, ferredoxin expression is decreased under most stress conditions (Ceccoli et al., 2011). In the absence of ferredoxin, photosystem I will pass electrons to O_2, generating ROS, and thus exacerbating the stress (Ceccoli et al., 2011). However, the overexpression of a ferredoxin from the cyanobacteria

Anabaena failed to improve stress tolerance (Ceccoli et al., 2011). This was potentially due to the fact that plant regulatory mechanisms appeared to be capable of regulating the *Anabaena* ferredoxin as well, successfully downregulating its expression under stress conditions (Ceccoli et al., 2011).

While cyanobacterial ferredoxin failed to enhance stress tolerance, cyanobacterial flavodoxin has shown to be an effective transgene. Flavodoxin is a small electron carrier protein similar to ferredoxin, but instead of an iron-sulfur cluster, it contains a flavin mononucleotide prosthetic group (Karlusich et al., 2014). While flavodoxin exists in many prokaryotes and in some algae, it is completely absent from plants and appears to have been lost in evolution in favor of the higher electron carrier efficiency of ferredoxin (Karlusich et al., 2014). In cyanobacteria, flavodoxin expression increases under stress while ferredoxin expression declines (Tognetti et al., 2006). To evaluate the effect of flavodoxin expression in plants, tobacco plants expressing *Anabaena* flavodoxin in the chloroplast were created. These plants were found to have very broad stress tolerance (methyl viologen, heat, drought, light, and UV), and resistance to iron starvation (Tognetti et al., 2007, 2006). It was also found that transforming ferredoxin deficient plants with cyanobacterial flavodoxin would restore wild type phenotype and resistance to oxidative stress (Blanco et al., 2011). This demonstrates that the flavodoxin is successfully able to participate in the same pathways as ferredoxin. Cyanobacterial flavodoxin has also been expressed in bent grass with similar results (Z. Li et al., 2016). The success of the expression of flavodoxin for enhancing stress tolerance highlights the importance of maintaining chloroplast redox balance and controlling ROS production.

Another component of plant ROS detoxification is the non-enzymatic antioxidants glutathione and ascorbic acid. In their reduced forms ascorbic acid and glutathione, scavenge and detoxify ROS in plant cells (Apel and Hirt, 2004). When these antioxidant molecules encounter ROS or interact with certain enzymes or proteins they become oxidized, and must be reduced enzymatically (Apel and Hirt, 2004). Oxidized ascorbate, monodehydroascorbate (MDA), can be reduced by monodehydroascorbate reductase (MDAR). However, MDA is unstable and will rapidly disproportionate into dehydroascorbate (DHA), which requires reduction to ascorbate by dehydroascorbate reductase (DHAR). In order for DHAR to reduce DHA to ascorbate, it must oxidize a molecule of reduced glutathione (GSH) producing oxidized glutathione (GSSG). The activity of glutathione reductase (GR) is required to reduce GSSG to GSH, maintaining cellular redox balance (Noctor et al., 2012). This process is called the Ascorbate-Glutathione cycle, and it is a key element of plant stress tolerance. While ascorbic acid is a vital component of plant ROS defenses, it is not commonly synthesized by bacteria or archaea, except for some cyanobacteria (Ziegelhoffer and Donohue, 2009). However, glutathione is widely used and important in microbial and plant defenses against ROS (Ziegelhoffer and Donohue, 2009).

Glutathione is a thiol tripeptide consisting of glutamate, cysteine, and glycine (Gill et al., 2013). Reduced glutathione (GSH) is abundant in plant tissues and cellular compartments and is involved in a variety of cellular processes including heavy metal detoxification, redox balance, and ROS scavenging (Gill et al., 2013; Noctor et al., 2012). With such an important role in the scavenging of ROS, it raises the question whether modulating the amount of GSH or the ratio of GSH:GSSG in the cell would lead to stress tolerance in plants. One method for increasing the GSH content in plants is through increasing the expression of GR. As

mentioned previously, GR is the enzyme responsible for reducing GSSG to produce GSH. Due to the important role GR plays in the ascorbate-glutathione cycle, increasing the amount of GR in the cell has the capacity to shift cell antioxidant capabilities by increasing the amount of reduced ascorbate and GSH, and/or increasing the rate of turnover for the oxidized compounds (Gill et al., 2013). *E. coli* GR has been used to transform wheat (Melchiorre et al., 2009), tobacco (Aono et al., 1993; Foyer et al., 1991; Le Martret et al., 2011), and poplar (Foyer et al., 1995). Unfortunately, the effect of expression of *E. coli* GR in plants did not yield a consistent result in all cases. While increased tolerance to oxidative stress was found in some transgenic plants (tobacco chloroplast and poplar chloroplast) (Aono et al., 1993; Foyer et al., 1995; Le Martret et al., 2011), others showed little to no difference (tobacco cytosol and wheat protoplasts) (Foyer et al., 1991; Melchiorre et al., 2009). Interestingly, plants with enhanced oxidative stress tolerance had the GR expressed or targeted to the chloroplast, which suggests that localization plays an important role (Le Martret et al., 2011).

Another strategy to increase GSH is to enhance its biosynthesis. Glutathione is synthesized in a two-step process from its constituent amino acids. The first step is catalyzed by γ-glutamylcysteine synthetase (γ-ECS), while the second step is catalyzed by glutathione synthetase (GS) forming glutathione (Noctor et al., 2012). In order to increase glutathione concentration, heterologous expression of *E. coli* γ-ECS and GS has been studied in poplar (Foyer et al., 1995; He et al., 2015; Herschbach et al., 1998; Noctor et al., 1998, 1996; Strohm et al., 1995), Indian mustard (Reisinger et al., 2008; Y L Zhu et al., 1999; Yong Liang Zhu et al., 1999), and tobacco (Creissen et al., 1999). While GS expression failed to significantly increase GSH content (Foyer et al., 1995; Herschbach et al., 1998; Strohm et al., 1995; Yong Liang Zhu et al., 1999), expression of γ-ECS in either chloroplast or cytosol

showed increases in GSH over control plants (Creissen et al., 1999; Herschbach et al., 1998; Noctor et al., 1998; Reisinger et al., 2008; Y L Zhu et al., 1999). In addition to its role in oxidative stress, glutathione is an important precursor for phytochelatin (PC) biosynthesis (Noctor et al., 2012). PCs are responsible for sequestering heavy metals, such as cadmium and arsenic, in the vacuole. In Brassica and poplar, plants expressing γ-ECS had increased tolerance to heavy metals, particularly cadmium, and increased amounts of PCs (He et al., 2015; Reisinger et al., 2008; Y L Zhu et al., 1999). In addition, γ-ECS expressing poplar plants were also shown to be resistant and to sequester chloroacetanilide herbicides (Gullner et al., 2001). The ability to tolerate and sequester heavy metals and other chemicals is valuable for phytoremediation. While there did not appear to be detrimental effects of γ-ECS expression in Indian mustard and poplar, tobacco plants expressing γ-ECS in the plastid showed increased sensitivity to oxidative stress and resultant chlorosis (Creissen et al., 1999). These results are further complicated by the recent creation of transgenic tobacco plants with 20-30 fold increases in GSH. These high accumulating tobacco plants, were transformed with a bifunctional γ-glutamylcysteine lyase from *Streptococcus thermophilus* (StGCL-GS) which performs both of the glutathione synthesis reactions simultaneously (Liedschulte et al., 2010). The StGCL-GS enzyme is beneficial over the plant or the *E. coli* γ-ECS as it is not as sensitive to feedback inhibition by GSH allowing GSH to accumulate to high levels without decreasing activity (Liedschulte et al., 2010). In addition to accumulating extremely high amounts of GSH, the transgenic plants were found to have increased resistance to oxidative stress and tolerance to Cd (Liedschulte et al., 2010). The difference in phenotype between StGCL-GS and γ-ECS transgenic tobacco may partially be explained by the need for balance between the two reactions. Further research is needed to elucidate the application of

increased GSH for stress tolerance and phytoremediation. Figure 1-3 provides a summary of the antioxidant targets that have been used to generate transgenic plants.

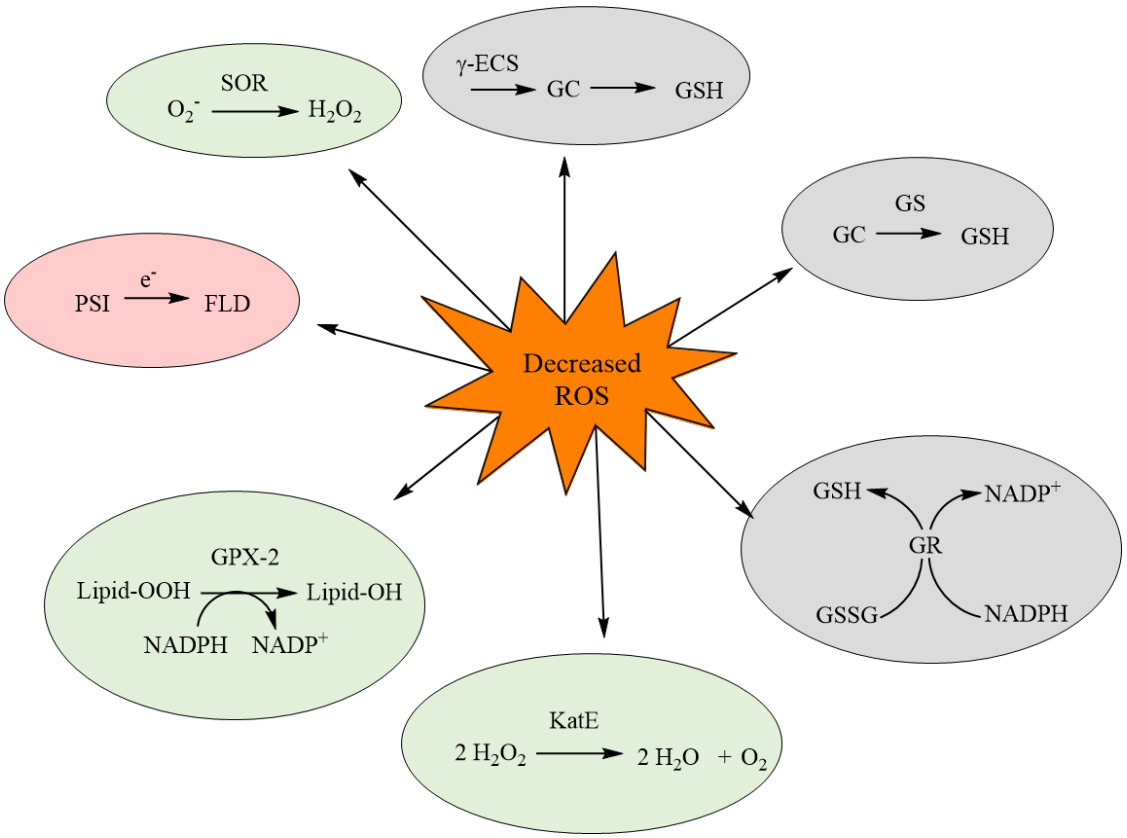

Figure 1-3. Antioxidant strategies used to increase abiotic stress tolerance through the expression of microbial genes. Green ovals represent enzymes that directly reduce reactive oxygen species (ROS) or in the case of GPX-2 reactive lipids created by ROS. Grey ovals represent enzymes involved in glutathione biosynthesis or reduction, which is a vital non-enzymatic ROS detoxification molecule. The pink oval contains flavodoxin, which has an indirect method for decreasing ROS, through accepting electrons from PSI under stress conditions preventing the creation of ROS. Abbreviations: Superoxide reductase (SOR), γ-glutamylcysteine synthetase (γ-ECS), glutamylcysteine (GC), reduced glutathione (GSH), glutathione synthetase (GS), oxidized glutathione (GSSG), glutathione reductase (GR), catalase (KatE), lipid-OOH (lipid hydrorperoxide), GPX-2 (glutathione peroxidase-like protein), lipid-OH (lipid alcohol), photosystem 1 (PSI), flavodoxin (FLD), e^- (electron).

1.4 Nutrient Acquisition

The availability and efficient usage of soil nutrients is vital to plant survival and a key component of increasing crop yield. While plants obtain many of their required nutrients from the soil, phosphorous and nitrogen are the most important (Schroeder et al., 2013). In addition to their role in crop productivity, applied nitrogen and phosphorous fertilizers are responsible for significant environmental disturbances caused by their runoff into waterways (López-Arredondo et al., 2015). Plants capable of efficient use of these nutrients could reduce over-application of fertilizers and enhance crop yields.

1.4.1 Nitrogen

Nitrogen is arguably the most important nutrient for plants. It is utilized in the biosynthesis of nucleic acids, proteins, and storage molecules, in various metabolic reactions, and also serves as a vital signaling molecule. The most common forms of nitrogen taken up by plants are nitrate (NO_3^-), ammonium (NH_4^+), and proteins or amino acids, with nitrate being the most abundant (Mcallister et al., 2012). While nitrogen is vital to plant growth and development, it is often limiting. In order to overcome this limitation, nitrogen fertilizer is added in agriculture. Despite the addition of large quantities of nitrogen, only 30-50% of applied nitrogen is utilized by the crops (Cassman et al., 2002). The remaining portion of the applied nitrogen is lost due to leaching, run-off, volatilization, and soil microbe competition. Heavy application of nitrogen fertilizers have had a variety of environmental impacts including excessive energy consumption to produce the fertilizer, contamination of fresh water with excess nitrogen leading to algal blooms, and adding to climate change and ozone depletion through the release of nitrous oxide (Mcallister et al., 2012).

Enhancing nitrogen use efficiency could limit waste of applied nitrogen and increase nitrogen assimilation in plants. In plants the assimilation of nitrogen involves the reduction of nitrogen to NH_4^+, which is incorporated into the amino acids glutamine and glutamate by glutamine synthetase (GS) and glutamate synthetase (GOGAT), respectively (Martínez-Andújar et al., 2013). Subsequently, glutamate and glutamine can be used by aspartate aminotransferase (AspAT) and asparagine synthetase (AS) to produce aspartate and asparagine, respectively (Martínez-Andújar et al., 2013). These amino acids act as nitrogen transport compounds throughout the plant, which are involved in biosynthesis of a wide variety of molecules (Martínez-Andújar et al., 2013). Asparagine in particular is a good transport amino acid for long distance transport and storage as it has a higher N/C ratio and is less reactive (Giannino et al., 2008). In plants, asparagine is synthesized through the transfer of an amino group from glutamine to aspartate, in a reaction requiring ATP. The activity of AS is regulated by N/C status as well as by light in plants (Martínez-Andújar et al., 2013). In *E. coli* the gene *asnA* encodes an AS (AS-A), which utilizes ammonium instead of glutamine for asparagine synthesis. The use of this gene in plants represents a more direct route for nitrogen assimilation, as well as alleviating the regulation of AS by light allowing for more activity (Martínez-Andújar et al., 2013). Various plant species have been transformed with *asnA* and have shown variable phenotypes. Transgenic *Lactuca sativa* L. (lettuce) expressing *asnA* showed greater leaf area, increased amino acids and protein content, and reduced nitrate (Giannino et al., 2008; Sobolev et al., 2010). However, *Lotus corniculatus* (Bellucci et al., 2004), tomato (Martínez-Andújar et al., 2013), and *Brassica napus* (rapeseed) (Seiffert et al., 2004) plants expressing *asnA* had reduced growth, particularly under nitrogen limiting

conditions. Further research is needed to evaluate the benefits of *asnA* overexpression on plant growth and nitrogen accumulation.

Despite the nitrogen limitations faced by agriculture, nitrogen (N_2) is not a scarce molecule as it composes 78% of the air. However, due to the stability of N_2 it is difficult for organisms to fix and requires a specific nitrogenase enzyme, which only evolved in bacteria and archaea (Oldroyd and Dixon, 2014). The canonical nitrogenase enzyme is a complex, where the catalytic portion is composed of a molybdenum containing subunit and an iron containing subunit, which fixes 1 mole of N_2 to 2 moles of NH_3 (Oldroyd and Dixon, 2014). Some plants, primarily legumes, have developed symbiotic relationships with nitrogenase containing microorganisms in order to ensure a supply of fixed nitrogen through nodulation. Engineering plants to express nitrogenase has been hypothesized for many years (Merrick and Dixon, 1984), but has recently garnered more interest (Oldroyd and Dixon, 2014). While the capability of expressing nitrogenase in plants is very attractive, there are also a number of factors which could interfere with the enzyme's function in plants. The first of which is that nitrogenase is irreversibly damaged by oxygen and thus requires protection of its catalytic subunits from oxygen. Another challenge is in the complexity of genes required for the assembly of the nitrogenase complex. Additionally, fixation of N_2 requires 16 ATP molecules and 8 electrons per N_2 fixed (Oldroyd and Dixon, 2014). Strategies to cope with these requirements involve both spatial and potentially temporal separation of the nitrogenase from other non-compatible plant metabolic processes.

One promising site for nitrogenase activity is the mitochondrial matrix. As the plant mitochondria contains oxygen-consuming enzymes and is the primary site of metalloenzyme synthesis in plants, it could provide a suitable environment for nitrogenase reconstitution and

activity (Allen et al., 2017; Oldroyd and Dixon, 2014). Additionally, the mitochondria could supply the required amounts of ATP and reductant for successful nitrogenase function. In order to evaluate the possibility of expressing a functional nitrogenase in plants, research is first being conducted to evaluate the expression and targeting of the *nif* genes in plant mitochondria. Allen et al. expressed 16 of the *nif* genes from the diazatrophic bacterium *Klebsiella pneumonia*e transiently in the *Nicotiana benthamiana* mitochondrial matrix. In addition to the catalytic nitrogenase subunits, NifD and NifK, 14 other genes were successfully expressed which are vital for nitrogenase assembly and electron transport (Allen et al., 2017). While no functional characterization was conducted, demonstrating that the *nif* genes can be successfully expressed and targeted to the mitochondrial matrix is a significant step to a functional nitrogenase in plants.

In addition to the mitochondria, the plastid is also being evaluated as a potential site for nitrogenase expression and activity (Ivleva et al., 2016; Oldroyd and Dixon, 2014). The presence of oxygen in photosynthetic plastids could be problematic, though plastids in non-photosynthetic tissue or temporally separating nitrogenase activity during the dark period could be utilized. The validity of the plastid as a site for nitrogenase activity was demonstrated through the functional expression of the iron containing subunit of nitrogenase in leaf plastids of tobacco (Ivleva et al., 2016). The iron containing subunit was chosen as it is most sensitive to oxygen. Nitrogenase genes *nifh and nifm* were transformed into the plastid genome, and shown to not only be expressed but to be functional when plants were grown in low oxygen (10%) conditions (Ivleva et al., 2016). The dependence of the activity on lower oxygen suggests that oxygen will likely be a limiting factor, but expression in non-

photosynthetic tissue or using temporal regulation could alleviate this inhibition (Ivleva et al., 2016).

1.4.2 Phosphate

Phosphate is a primary component of a variety of cellular macromolecules (i.e. phospholipids, DNA, RNA) and as such is an essential macronutrient. It is also vital for cellular metabolism as part of ATP, ADP, NADPH, etc., which drive the majority of metabolic processes within the cell. Phosphate is acquired by plants as inorganic phosphate (P_i) from the soil (López-Arredondo et al., 2014). In agriculture, phosphate fertilizers are typically applied in order to supply plants with sufficient P_i for growth. The application of P_i containing fertilizers has led to increases in crop productivity in modern agriculture. However, as the P_i in fertilizers is acquired by mining, it is a finite resource with dwindling supplies (Heuer et al., 2016). It is predicted that P_i resources will be exhausted within 300-400 years. With the amount of fertilizer used predicted to increase in the future, this poses a significant problem. In addition to long-term issues with P_i fertilizer supply, only a small percentage of applied P_i can be readily accessed by crops due to immobilization and leaching (Hinsinger, 2001). In the soil, P_i readily forms complexes or precipitates with organic matter and mineral cations. This is a particular problem in acidic or alkaline soils where P_i will form complexes primarily with aluminum or calcium (Hinsinger, 2001). In addition, a significant portion of applied fertilizer ends up in bodies of water neighboring fields from run-off. This phosphate leaching can lead to algal blooms and eutrophication (Smith and Schindler, 2009). Thus enhancing P_i incorporation and usage by plants is important to increase productivity and limit over-usage of fertilizers.

While P_i is the only phosphate source that can be utilized by plants, it is not the only phosphorous compound available or the only compound that can be imported by plants. Phosphite (Phi), a reduced form of P_i, is also available and capable of being imported by plants (López-Arredondo and Herrera-Estrella, 2012). Phi has many beneficial characteristics compared to P_i such as higher solubility and lower reactivity with soil components, leading to higher availability of Phi after application. Phi has also been utilized in agriculture as a fungicide and herbicide (López-Arredondo and Herrera-Estrella, 2012). While plants cannot metabolize Phi, some bacteria have developed mechanisms to oxidize Phi to produce P_i using the enzyme phosphite oxidoreductase (PTXD) (Costas et al., 2001). In this reaction Phi is oxidized to P_i while reducing NAD^+ to NADH. To generate plants capable of incorporating Phi, the *ptxD* gene from *Pseudomonas stutzeri* WM88, was constitutively expressed in *Arabidopsis thaliana* and tobacco. These plants were capable of utilizing Phi as a sole phosphorous source, and required 30-50% less phosphorous input to achieve the same productivity when fertilized with Phi instead of P_i (López-Arredondo and Herrera-Estrella, 2012). Further evaluation of this technology in the field is still needed. Due to the ability of bacteria to metabolize a variety of phosphorous sources additional enzymes may exist to further increase incorporation, and utilization of phosphorous in plants.

1.5 Conclusion

Microbes inhabit the most inhospitable environments on the planet, and possess an incredibly diverse array of metabolic and enzymatic potential. Microbial genes have been used to generate a variety of transgenic plants with enhanced phenotypes. In some cases the use of bacterial genes and pathways have increased yields from 20-70% (Castiglioni et al.,

2008; Dalal et al., 2015). The expression of microbial genes has also led to the creation of transgenic plants able to withstand a wide variety of damaging environmental conditions that typically lead to detrimental losses in the field (Gaber et al., 2006; Garg et al., 2002; Im et al., 2009; Park et al., 2007; Tognetti et al., 2006). However, a significant amount of work remains to be done. Despite the wide variety of research being conducted, the vast majority of microbially-derived crop improvement traits come from a small handful of bacteria and archaea, primarily *E. coli* (Table 1-1). Further exploration and characterization of microbial species, genes, and metabolic pathways will be vital to the discovery of additional traits for crop improvement. Additionally, with a complex problem such as increasing yield, a complex answer is often required. It is unlikely that a single trait will be sufficient to solve the yield crisis. Stacking and combining traits, and introducing new metabolic pathways will likely lead to greater improvements. With the development of complex metabolic modeling tools, gaining insight into which genes and pathways will be most beneficial is becoming more straightforward (Ducat and Silver, 2012). Further characterization and detailed analysis of enzyme and pathway kinetics will help build these computational tools, and enhance our ability to predict where metabolic intervention will be most helpful to increase yield (Long et al., 2015).

Another microbially-derived tool that is paving the way for enhanced expression and targeted integration of transgenes is CRISPR. The utilization of CRISPR genome editing technology is revolutionizing the field of synthetic biology and genetic engineering across all systems. The earliest and best characterized use for CRISPR in plant biology is the introduction of double strand breaks in specific target genes resulting in knockout plants. This strategy has been used in an ever expanding number of crop plants (Soda et al., 2017).

Some of these knockout targets have created plants with important phenotypes, such as powdery mildew resistant wheat (Wang et al., 2014) and switchgrass with increased biomass (Liu et al., 2017). One of the most exciting applications of CRISPR is controlling the integration of a transgene to a particular locus on the genome (Puchta, 2017). Targeted integration could enhance transgene expression and reduce the risks of disruption of other genes (Yin et al., 2017). While only few examples of using CRISPR to introduce transgenes exist currently, as this method is optimized, it will become an invaluable tool moving forward (J. Li et al., 2016; Svitashev et al., 2015).

References

Abebe, T., Guenzi, A.C., Martin, B., Cushman, J.C., 2003. Tolerance of mannitol-accumulating transgenic wheat to water stress and salinity. Plant Physiol. 131, 1748–1755.

Ahmad, R., Kim, M.D., Back, K.-H., Kim, H.-S., Lee, H.-S., Kwon, S.-Y., Murata, N., Chung, W.-I., Kwak, S.-S., 2008. Stress-induced expression of choline oxidase in potato plant chloroplasts confers enhanced tolerance to oxidative, salt, and drought stresses. Plant Cell Rep. 27, 687–698.

Ahmad, R., Kim, Y.-H., Kim, M.-D., Kwon, S.-Y., Cho, K., Lee, H.-S., Kwak, S.-S., 2010. Simultaneous expression of choline oxidase, superoxide dismutase and ascorbate peroxidase in potato plant chloroplasts provides synergistically enhanced protection against various abiotic stresses. Physiol. Plant. 138, 520–533.

Ahuja, I., De Vos, R.C.H., Bones, A.M., Hall, R.D., 2010. Plant molecular stress responses face climate change. Trends Plant Sci. 15, 664–674.

Al-Taweel, K., Iwaki, T., Yabuta, Y., Shigeoka, S., Murata, N., Wadano, A., 2007. A Bacterial Transgene for Catalase Protects Translation of D1 Protein during Exposure of Salt-Stressed Tobacco Leaves to Strong Light. Plant Physiol. 145, 258–265.

Alia, H., Hayashi, H., Chen, T.H.H., Murata, N., 1998. Transformation with a gene for choline oxidase enhances the cold tolerance of *Arabidopsis* during germination and early growth. Plant. Cell Environ. 21, 232–239.

Alia, Kondo, Y., Sakamoto, A., Nonaka, H., Hayashi, H., Saradhi, P.P., Chen, T.H., Murata, N., 1999. Enhanced tolerance to light stress of transgenic *Arabidopsis* plants that express the *codA* gene for a bacterial choline oxidase. Plant Mol. Biol. 40, 279–288.

Allen, R.S., Tilbrook, K., Warden, A.C., Campbell, P.C., Rolland, V., Singh, S.P., Wood, C.C., 2017. Expression of 16 Nitrogenase Proteins within the Plant Mitochondrial Matrix. Front. Plant Sci. 8, 287.

Aono, M., Kubo, A., Saji, H., Tanaka, K., Kondo, N., 1993. Enhanced Tolerance to Photooxidative Stress of Transgenic *Nicotiana tabacum* with High Chloroplastic Glutathione Reductase Activity. Plant Cell Physiol. 34, 129–135.

Apel, K., Hirt, H., 2004. REACTIVE OXYGEN SPECIES: Metabolism, Oxidative Stress, and Signal Transduction. Annu. Rev. Plant Biol. 55, 373–399.

Atkinson, N.J., Urwin, P.E., 2012. The interaction of plant biotic and abiotic stresses: from genes to the field. J. Exp. Bot. 63, 3523–3544.

Bainbridge, G., Madgwick, P., Parmar, S., Mitchell, R., Paul, M., Pitts, J., Keys, A.J., Parry, M.A.J., 1995. Engineering Rubisco to change its catalytic properties. J. Exp. Bot. 46, 1269–1276.

Bar-Even, A., Noor, E., Lewis, N.E., Milo, R., 2010. Design and analysis of synthetic carbon fixation pathways. Proc. Natl. Acad. Sci. U. S. A. 107, 8889–8894.

Bela, K., Horváth, E., Gallé, Á., Szabados, L., Tari, I., Csiszár, J., 2015. Plant glutathione peroxidases: Emerging role of the antioxidant enzymes in plant development and stress responses. J. Plant Physiol. 176, 192–201.

Bellucci, M., Ederli, L., De Marchis, F., Pasqualini, S., Arcioni, S., 2004. Transformation of *Lotus corniculatus* Plants with *Escherichia coli* Asparagine Synthetase A: Effect on Nitrogen Assimilation and Plant Development. Plant Cell. Tissue Organ Cult. 78, 139–150.

Blanco, N.E., Ceccoli, R.D., Segretin, M.E., Poli, H.O., Voss, I., Melzer, M., Bravo-Almonacid, F.F., Scheibe, R., Hajirezaei, M.-R., Carrillo, N., 2011. Cyanobacterial flavodoxin complements ferredoxin deficiency in knocked-down transgenic tobacco plants. Plant J. 65, 922–935.

Bonacci, W., Teng, P.K., Afonso, B., Niederholtmeyer, H., Grob, P., Silver, P.A., Savage, D.F., 2012. Modularity of a carbon-fixing protein organelle. Proc. Natl. Acad. Sci. U. S. A. 109, 478–483.

Bonfil, D.J., Ronen-Tarazi, M., Sültemeyer, D., Lieman-Hurwitz, J., Schatz, D., Kaplan, A., 1998. A putative HCO − 3 transporter in the cyanobacterium *Synechococcus* sp. strain PCC 7942. FEBS Lett. 430, 236–240.

Carvalho, J., Madgwick, P.J., Powers, S.J., Keys, A.J., Lea, P.J., Parry, M.A., 2011. An engineered pathway for glyoxylate metabolism in tobacco plants aimed to avoid the release of ammonia in photorespiration. BMC Biotechnol. 11, 111.

Cassman, K.G., Dobermann, A., Walters, D.T., 2002. Agroecosystems, Nitrogen-use Efficiency, and Nitrogen Management. Ambio A J. Hum. Environ. 31, 132–140.

Castiglioni, P., Warner, D., Bensen, R.J., Anstrom, D.C., Harrison, J., Stoecker, M., Abad, M., Kumar, G., Salvador, S., D'Ordine, R., Navarro, S., Back, S., Fernandes, M., Targolli, J., Dasgupta, S., Bonin, C., Luethy, M.H., Heard, J.E., 2008. Bacterial RNA chaperones confer abiotic stress tolerance in plants and improved grain yield in maize under water-limited conditions. Plant Physiol. 147, 446–455.

Ceccoli, R.D., Blanco, N.E., Medina, M., Carrillo, N., 2011. Stress response of transgenic tobacco plants expressing a cyanobacterial ferredoxin in chloroplasts. Plant Mol. Biol. 76, 535–544.

Chen, T.H.H., Murata, N., 2011. Glycinebetaine protects plants against abiotic stress: mechanisms and biotechnological applications. Plant. Cell Environ. 34, 1–20.

Chen, T.H.H., Murata, N., 2002. Enhancement of tolerance of abiotic stress by metabolic engineering of betaines and other compatible solutes. Curr. Opin. Plant Biol. 5, 250–257.

Costas, A.M., White, A.K., Metcalf, W.W., 2001. Purification and characterization of a novel phosphorus-oxidizing enzyme from *Pseudomonas stutzeri* WM88. J. Biol. Chem. 276, 17429–17436.

Creissen, G., Firmin, J., Fryer, M., Kular, B., Leyland, N., Reynolds, H., Pastori, G., Wellburn, F., Baker, N., Wellburn, A., Mullineaux, P., 1999. Elevated Glutathione Biosynthetic Capacity in the Chloroplasts of Transgenic Tobacco Plants Paradoxically Causes Increased Oxidative Stress. Plant Cell Online 11, 1277–1291.

Dalal, J., Lopez, H., Vasani, N.B., Hu, Z., Swift, J.E., Yalamanchili, R., Dvora, M., Lin, X., Xie, D., Qu, R., Sederoff, H.W., 2015. A photorespiratory bypass increases plant growth and seed yield in biofuel crop *Camelina sativa*. Biotechnol. Biofuels 8, 175.

Duan, X., Song, Y., Yang, A., Zhang, J., 2009. The transgene pyramiding tobacco with betaine synthesis and heterologous expression of *AtNHX1* is more tolerant to salt stress than either of the tobacco lines with betaine synthesis or *AtNHX1*. Physiol. Plant. 135, 281–295.

Ducat, D.C., Silver, P.A., 2012. Improving carbon fixation pathways. Curr. Opin. Chem. Biol. 16, 337–344.

Empadinhas, N., da Costa, M.S., 2008. Osmoadaptation mechanisms in prokaryotes: distribution of compatible solutes. Int. Microbiol. 11, 151–161.

Erb, T.J., Zarzycki, J., 2018. A short history of RubisCO: the rise and fall (?) of Nature's predominant CO2 fixing enzyme. Curr. Opin. Biotechnol. 49, 100–107.

Evans, J.R., 2013. Improving photosynthesis. Plant Physiol. 162, 1780–1793.

Foyer, C., Lelandais, M., Galap, C., Kunert, K.J., 1991. Effects of Elevated Cytosolic Glutathione Reductase Activity on the Cellular Glutathione Pool and Photosynthesis in Leaves under Normal and Stress Conditions. Plant Physiol. 97, 863–872.

Foyer, C.H., Souriau, N., Perret, S., Lelandais, M., Kunert, K.-J., Pruvost, C., Jouanin, L., 1995. Overexpression of Glutathione Reductase but Not Glutathione Synthetase Leads to lncreases in Antioxidant Capacity and Resistance to Photoinhibition in Poplar Trees. Plant Physiol. 109, 1047–1057.

Gaber, A., Yoshimura, K., Yamamoto, T., Yabuta, Y., Takeda, T., Miyasaka, H., Nakano, Y., Shigeoka, S., 2006. Glutathione peroxidase-like protein of *Synechocystis* PCC 6803 confers tolerance to oxidative and environmental stresses in transgenic Arabidopsis. Physiol. Plant. 128, 251–262.

Gao, M., Sakamoto, A., Miura, K., Murata, N., Sugiura, A., Tao, R., 2000. Transformation of Japanese persimmon (*Diospyros kaki* Thunb.) with a bacterial gene for choline oxidase. Mol. Breed. 6, 501–510.

Garg, A.K., Kim, J.-K., Owens, T.G., Ranwala, A.P., Choi, Y.D., Kochian, L. V, Wu, R.J.,

2002. Trehalose accumulation in rice plants confers high tolerance levels to different abiotic stresses. Proc. Natl. Acad. Sci. U. S. A. 99, 15898–15903.

Geng, X.-M., Liu, X., Ji, M., Hoffmann, W.A., Grunden, A., Xiang, Q.-Y.J., 2016. Enhancing Heat Tolerance of the Little Dogwood *Cornus canadensis* L. f. with Introduction of a Superoxide Reductase Gene from the Hyperthermophilic Archaeon *Pyrococcus furiosus*. Front. Plant Sci. 7, 26.

Giannino, D., Nicolodi, C., Testone, G., Frugis, G., Pace, E., Santamaria, P., Guardasole, M., Mariotti, D., 2008. The overexpression of asparagine synthetase A from *E. coli* affects the nitrogen status in leaves of lettuce (*Lactuca sativa* L.) and enhances vegetative growth. Euphytica 162, 11–22.

Gill, S.S., Anjum, N.A., Hasanuzzaman, M., Gill, R., Trivedi, D.K., Ahmad, I., Pereira, E., Tuteja, N., 2013. Glutathione and glutathione reductase: A boon in disguise for plant abiotic stress defense operations. Plant Physiol. Biochem. 70, 204–212.

Gill, S.S., Tuteja, N., 2010. Reactive oxygen species and antioxidant machinery in abiotic stress tolerance in crop plants. Plant Physiol. Biochem. 48, 909–930.

Goddijn, O.J.M., Verwoerd, T.C., Voogd, E., Krutwagen, R.W.H.H., De Graaf, P.T.H.M., Poels, J., Van Dun, K., Ponstein, A.S., Damm, B., Pen, J., 1997. Inhibition of Trehalase Activity Enhances Trehalose Accumulation in Transgenic Plants. Plant Physiol. 113, 181–190.

Goel, D., Singh, A.K., Yadav, V., Babbar, S.B., Murata, N., Bansal, K.C., 2011. Transformation of tomato with a bacterial *codA* gene enhances tolerance to salt and water stresses. J. Plant Physiol. 168, 1286–1294.

Gong, H.Y., Li, Y., Fang, G., Hu, D.H., Jin, W.B., Wang, Z.H., Li, Y.S., 2015. Transgenic Rice Expressing Ictb and FBP/Sbpase Derived from Cyanobacteria Exhibits Enhanced Photosynthesis and Mesophyll Conductance to CO2. PLoS One 10, e0140928.

Grunden, A.M., Jenney, F.E., Ma, K., Ji, M., Weinberg, M. V, Adams, M.W.W., 2005. In vitro reconstitution of an NADPH-dependent superoxide reduction pathway from *Pyrococcus furiosus*. Appl. Environ. Microbiol. 71, 1522–1530.

Gullner, G., Kömives, T., Rennenberg, H., 2001. Enhanced tolerance of transgenic poplar plants overexpressing γ□glutamylcysteine synthetase towards chloroacetanilide herbicides. J. Exp. Bot. 52, 971–979.

Halliwell, B., 2006. Reactive Species and Antioxidants. Redox Biology Is a Fundamental Theme of Aerobic Life. Plant Physiol. 141, 312–322.

Harrison, E.P., Olcer, H., Lloyd, J.C., Long, S.P., Raines, C.A., 2001. Small decreases in SBPase cause a linear decline in the apparent RuBP regeneration rate, but do not affect Rubisco carboxylation capacity. J. Exp. Bot. 52, 1779–1784.

Hay, W.T., Bihmidine, S., Mutlu, N., Hoang, K.L., Awada, T., Weeks, D.P., Clemente, T., Long, S.P., 2017. Enhancing soybean photosynthetic CO_2 assimilation using a cyanobacterial membrane protein, ictB. J. Plant Physiol. 212, 56–68.

Hayashi, H., Alia, L., Mustardy, L., Deshnium, P., Ida, M., Murata, N., 1997. Transformation of *Arabidopsis thaliana* with the *codA* gene for choline oxidase; accumulation of glycinebetaine and enhanced tolerance to salt and cold stress. Plant J. 12, 133–142.

Hayashi, H., Alia, Sakamoto, A., Nonaka, H., Chen, T.H.H., Murata, N., 1998. Enhanced germination under high-salt conditions of seeds of transgenic *Arabidopsis* with a bacterial gene (*codA*) for choline oxidase. J. Plant Res. 111, 357–362.

He, C., Zhang, W., Gao, Q., Yang, A., Hu, X., Zhang, J., 2011. Enhancement of drought resistance and biomass by increasing the amount of glycine betaine in wheat seedlings. Euphytica 177, 151–167.

He, J., Li, H., Ma, C., Zhang, Y., Polle, A., Rennenberg, H., Cheng, X., Luo, Z.-B., 2015. Overexpression of bacterial γ-glutamylcysteine synthetase mediates changes in cadmium influx, allocation and detoxification in poplar. New Phytol. 205, 240–254.

Herschbach, C., Jouanin, L., Rennenberg, H., 1998. Overexpression of 7-Glutamylcysteine Synthetase, but not of Glutathione Synthetase, Elevates Glutathione Allocation in the Phloem of Transgenic Poplar Trees. Plant Cell Physiol. 39, 447–451.

Heuer, S., Gaxiola, R., Schilling, R., Herrera-Estrella, L., López-Arredondo, D., Wissuwa, M., Delhaize, E., Rouached, H., 2016. Improving phosphorus use efficiency - a complex trait with emerging opportunities. Plant J. 90, 868–885.

Hibino, T., Kaku, N., Yoshikawa, H., Takabe, T., Takabe, T., 1999. Molecular characterization of DnaK from the halotolerant cyanobacterium *Aphanothece halophytica* for ATPase, protein folding, and copper binding under various salinity conditions. Plant Mol. Biol. 40, 409–418.

Hinsinger, P., 2001. Bioavailability of soil inorganic P in the rhizosphere as affected by root-induced chemical changes: a review. Plant Soil 237, 173–195.

Holmström, K.-O., Somersalo, S., Mandal, A., Palva, T.E., Welin, B., 2000. Improved tolerance to salinity and low temperature in transgenic tobacco producing glycine betaine. J. Exp. Bot. 51, 177–185.

Hu, L., Lu, H., Liu, Q., Chen, X., Jiang, X., 2005. Overexpression of *mtlD* gene in transgenic *Populus tomentosa* improves salt tolerance through accumulation of mannitol. Tree Physiol. 25, 1273–1281.

Ikuta, S., Imamura, S., Misaki, H., Horiuti, Y., 1977. Purification and characterization of choline oxidase from *Arthrobacter globiformis*. J. Biochem. 82, 1741–1749.

Im, Y.J., Ji, M., Lee, A., Killens, R., Grunden, A.M., Boss, W.F., 2009. Expression of

Pyrococcus furiosus superoxide reductase in *Arabidopsis* enhances heat tolerance. Plant Physiol. 151, 893–904.

Im, Y.J., Ji, M., Lee, A.M., Boss, W.F., Grunden, A.M., 2005. Production of a thermostable archaeal superoxide reductase in plant cells. FEBS Lett. 579, 5521–5526.

Iordachescu, M., Imai, R., 2008. Trehalose Biosynthesis in Response to Abiotic Stresses. J. Integr. Plant Biol. 50, 1223–1229.

Ivleva, N.B., Groat, J., Staub, J.M., Stephens, M., 2016. Expression of active subunit of nitrogenase via integration into plant organelle genome. PLoS One 11, e0160951.

Jacob, P., Hirt, H., Bendahmane, A., 2017. The heat-shock protein/chaperone network and multiple stress resistance. Plant Biotechnol. J. 15, 405–414.

Jang, I.-C., Oh, S.-J., Seo, J.-S., Choi, W.-B., Song, S.I., Kim, C.H., Kim, Y.S., Seo, H.-S., Choi, Y.D., Nahm, B.H., Kim, J.-K., 2003. Expression of a bifunctional fusion of the *Escherichia coli* genes for trehalose-6-phosphate synthase and trehalose-6-phosphate phosphatase in transgenic rice plants increases trehalose accumulation and abiotic stress tolerance without stunting growth. Plant Physiol. 131, 516–524.

Jenney, F.E., Verhagen, M.F., Cui, X., Adams, M.W., 1999. Anaerobic microbes: oxygen detoxification without superoxide dismutase. Science. 286, 306–309.

Kanevski, I., Maliga, P., Rhoades, D.F., Gutteridge, S., 1999. Plastome engineering of ribulose-1,5-bisphosphate carboxylase/oxygenase in tobacco to form a sunflower large subunit and tobacco small subunit hybrid. Plant Physiol. 119, 133–142.

Karakas, B., Ozias-Akins, P., Stushnoff, C., Suefferheld, M., Rieger, M., 1997. Salinity and drought tolerance of mannitol-accumulating transgenic tobacco. Plant. Cell Environ. 20, 609–616.

Karlusich, J.J.P., Lodeyro, A.F., Carrillo, N., 2014. The long goodbye: the rise and fall of flavodoxin during plant evolution. J. Exp. Bot. 65, 5161–5178.

Kebeish, R., Niessen, M., Thiruveedhi, K., Bari, R., Hirsch, H.-J., Rosenkranz, R., Stäbler, N., Schönfeld, B., Kreuzaler, F., Peterhänsel, C., 2007. Chloroplastic photorespiratory bypass increases photosynthesis and biomass production in *Arabidopsis* thaliana. Nat. Biotechnol. 25, 593–599.

Klahn, S., Marquardt, D.M., Rollwitz, I., Hagemann, M., 2009. Expression of the *ggpPS* gene for glucosylglycerol biosynthesis from *Azotobacter vinelandii* improves the salt tolerance of *Arabidopsis thaliana*. J. Exp. Bot. 60, 1679–1689.

Köhler, I.H., Ruiz-Vera, U.M., VanLoocke, A., Thomey, M.L., Clemente, T., Long, S.P., Ort, D.R., Bernacchi, C.J., 2016. Expression of cyanobacterial FBP/SBPase in soybean prevents yield depression under future climate conditions. J. Exp. Bot. 61, 715–726.

Konstantinova, T., Parvanova, D., Atanassov, A., Djilianov, D., 2002. Freezing tolerant tobacco, transformed to accumulate osmoprotectants. Plant Sci. 163, 157–164.

Le Martret, B., Poage, M., Shiel, K., Nugent, G.D., Dix, P.J., 2011. Tobacco chloroplast transformants expressing genes encoding dehydroascorbate reductase, glutathione reductase, and glutathione-S-transferase, exhibit altered anti-oxidant metabolism and improved abiotic stress tolerance. Plant Biotechnol. J. 9, 661–673.

Li, J., Meng, X., Zong, Y., Chen, K., Zhang, H., Liu, J., Li, J., Gao, C., 2016. Gene replacements and insertions in rice by intron targeting using CRISPR–Cas9. Nat. Plants 2, 16139.

Li, S., Li, F., Wang, J., Zhang, W., Meng, Q., Chen, T.H.H., Murata, N., Yang, X., 2011. Glycinebetaine enhances the tolerance of tomato plants to high temperature during germination of seeds and growth of seedlings. Plant. Cell Environ. 34, 1931–1943.

Li, Z., Yuan, S., Jia, H., Gao, F., Zhou, M., Yuan, N., Wu, P., Hu, Q., Sun, D., Luo, H., 2016. Ectopic expression of a cyanobacterial flavodoxin in creeping bentgrass impacts plant development and confers broad abiotic stress tolerance. Plant Biotechnol. J. 15, 433–446.

Liedschulte, V., Wachter, A., Zhigang, A., Rausch, T., 2010. Exploiting plants for glutathione (GSH) production: Uncoupling GSH synthesis from cellular controls results in unprecedented GSH accumulation. Plant Biotechnol. J. 8, 807–820.

Lieman-Hurwitz, J., Rachmilevitch, S., Mittler, R., Marcus, Y., Kaplan, A., 2003. Enhanced photosynthesis and growth of transgenic plants that express *ictB* , a gene involved in HCO_3^- accumulation in cyanobacteria. Plant Biotechnol. J. 1, 43–50.

Lin, M.T., Occhialini, A., Andralojc, P.J., Devonshire, J., Hines, K.M., Parry, M.A.J., Hanson, M.R., 2014a. β-Carboxysomal proteins assemble into highly organized structures in *Nicotiana* chloroplasts. Plant J. 79, 1–12.

Lin, M.T., Occhialini, A., Andralojc, P.J., Parry, M.A.J., Hanson, M.R., 2014b. A faster Rubisco with potential to increase photosynthesis in crops. Nature 513, 547–550.

Liu, Y., Merrick, P., Zhang, Z., Ji, C., Yang, B., Fei, S., 2017. Targeted mutagenesis in tetraploid switchgrass (*Panicum virgatum* L.) using CRISPR/Cas9. Plant Biotechnol. J. 1–13.

Long, B.M., Rae, B.D., Rolland, V., Förster, B., Price, G.D., 2016. Cyanobacterial CO_2 - concentrating mechanism components: function and prospects for plant metabolic engineering. Curr. Opin. Plant Biol. 31, 1–8.

Long, S.P., Marshall-Colon, A., Zhu, X.-G., 2015. Meeting the Global Food Demand of the Future by Engineering Crop Photosynthesis and Yield Potential. Cell 161, 56–66.

López-Arredondo, D., González-Morales, S.I., Bello-Bello, E., Alejo-Jacuinde, G., Herrera,

L., 2015. Engineering food crops to grow in harsh environments. F1000Research 4, 651.

López-Arredondo, D.L., Herrera-Estrella, L., 2012. Engineering phosphorus metabolism in plants to produce a dual fertilization and weed control system. Nat. Biotechnol. 30, 889–893.

López-Arredondo, D.L., Leyva-González, M.A., González-Morales, S.I., López-Bucio, J., Herrera-Estrella, L., 2014. Phosphate Nutrition: Improving Low-Phosphate Tolerance in Crops. Annu. Rev. Plant Biol. 65, 95–123.

Lv, S., Yang, A., Zhang, K., Wang, L., Zhang, J., 2007. Increase of glycinebetaine synthesis improves drought tolerance in cotton. Mol. Breed. 20, 233–248.

Marco, F., Bitrián, M., Carrasco, P., Rajam, M.V., Alcázar, R., Tiburcio, A.F., 2015. Genetic Engineering Strategies for Abiotic Stress Tolerance in Plants, in: Plant Biology and Biotechnology. Springer India, New Delhi, pp. 579–609.

Martínez-Andújar, C., Ghanem, M.E., Albacete, A., Pérez-Alfocea, F., 2013. Response to nitrate/ammonium nutrition of tomato (*Solanum lycopersicum* L.) plants overexpressing a prokaryotic NH4+-dependent asparagine synthetase. J. Plant Physiol. 170, 676–687.

Mcallister, C.H., Beatty, P.H., Good, A.G., 2012. Engineering nitrogen use efficient crop plants: The current status. Plant Biotechnol. J. 10, 1011–1025.

McGrath, J.M., Long, S.P., 2014. Can the cyanobacterial carbon-concentrating mechanism increase photosynthesis in crop species? A theoretical analysis. Plant Physiol. 164, 2247–2261.

Medrano, H., Keys, A.J., Lawlor, D.W., Parry, M.A.J., Azcon-Bieto, J., Delgado, E., 1995. Improving plant production by selection for survival at low CO_2 concentrations. J. Exp. Bot. 46, 1389–1396.

Melchiorre, M., Robert, G., Trippi, V., Racca, R., Lascano, H.R., 2009. Superoxide dismutase and glutathione reductase overexpression in wheat protoplast: photooxidative stress tolerance and changes in cellular redox state. Plant Growth Regul. 57, 57–68.

Merrick, M., Dixon, R., 1984. Why don't plants fix nitrogen? Trends Biotechnol. 2, 162–166.

Mickelbart, M. V., Hasegawa, P.M., Bailey-Serres, J., 2015. Genetic mechanisms of abiotic stress tolerance that translate to crop yield stability. Nat. Rev. Genet. 16, 237–251.

Miyagawa, Y., Tamoi, M., Shigeoka, S., 2001. Overexpression of a cyanobacterial fructose-1,6-/sedoheptulose-1,7-bisphosphatase in tobacco enhances photosynthesis and growth. Nat. Biotechnol. 19, 965–969.

Miyagawa, Y., Tamoi, M., Shigeoka, S., 2000. Evaluation of the Defense System in Chloroplasts to Photooxidative Stress Caused by Paraquat Using Transgenic Tobacco

Plants Expressing Catalase from Escherichia coli. Plant Cell Physiol. 41, 311–320.

Miyake, C., 2010. Alternative Electron Flows (Water–Water Cycle and Cyclic Electron Flow Around PSI) in Photosynthesis: Molecular Mechanisms and Physiological Functions. Plant Cell Physiol. 51, 1951–1963.

Moghaieb, R.E.A., Nakamura, A., Saneoka, H., Fujita, K., 2017. GM Crops Evaluation of salt tolerance in ectoine-transgenic tomato plants (*Lycopersicon esculentum*) in terms of photosynthesis, osmotic adjustment, and carbon partitioning. GM Crops 2, 58–65.

Moghaieb, R.E.A., Tanaka, N., Saneoka, H., Murooka, Y., Ono, H., Morikawa, H., Nakamura, A., Nguyen, N.T., Suwa, R., Fujita, K., 2006. Characterization of salt tolerance in ectoine-transformed tobacco plants (*Nicotiana tabaccum*): photosynthesis, osmotic adjustment, and nitrogen partitioning. Plant. Cell Environ. 29, 173–182.

Mohamed, E.-A., Iwaki, T., Munir, I., Tamoi, M., Shigeoka, S., Wadano, A., 2003. Overexpression of bacterial catalase in tomato leaf chloroplasts enhances photo-oxidative stress tolerance. Plant. Cell Environ. 26, 2037–2046.

Mohanty, A., Kathuria, H., Ferjani, A., Sakamoto, A., Mohanty, P., Murata, N., Tyagi, A., 2002. Transgenics of an elite indica rice variety Pusa Basmati 1 harbouring the codA gene are highly tolerant to salt stress. Theor. Appl. Genet. 106, 51–57.

Moriwaki, T., Yamamoto, Y., Aida, T., Funahashi, T., Shishido, T., Asada, M., Prodhan, S.H., Komamine, A., Motohashi, T., 2008. Overexpression of the *Escherichia coli* catalase gene, *katE*, enhances tolerance to salinity stress in the transgenic indica rice cultivar, BR5. Plant Biotechnol. Rep. 2, 41–46.

Nagamiya, K., Motohashi, T., Nakao, K., Prodhan, S.H., Hattori, E., Hirose, S., Ozawa, K., Ohkawa, Y., Takabe, T., Takabe, T., Komamine, A., 2007. Enhancement of salt tolerance in transgenic rice expressing an *Escherichia coli* catalase gene, *katE*. Plant Biotechnol. Rep. 1, 49–55.

Nakayama, H., Yoshida, K., Ono, H., Murooka, Y., Shinmyo, A., 2000. Ectoine, the Compatible Solute of *Halomonas elongata*, Confers Hyperosmotic Tolerance in Cultured Tobacco Cells. Plant Physiol. 122, 1239–1247.

Noctor, G., Arisi, A.-C.M., Jouanin, L., Foyer, C.H., 1998. Manipulation of Glutathione and Amino Acid Biosynthesis in the Chloroplast. Plant Physiol. 118, 471–482.

Noctor, G., Mhamdi, A., Chaouch, S., Han, Y., Neukermans, J., Marquez-Garcia, B., Queval, G., Foyer, C.H., 2012. Glutathione in plants: an integrated overview. Plant. Cell Environ. 35, 454–484.

Noctor, G., Strohm, M., Jouanin, L., Kunert, K.-J., Foyer, C.H., Rennenberg, H., 1996. Synthesis of Glutathione in Leaves of Transgenic Poplar Overexpressing y-Glutamylcysteine Synthetase. Plant Physiol. 112, 1071–1078.

Nolke, G., Houdelet, M., Kreuzaler, F., Peterhansel, C., Schillberg, S., 2014. The expression of a recombinant glycolate dehydrogenase polyprotein in potato (*Solanum tuberosum*) plastids strongly enhances photosynthesis and tuber yield. Plant Biotechnol. J. 12, 734–742.

Occhialini, A., Lin, M.T., Andralojc, P.J., Hanson, M.R., Parry, M.A.J., 2016. Transgenic tobacco plants with improved cyanobacterial Rubisco expression but no extra assembly factors grow at near wild-type rates if provided with elevated CO2. Plant J. 85, 148–160.

Ogren, W.L., 1984. Photorespiration: Pathways, Regulation, and Modification. Annu. Rev. Plant Physiol. 35, 415–442.

Oldroyd, G.E., Dixon, R., 2014. Biotechnological solutions to the nitrogen problem. Curr. Opin. Biotechnol. 26, 19–24.

Ono, K., Hibino, T., Kohinata, T., Suzuki, S., Tanaka, Y., Nakamura, T., Takabe, T., Takabe, T., 2001. Overexpression of DnaK from a halotolerant cyanobacterium *Aphanothece halophytica* enhances the high-temperatue tolerance of tobacco during germination and early growth. Plant Sci. 160, 455–461.

Park, E.-J., Jeknic, Z., Pino, M.-T., Norio, M., Chen, T.H.-H., 2007. Glycinebetaine accumulation is more effective in chloroplasts than in the cytosol for protecting transgenic tomato plants against abiotic stress. Plant. Cell Environ. 30, 994–1005.

Park, E.-J., Jeknić, Z., Sakamoto, A., DeNoma, J., Yuwansiri, R., Murata, N., Chen, T.H.H., 2004. Genetic engineering of glycinebetaine synthesis in tomato protects seeds, plants, and flowers from chilling damage. Plant J. 40, 474–487.

Pellny, T.K., Ghannoum, O., Conroy, J.P., Schluepmann, H., Smeekens, S., Andralojc, J., Krause, K.P., Goddijn, O., Paul, M.J., 2004. Genetic modification of photosynthesis with *E. coli* genes for trehalose synthesis. Plant Biotechnol. J. 2, 71–82.

Pengelly, J.J.L., Förster, B., von Caemmerer, S., Badger, M.R., Price, G.D., Whitney, S.M., 2014. Transplastomic integration of a cyanobacterial bicarbonate transporter into tobacco chloroplasts. J. Exp. Bot. 65, 3071–3080.

Peterhansel, C., Maurino, V.G., 2011. Photorespiration Redesigned. Plant Physiol. 155, 49–55.

Pilon-Smits, E.A.H., Terry, N., Sears, T., Kim, H., Zayed, A., Hwang, S., van Dun, K., Voogd, E., Verwoerd, T.C., Krutwagen, R.W.H.H., Goddijn, O.J.M., 1998. Trehalose-producing transgenic tobacco plants show improved growth performance under drought stress. J. Plant Physiol. 152, 525–532.

Prabhavathi, V., Yadav, J.S., Kumar, P.A., Rajam, M.V., 2002. Abiotic stress tolerance in transgenic eggplant (*Solanum melongena* L.) by introduction of bacterial mannitol phosphodehydrogenase gene. Mol. Breed. 9, 137–147.

Prasad, K.V.S.K., Sharmila, P., Kumar, P.A., Saradhi, P.P., 2000. Transformation of *Brassica juncea* (L.) Czern with bacterial *codA* gene enhances its tolerance to salt stress. Mol. Breed. 6, 489–499.

Price, G.D., Badger, M.R., von Caemmerer, S., 2011. The Prospect of Using Cyanobacterial Bicarbonate Transporters to Improve Leaf Photosynthesis in C3 Crop Plants. Plant Physiol. 155, 20–26.

Puchta, H., 2017. Applying CRISPR/Cas for genome engineering in plants: the best is yet to come. Curr. Opin. Plant Biol. 36, 1–8.

Pujni, D., Chaudhary, A., Rajam, M. V., 2007. Increased Tolerance to Salinity and Drought in Transgenic Indica Rice by Mannitol Accumulation. J. Plant Biochem. Biotechnol. 16, 1–7.

Quan, R., Shang, M., Zhang, H., Zhao, Y., Zhang, J., 2004a. Improved chilling tolerance by transformation with *betA* gene for the enhancement of glycinebetaine synthesis in maize. Plant Sci. 166, 141–149.

Quan, R., Shang, M., Zhang, H., Zhao, Y., Zhang, J., 2004b. Engineering of enhanced glycine betaine synthesis improves drought tolerance in maize. Plant Biotechnol. J. 2, 477–486.

Rae, B.D., Long, B.M., Förster, B., Nguyen, N.D., Velanis, C.N., Atkinson, N., Hee, W.Y., Mukherjee, B., Price, G.D., McCormick, A.J., 2017. Progress and challenges of engineering a biophysical CO_2-concentrating mechanism into higher plants. J. Exp. Bot. 68, 3717–3737.

Rai, M., Pal, M., Sumesh, K.V., Jain, V., Sankaranarayanan, A., 2006. Engineering for biosynthesis of ectoine (2-methyl 4-carboxy tetrahydro pyrimidine) in tobacco chloroplasts leads to accumulation of ectoine and enhanced salinity tolerance. Plant Sci. 170, 291–306.

Reguera, M., Peleg, Z., Blumwald, E., 2012. Targeting metabolic pathways for genetic engineering abiotic stress-tolerance in crops. Biochim. Biophys. Acta 1819, 186–194.

Reisinger, S., Schiavon, M., Terry, N., Pilon-Smits, E.A.H., 2008. Heavy Metal Tolerance and Accumulation in Indian Mustard (*Brassica Juncea* L.) Expressing Bacterial γ-Glutamylcysteine Synthetase or Glutathione Synthetase. Int. J. Phytoremediation 10, 440–454.

Rhodes, D., Hanson, A.D., 1993. Quaternary Ammonium and Tertiary Sulfonium Compounds in Higher Plants. Annu. Rev. Plant Physiol. Plant Mol. Biol. 44, 357–384.

Rolland, V., Badger, M.R., Price, G.D., 2016. Redirecting the Cyanobacterial Bicarbonate Transporters BicA and SbtA to the Chloroplast Envelope: Soluble and Membrane Cargos Need Different Chloroplast Targeting Signals in Plants. Front. Plant Sci. 7, 185.

Sakamoto, A., Alia, Murata, N., Murata, A., 1998. Metabolic engineering of rice leading to biosynthesis of glycinebetaine and tolerance to salt and cold. Plant Mol. Biol. 38, 1011–1019.

Schroeder, J.I., Delhaize, E., Frommer, W.B., Guerinot, M. Lou, Harrison, M.J., Herrera-Estrella, L., Horie, T., Kochian, L. V, Munns, R., Nishizawa, N.K., Tsay, Y.-F., Sanders, D., 2013. Using membrane transporters to improve crops for sustainable food production. Nature 497, 60–66.

Schwander, T., Schada von Borzyskowski, L., Burgener, S., Cortina, N.S., Erb, T.J., 2016. A synthetic pathway for the fixation of carbon dioxide in vitro. Science. 354, 900–904.

Seiffert, B., Zhou, Z., Wallbraun, M., Lohaus, G., Mollers, C., 2004. Expression of a bacterial asparagine synthetase gene in oilseed rape (*Brassica napus*) and its effect on traits related to nitrogen efficiency. Physiol. Plant. 121, 656–665.

Shih, P.M., Occhialini, A., Cameron, J.C., Andralojc, P.J., Parry, M.A.J., Kerfeld, C.A., 2016. Biochemical characterization of predicted Precambrian RuBisCO. Nat. Commun. 7, 10382.

Shikanai, T., Takeda, T., Yamauchi, H., Sano, S., Tomizawa, K.-I., Yokota, A., Shigeoka, S., 1998. Inhibition of ascorbate peroxidase under oxidative stress in tobacco having bacterial catalase in chloroplasts. FEBS Lett. 428, 47–51.

Sievers, N., Muders, K., Henneberg, M., Klähn, S., Effmert, M., Junghans, H., Hagemann, M., 2013. Establishing glucosylglycerol synthesis in potato (*Solanum tuberosum* l. cv. Albatros) by expression of the *ggpPS* gene from *Azotobacter vinelandii*. J. Plant Sci. Mol. Breed. 2.

Smith, V.H., Schindler, D.W., 2009. Eutrophication science: where do we go from here? Trends Ecol. Evol. 24, 201–207.

Sobolev, A.P., Testone, G., Santoro, F., Nicolodi, C., Iannelli, M.A., Amato, M.E., Ianniello, A., Brosio, E., Giannino, D., Mannina, L., 2010. Quality Traits of Conventional and Transgenic Lettuce (*Lactuca sativa* L.) at Harvesting by NMR Metabolic Profiling. J. Agric. Food Chem. 58, 6928–6936.

Soda, N., Verma, L., Giri, J., 2017. CRISPR/Cas9 based plant genome editing: Significance, opportunities and recent advances. Plant Physiol. Biochem. in press.

Somerville, C.R., 2001. An Early *Arabidopsis* Demonstration. Resolving a Few Issues Concerning Photorespiration. Plant Physiol. 125, 20–24.

Strohm, M., Jouanin, L., Kunert, K.J., Pruvost, C., Polle, A., Foyer, C.H., Rennenberg, H., 1995. Regulation of glutathione synthesis in leaves of transgenic poplar (*Populus tremula* X P. alba) overexpressing glutathione synthetase. Plant J. 7, 141–145.

Sugino, M., Hibino, T., Tanaka, Y., Nii, N., Takabe, T., Takabe, T., 1999. Overexpression of

DnaK from a halotolerant cyanobacterium *Aphanothece halophytica* acquires resistance to salt stress in transgenic tobacco plants. Plant Sci. 146, 81–88.

Sulpice, R., Tsukaya, H., Nonaka, H., Mustardy, L., Chen, T.H.H., Murata, N., 2003. Enhanced formation of flowers in salt-stressed *Arabidopsis* after genetic engineering of the synthesis of glycine betaine. Plant J. 36, 165–176.

Suzuki, N., Koussevitzky, S., Mittler, R., Miller, G., 2012. ROS and redox signalling in the response of plants to abiotic stress. Plant. Cell Environ. 35, 259–270.

Svitashev, S., Young, J.K., Schwartz, C., Gao, H., Falco, S.C., Cigan, A.M., 2015. Targeted Mutagenesis, Precise Gene Editing, and Site-Specific Gene Insertion in Maize Using Cas9 and Guide RNA. Plant Physiol. 169, 931–945.

Tamoi, M., Nagaoka, M., Miyagawa, Y., Shigeoka, S., 2006. Contribution of Fructose-1,6-bisphosphatase and Sedoheptulose-1,7-bisphosphatase to the Photosynthetic Rate and Carbon Flow in the Calvin Cycle in Transgenic Plants. Plant Cell Physiol. 47, 380–390.

Tarczynski, M.C., Jensen, R.G., Bohnert, H.J., 1992. Expression of a bacterial *mtlD* gene in transgenic tobacco leads to production and accumulation of mannitol. Proc. Natl. Acad. Sci. U. S. A. 89, 2600–2604.

Tcherkez, G.G.B., Farquhar, G.D., Andrews, T.J., Lorimer, G.H., 2006. Despite slow catalysis and confused substrate specificity, all ribulose bisphosphate carboxylases may be nearly perfectly optimized. Proc. Natl. Acad. Sci. U. S. A. 103, 7246–7251.

Thomas, J.C., Sepahi, M., B., A., Bohnert, H.J., 1995. Enhancement of seed germination in high salinity by engineering mannitol expression in *Arabidopsis thaliana*. Plant. Cell Environ. 18, 801–806.

Tilman, D., Balzer, C., Hill, J., Befort, B.L., 2011. Global food demand and the sustainable intensification of agriculture. Proc. Natl. Acad. Sci. U. S. A. 108, 20260–20264.

Tognetti, V.B., Palatnik, J.F., Fillat, M.F., Melzer, M., Hajirezaei, M.-R., Valle, E.M., Carrillo, N., 2006. Functional replacement of ferredoxin by a cyanobacterial flavodoxin in tobacco confers broad-range stress tolerance. Plant Cell 18, 2035–2050.

Tognetti, V.B., Zurbriggen, M.D., Morandi, E.N., Fillat, M.F., Valle, E.M., Hajirezaei, M.-R., Carrillo, N., 2007. Enhanced plant tolerance to iron starvation by functional substitution of chloroplast ferredoxin with a bacterial flavodoxin. Proc. Natl. Acad. Sci. U. S. A. 104, 11495–11500.

Uchida, A., Hibino, T., Shimada, T., Saigusa, M., Takabe, T., Araki, E., Kajita, H., Takabe, T., 2008. Overexpression of DnaK chaperone from a halotolerant cyanobacterium *Aphanothece halophytica* increases seed yield in rice and tobacco. Plant Biotechnol. 25, 141–150.

Uehara, S., Adachi, F., Ito-Inaba, Y., Inaba, T., 2016. Specific and Efficient Targeting of

Cyanobacterial Bicarbonate Transporters to the Inner Envelope Membrane of Chloroplasts in *Arabidopsis*. Front. Plant Sci. 7.

Wang, Y., Cheng, X., Shan, Q., Zhang, Y., Liu, J., Gao, C., Qiu, J.-L., 2014. Simultaneous editing of three homoeoalleles in hexaploid bread wheat confers heritable resistance to powdery mildew. Nat. Biotechnol. 32, 947–951.

Wei, A., He, C., Li, B., Li, N., Zhang, J., 2011. The pyramid of transgenes TsVP and BetA effectively enhances the drought tolerance of maize plants. Plant Biotechnol. J. 9, 216–229.

Whitney, S.M., Andrews, T.J., 2001. Plastome-encoded bacterial ribulose-1,5-bisphosphate carboxylase/oxygenase (RubisCO) supports photosynthesis and growth in tobacco. Proc. Natl. Acad. Sci. U. S. A. 98, 14738–14743.

Whitney, S.M., Houtz, R.L., Alonso, H., 2011. Advancing Our Understanding and Capacity to Engineer Nature's CO2-Sequestering Enzyme, Rubisco. Plant Physiol. 155, 27–35.

Wu, L., Fan, Z., Guo, L., Li, Y., Chen, Z.-L., Qu, L.-J., 2005. Over-expression of the bacterial *nhaA* gene in rice enhances salt and drought tolerance. Plant Sci. 168, 297–302.

Xin, C.-P., Tholen, D., Devloo, V., Zhu, X.-G., 2015. The Benefits of Photorespiratory Bypasses: How Can They Work? Plant Physiol. 167, 574–585.

Yin, K., Gao, C., Qiu, J.-L., 2017. Progress and prospects in plant genome editing. Nat. Plants 3, 17107.

Zhang, K., Wang, J., Lian, L., Fan, W., Guo, N., Lv, S., 2012. Increased Chilling Tolerance Following Transfer of a betA Gene Enhancing Glycinebetaine Synthesis in Cotton (*Gossypium hirsutum* L.). Plant Mol. Biol. Report. 30, 1158–1171.

Zhu, G., Spreitzer, R.J., 1996. Directed mutagenesis of chloroplast ribulose-1,5-bisphosphate carboxylase/oxygenase. Loop 6 substitutions complement for structural stability but decrease catalytic efficiency. J. Biol. Chem. 271, 18494–18498.

Zhu, X.-G., De Sturler, E., Long, S.P., 2007. Optimizing the Distribution of Resources between Enzymes of Carbon Metabolism Can Dramatically Increase Photosynthetic Rate: A Numerical Simulation Using an Evolutionary Algorithm. Plant Physiol. 145, 513–526.

Zhu, X.-G., Long, S.P., Ort, D.R., 2010. Improving Photosynthetic Efficiency for Greater Yield. Annu. Rev. Plant Biol. 61, 235–261.

Zhu, Y.L., Pilon-Smits, E.A., Tarun, A.S., Weber, S.U., Jouanin, L., Terry, N., 1999. Cadmium tolerance and accumulation in Indian mustard is enhanced by overexpressing gamma-glutamylcysteine synthetase. Plant Physiol. 121, 1169–1178.

Zhu, Y.L., Pilon-Smits, E.A.H., Jouanin, L., Terry, N., 1999. Overexpression of Glutathione Synthetase in Indian Mustard Enhances Cadmium Accumulation and Tolerance. Plant Physiol. 119, 73–80.

Ziegelhoffer, E.C., Donohue, T.J., 2009. Bacterial responses to photo-oxidative stress. Nat. Rev. Microbiol. 7, 856–863.

Zurbriggen, M.D., Tognetti, V.B., Fillat, M.F., Hajirezaei, M.-R., Valle, E.M., Carrillo, N., 2008. Combating stress with flavodoxin: a promising route for crop improvement. Trends Biotechnol. 26, 531–537.

CHAPTER 2

A Synthetic Condensed Reverse TCA Cycle to Enhance Carbon Fixation in Plants

Caroline M. Smith-Moore, Kai Li, Denise Aslett, Mikyoung Ji, Xuli Lin, Deyu Xie, Heike Sederoff, and Amy Grunden

Contribution Statement:

From the outset of this research, I was responsible for the identification and selection of all SCS, KOR, and ferredoxin proteins. Following enzyme selection, I cloned these genes into their respective expression vectors, expressed, purified, and evaluated their activity. For the KOR enzymes, I designed and optimized the benzyl viologen reduction assay. As the producer of these enzymes, I provided the enzymes used in the original 5-step LC-MS assays assessing the crTCA cycle.

Additionally, I theorized, designed, and assessed the function of the 4 step crTCA cycle. This involved the implementation and design of assays to evaluate the OSR enzyme for carboxylation activity and the OGC enzyme for pyruvate carboxylase activity. Additionally, I prepared the LC-MS reactions and analyzed the resulting data.

I also implemented a *Nicotiana benthamiana* transient expression system for higher efficiency production of the HyTh KOR through collaboration with the Perera lab and cloned the HyTh KOR for expression in tobacco as well as conducted all western blots and activity assays for this construct.

Overall, I contributed in every aspect of this project and made significant contributions to both data generation and interpretation as well as experimental design. Lastly, I authored the majority of this manuscript.

Abstract

CO_2 fixation is a rate-limiting factor in biomass production of C_3 crops due to the low activity and specificity of ribulose-1,5-bisphosphate carboxylase/oxygenase. To overcome this bottleneck, alternative CO_2 fixation pathways are of interest for evaluation in plants. We demonstrate the *in vitro* function of a synthetic CO_2 fixation cycle based on a condensed reverse tricarboxylic acid cycle (crTCA). The crTCA cycle as designed consists of five enzymes of bacterial origin that utilize succinate and bicarbonate to generate glyoxylate, but it was shown to be fully functional using four of the five enzymes. Purified recombinant enzymes of this crTCA cycle are able to assimilate CO_2 *in vitro* and generate glyoxylate. To assess the feasibility of this approach *in planta*, the individual crTCA cycle enzymes were expressed using a transient tobacco system and shown to be functional. Implementation of this crTCA cycle in plants could lead to increases in plant biomass and yield.

2.1 Introduction

Most atmospheric CO_2 is assimilated into the organic matter of the biosphere by Ribulose-1,5-Bisphosphate Carboxylase/Oxygenase (RuBisCO). Because the RuBisCO catalytic velocity for CO_2 fixation is so slow, the RuBisCO protein is about 50% of the soluble protein in a plant leaf (Ellis, 1979), making it the most abundant single protein in the biosphere. The RuBisCO protein itself is a major sink for assimilated carbon and nitrogen in a plant, reducing its productivity and nitrogen use efficiency.

In addition to its carboxylase activity, RuBisCO reacts with oxygen producing 2-phosphoglycolate (Ogren and Bowes, 1971). Phosphoglycolate is removed through photorespiration, resulting in a loss of energy and assimilated carbon (Ogren, 1984). The net loss of plant productivity due to oxygenase activity of RuBisCO and photorespiration is approximately 30% in C_3 plants such as soybean (Zhu et al., 2010). To compensate, photosynthetic organisms have evolved different carbon-concentrating mechanisms (CCMs) including carboxysomes in cyanobacteria (Hanson et al., 2016), C_4 metabolism (Leegood, 2013), and crassulacean acid metabolism in plants (Borland et al., 2014).

Attempts have been made to modify RuBisCO (Bainbridge et al., 1995) and its regulatory proteins (Kurek et al., 2007), introduce CCM structures and enzymes into C_3 plants (Lin et al., 2014), or alter the photorespiratory pathway (Dalal et al., 2015a; Kebeish et al., 2007). Engineering RuBisCO has proved unsuccessful, while creating a photorespiratory bypass has, increased biomass and yield (Dalal et al., 2015a; Kebeish et al., 2007).

Non-photosynthetic autotrophs have RuBisCO-independent CO_2 fixation pathways, suggesting that alternative CO_2 fixation cycles might work in plants (Bar-Even et al., 2010; Ducat and Silver, 2012). The reverse TCA (rTCA) cycle is a CO_2 fixation cycle identified in

anaerobic organisms and some microaerophiles due to the oxygen sensitivity of cycle enzymes (Hügler and Sievert, 2011). Bar-Even, et al. (2010) computationally evaluated a five-step CO_2 fixation cycle using rTCA cycle enzymes, which appeared to be energetically feasible under diverse physiological conditions. The oxygen sensitivity of the 2-oxoglutarate ferredoxin oxidoreductase (KOR) and the strict thermophilic activity of the 2-oxoglutarate carboxylase (OGC) made the implementation of the cycle in a plant uncertain (Bar-Even et al., 2010).

To create a functional five-step or condensed rTCA cycle, (designated crTCA cycle), BLAST was used to search for rTCA enzyme homologs in mesophilic, microaerobic/aerobic organisms. The crTCA cycle consists of five enzyme catalyzed steps. Step 1 is catalyzed by succinyl CoA synthetase (SCS; E.C. 6.2.1.5), which converts succinate to succinyl CoA with the hydrolysis of ATP. Step 2 converts succinyl CoA to 2-oxoglutarate (2-OG), fixing CO_2 and oxidizing ferredoxin and is catalyzed by KOR (E.C. 1.2.7.3). OGC (E.C. 6.4.1.7) catalyzes step 3 by adding one more carbon to 2-OG and producing oxalosuccinate with the hydrolysis of ATP. Step 4 is catalyzed by oxalosuccinate reductase (OSR in this article, more commonly ICDH; E.C. 1.1.1.42), which converts oxalosuccinate to isocitrate and oxidizes NADPH. Isocitrate lyase (ICL; E.C. 4.1.3.1) catalyzes step 5; it hydrolyzes isocitrate to produce glyoxylate and succinate, thus beginning the cycle again. A diagram of the crTCA cycle can be seen in Figure 2-1.

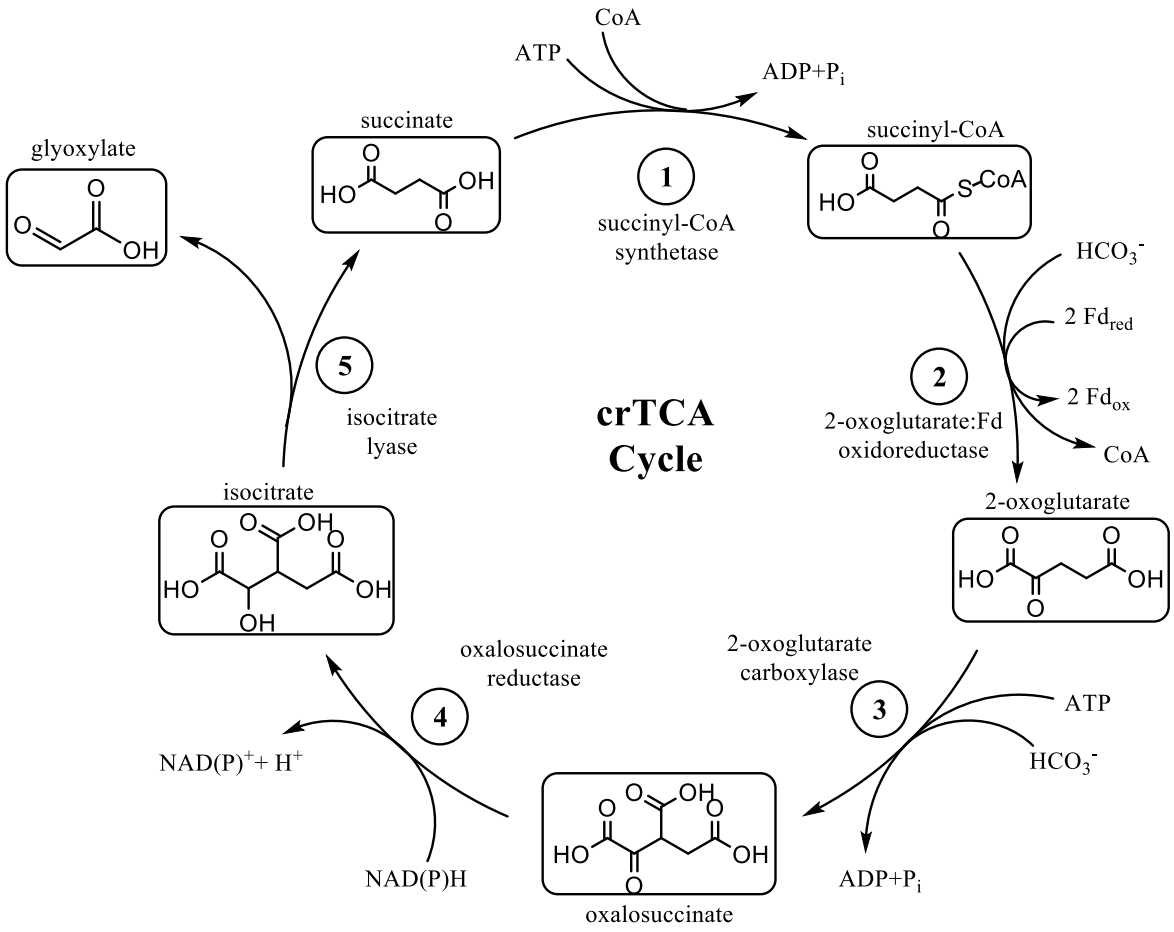

Figure 2-1. Diagram of the crTCA cycle. Diagram highlights the enzymes, cofactors, and metabolites produced and includes the following abbreviations: ferredoxin (Fd).

The product of this crTCA cycle, glyoxylate, can be metabolized via the photorespiratory pathway. Recent work on a bacterial bypass to reduce photorespiratory energy and carbon loss has shown that glyoxylate produced in the chloroplast can be metabolized and contributes to increased biomass (Dalal et al., 2015a; Kebeish et al., 2007). Here we demonstrate the function of the crTCA cycle *in vitro* and the activity of the cycle enzymes *in planta* using a transient tobacco expression system.

2.2 Materials and Methods

2.2.1 Selection of crTCA Cycle Enzyme Candidates

To generate a robust synthetic gene candidate list (3-5 target genes) for each of the five enzyme steps of the proposed synthetic crTCA cycle, BLAST-p (NCBI) alignments and Conserved Domain (NCBI) analysis were used to identify target crTCA cycle enzymes and appropriate catalytic/substrate binding domains. The query sequences for the BLAST-p alignments were from enzymes known to have activity for crTCA cycle functions. MODELLER (Eswar et al., 2007) was used to predict the binding affinity of the candidates for the cycle substrates. The selected genes were synthesized by GenScript (Piscataway, NJ) with codon optimization for *Escherichia coli* and ligated into pUC57. Enzymes 1-3 are multi-subunit, and the sequences for these enzymes were synthesized consistent with the NCBI genome sequence for each organism including intergenic spacer regions, which were not codon optimized. Ferredoxin from *Hydrogenobacter thermophilus* TK-6 was also synthesized to supplement the KOR enzyme in the proposed crTCA cycle. The selected candidates are listed in Table 2-1.

Table 2-1. Selected gene candidates for the crTCA cycle.

Enzyme class	Source Organism	Protein ID
Step #1 Succinyl CoA Synthetase (SCS)	*Bradyrhizobium* sp. BTAi1	α: WP_012040734.1
		β: WP_012040733.1
	Azotobacter vinelandii DJ	α: WP_012701526.1
		β: WP_012701527.1
	Azospirillum sp. B510	α: WP_012975136.1
		β: WP_012975135.1
	Escherichia coli K-12 substr. MG1655	α: NP_415257.1
		β: NP_415256.1
Step #2 2-oxoglutarate: ferredoxin oxidoreductase (KOR)	*Hydrogenobacter thermophilus* TK-6	α: WP_012963731.1
		β: WP_012963730.1
	Bacillus sp. M3-13	α: ZP_07708142.1
		β: WP_010193262.1
	Haladaptatus paucihalophilus DX253	α: WP_007979610.1
		β: WP_007979608.1
	Halobacterium sp. NRC-1	α: WP_012289282.1
		β: WP_010902808.1
	Magnetococcus sp. MC-1	α: WP_011713405
		β: WP_011713406.1
	Paenibacillus larvae subsp. larvae B-3650	α: WP_036654064.1
		β: WP_036654066.1
Step #3 2-oxoglutarate carboxylase (OGC)	*Mariprofundus ferrooxydans* PV-1	α: WP_009849086.1
		β: WP_009849087.1
	Hydrogenobacter thermophilus TK-6	α: WP_012964024.1
		β: WP_012964023.1
	Candidatus Nitrospira defluvii	α: WP_013247788.1
		β: CBK40961.1
	Thiocystis violascens DSM198	α: WP_014776649.1
		β: WP_014776651.1
	Pseudomonas stutzeri ATCC14405	α: ABP77893.1
		β: WP_011911433.1
Step #4 Oxalosuccinate reductase (OSR)	*Nitrosococcus halophilus Nc4*	WP_013033479.1
	Marine gamma proteobacterium HTCC2080	WP_007233843.1
	Kosmotoga olearia TBF 19.5.1	WP_015868581.1
	Chlorobium limicola DSMZ245	BAC00856.1
	Acinetobacter baumannii ACICU	WP_000542119.1

Table 2-1 (continued)

Enzyme class	Source Organism	Protein ID
Step #5 Isocitrate Lyase (ICL)	*Nocardia farcinica* IFM 10152	WP_011211764.1
	Gordonia alkanivorans NBRC 16433	WP_005200301.1
	Corynebacterium glutamicum ATCC 13032	NP_601531.1
	Rhodococcus jostii RHA1	WP_009474796.1
	Rhodococcus pyridinivorans AK37	WP_006553580.1
Supplemental Protein: Ferredoxin	*Hydrogenobacter thermophilus* TK-6	WP_012964515.1|

2.2.2 crTCA Cycle Gene Cloning

The Qiagen (Valencia, CA) pQE vector system was chosen for overexpression of the crTCA cycle enzymes because it enables expression of His-tagged fusion proteins for purification. Some of the crTCA enzymes did not express well with the pQE vector and were instead expressed using pET21b or pET28a (EMD Millipore, Burlington, MA) as indicated in Supplemental Table 2-1.

The primers and annealing temperatures used to amplify the candidate crTCA cycle genes are also listed in Supplemental Table 2-1. For cloning the genes into pQE-1, forward primers were designed to amplify the sequence beginning with the 5' ATG to limit additional amino acids on the N-terminus. Reverse primers included the *Hind*III or *Sac*I sites of pUC57. The synthesized crTCA cycle genes in pUC57 were used as template DNA with iProof High-Fidelity DNA polymerase (BioRad, Hercules, CA). The PCR products were gel purified, digested with *Hind*III or *Sac*I, and precipitated with ethanol. Following phosphorylation with T4 polynucleotide kinase (New England BioLabs, Ipswich, MA), the PCR products were ligated into expression vector pQE-1 (Qiagen) with T4 ligase (New England BioLabs), and the ligation mix was transformed into *E. coli* strain XL-1 Blue.

Plasmid DNA was confirmed by sequence and then transformed into expression strain *E. coli* M15.

Genes for BrBT-SCS, BaM3-KOR, HyTh-KOR, and PaLa-KOR were also cloned into pET21b (SCS and KOR) and pET28a (only the KOR genes). PCR products were ligated into pPCRscript and transformed into *E. coli* XL-1 Blue. Digestion with *Nde*I and *Xho*I was conducted to extract the PCR product from pPCRscript using sites in the PCR primers. The digested PCR product was gel extracted, ligated into pET21b or pET28a and transformed into *E.coli* XL-1 Blue. Plasmid DNA was confirmed by sequencing before transformation into expression strain *E.coli* BL21 (DE3).

2.2.3 crTCA Cycle Protein Expression

The crTCA cycle candidate proteins were expressed, purified and evaluated for activity. Enzymes with the highest activity were selected for LC-MS assays and transient expression in tobacco. BrBT-SCS was expressed in *E. coli* BL21 (DE3) transformed with BrBT-SCS in pET21b. The cells, grown in LB at 37 °C and 200 rpm to mid-log phase (OD_{600} 0.6-0.8), were induced with 0.1 mM IPTG and the temperature was reduced to 18 °C for 18-20 h. HyTh-KOR was expressed in *E. coli* BL21 (DE3) transformed with HyTh-KOR in pET28a. The cells, grown in LB, supplemented with 1 mM thiamine, at 37 °C and 200 rpm to mid log phase (OD_{600} 0.6-0.8), were then induced with 0.1 mM IPTG. $FeSO_4$ (0.5 mM) was added to increase iron availability for Fe-S cluster biosynthesis. The temperature was then reduced to 18 °C for 18-20 h. MaFe-OGC was expressed in *E. coli* M15 transformed with MaFe-OGC in pQE1. Cells were grown in LB, with 1 mg/L biotin, at 25 °C, 200 rpm to OD_{600} 0.6-0.8, and expression was induced with 0.05 mM IPTG. The temperature was

reduced to 18 °C and incubated for an additional 18-20 h at 200 rpm. For NiHa-OSR and NoFa-ICL enzymes, freshly transformed *E. coli* M15 cultures were grown at 25°C, 200 rpm, to mid log phase (OD_{600} 0.6 to 0.8). IPTG was added (to 0.05 mM) and cultures were shaken at 200 rpm and 15 °C, for 16 to 18 h. For all enzymes, prior to increasing the cultures to 1 L, soluble protein expression was confirmed from a 30 ml culture using SDS-PAGE and/or Western blot analysis.

2.2.4 Purification of Recombinant crTCA Cycle Enzymes

All purifications used a BioRad DuoFlow system. Cell pellets containing the recombinant crTCA cycle proteins were resuspended in 50 mM sodium phosphate, pH 7.5, containing 1 mM benzamidine–HCl. All buffers for the KOR enzymes contained 0.01% Triton X100 during the purification [17]. The bacteria were passed through a French pressure cell (1,100 lb/in^2) two or three times. The lysate was centrifuged at 15,000 x g for 40 min at 4 °C to remove cell debris, then passed through a 0.45 μm syringe filter. The filtrate was applied to a 5 mL HisTrap HP Nickel Sepharose™ affinity column (GE Healthcare Life Sciences) and washed with five column volumes of binding buffer (50 mM sodium phosphate buffer, 500 mM NaCl, 30 mM imidazole, pH 7.5). The elution buffer was 50 mM sodium phosphate buffer, 300 mM NaCl, 250 mM imidazole, pH 7.5. Elution was done via a linear gradient from 0% to 100% elution buffer. Fractions were analyzed by SDS-PAGE (12.5%) and protein concentration was estimated using the BioRad Bradford Assay (with a BSA standard). Fractions containing recombinant protein were pooled prior to additional purification. Additional treatment of crTCA cycle enzymes is described below and purified crTCA enzymes are shown in Figure 2-2.

BrBT-SCS:

Pooled fractions were dialyzed using (20 kDa MWCO) Slide-A-Lyzer (Thermo Fisher Scientific), in 50mM Tris-HCl (pH 8) overnight at 4 °C. Dialyzed protein was then loaded onto a 5 ml HiTrap Q HP anion exchange column (GE Healthcare Life Sciences) and eluted with a gradient of 0-100% elution buffer (50 mM Tris-HCl (pH 8), 1 M NaCl). Fractions containing BrBT-SCS were dialyzed again as described, quantified, and stored at -80 °C in 15% glycerol.

HyTh-KOR:

Microaerobic handling was required for the KOR enzymes, which involved de-gassing and sparging of all purification buffers with argon and anaerobic collection of elution fractions. After affinity chromatography, HyTh-KOR was desalted into 20 mM Tris-HCl (pH 8), 0.01% Triton X100 using a 30 kDa MWCO centrifugation filter (Millipore) in an anaerobic glovebox. Purified enzymes were quantified, and stored anaerobically at -80 °C in stoppered vials in 15% glycerol.

MaFe-OGC:

Pooled fractions were dialyzed using Slide-A-Lyzer (Thermo Scientific) cassettes (30 kDa MWCO) against 50 mM Tris-HCl (pH 8) then stored at -80 °C in 15% glycerol.

NiHa-OSR and NoFa-ICL:

Fractions containing recombinant protein were pooled and dialyzed using a Slide-A-Lyzer (Thermo Fisher Scientific) cassette (20 kDa MWCO) against 50 mM Tris-HCl, 1 mM benzamidine, 0.25 mM EDTA, pH 8.0. The dialyzed samples were applied to a 5 ml HiTrap Q HP anion exchange column (GE Healthcare Life Sciences). The Q anion exchange column

was eluted via linear gradients from 0% to 100% elution buffer (50 mM Tris, 1 M NaCl, 1 mM benzamidine, 0.5 mM EDTA, pH 8). Appropriate fractions were pooled and dialyzed using a Slide-A-Lyzer (Thermos Fisher Scientific) cassette (20 kDa MWCO) against 50 mM Tris-HCl, 1mM benzamidine, 0.25 mM EDTA, pH 8.0. The purified enzymes were stored at -80 °C. in 15% glycerol.

HyTh-FDX:

Fractions were pooled and loaded onto a HiPrep 26/10 desalting column (GE Life Sciences) into 50 mM Tris-HCl, pH 8. Protein was stored at -80 °C in 15% glycerol.

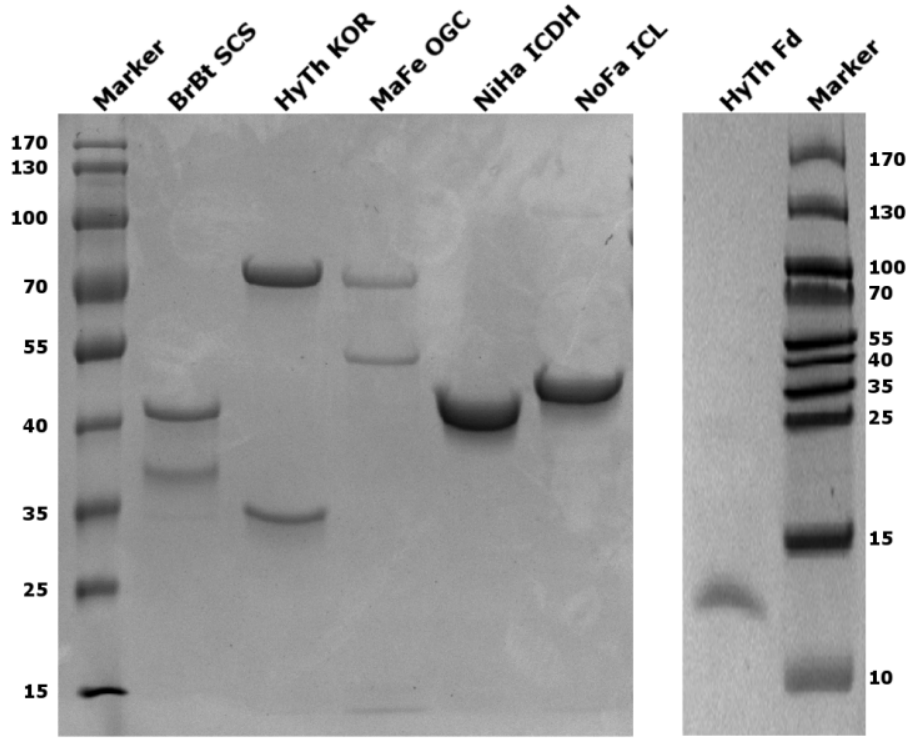

Figure 2-2. Purified crTCA cycle enzymes. SDS-PAGE (12.5%) showing all of the purified enzymes used in the subsequent *in vitro* analysis of the full cycle. The expected molecular weights are as follows: BrBT SCS (α: 43 kDa, β: 30 kDa); HyTh KOR (α: 65 kDa, β: 31 kDa); MaFe OGC (α: 53 kDa, β: 68 kDa); NiHa OSR (46 kDa); NoFa ICL (48 kDa); and HyTh Ferredoxin (9.1 kDa).

2.2.5 Spectrophotometric Assays for crTCA Cycle Enzymes

Spectrophotometric assays were carried out to screen the candidate enzymes for each crTCA cycle step *in vitro* as well as to detect *in planta* expression in tobacco. A Biomate 3 spectrophotometer from Thermo Fisher Scientific and a Shimadzu UV-2401PC UV-visible spectrophotometer with a temperature controlled cuvette holder were used for the assays. In all cases, individual enzyme reactions were conducted in triplicate using purified enzymes from the same batch of purification that had been stored in aliquots at -80°C.

SCS:

The standard reaction consisted of 10 mM sodium succinate, 10 mM $MgCl_2$, 0.1 mM CoA, 0.1 mM DTT, 0.4 mM nucleotide ATP and 0.1 M KCl in 50 mM Tris-HCl (pH 7.4). Reactions were started with purified enzyme or extracts of cells transformed with BrBT-SCS. The reaction was monitored by absorbance at 230 nm in response to thioester formation at RT (Bridger et al., 1969).

KOR:

The decarboxylase activity of KOR was detected in a continuous spectrophotometric assay following the enzyme-, substrate-, and time-dependent reduction of oxidized benzyl viologen (at 600 nm). Reaction mixtures were prepared aerobically, then sparged with argon. The assay was performed in anaerobic gas-tight glass cuvettes. The KOR enzyme was treated with 5 mM DTT (15 min) prior to adding the enzyme to the reaction mix. The reaction mix contained 100 mM sodium phosphate (pH 7.5), 1 mM benzyl viologen, 2.5 mM 2-OG, 0.5 mM coenzyme A, 4 mM MgCl2, and 0.025 mM sodium dithionite. The reactions were started by adding 2-OG using gas-tight glass syringes. The assay was conducted at RT or 30 °C.

OGC:

A two-step, coupled spectrophotometric assay was developed for the ATPase activity of OGC using phosphoenolpyruvate kinase (PK) and lactate dehydrogenase (LDH). PK utilizes ADP hydrolyzed by OGC to produce pyruvate from phosphoenolpyruvate, which is converted to lactate by LDH by the oxidation of NADH. The oxidation of NADH is observed by absorbance at 340 nm. The first step reaction mixture is composed of 100 mM PIPES (pH 6.5), 5 mM $MgCl_2$, 20 mM 2-OG, 50 mM $NaHCO_3$, and 5 mM ATP. The reaction was initiated by OGC. The reaction mixture with OGC was held for 30 min at RT (65 °C for the thermophilic enzyme). For the second step, 0.1 mM β-NADH, 2 mM phosphoenolpyruvate and PK/LDH were added to the first step reaction, and NADH oxidation was monitored by absorbance at 340 nm. The amount of ADP produced was estimated using a standard curve.

OSR:

The assay evaluates the dehydrogenase activity of OSR, monitored at 340 nm, measuring the reduction of NADP+. The reaction mixture is composed of 50 mM Tris (pH 7.4), 10 mM $MgCl_2$, 100 mM KCl, 4 mM isocitrate, 4 mM β-$NADP^+$. The reaction was initiated by addition of purified enzymes or tobacco cell extracts and monitored by $NADP^+$ reduction (340 nm at RT). The OSR carboxylation assay was adapted from a published method (Kanao et al., 2002). The reaction mixture contained 50 mM PIPES (pH 6.5), 10 mM 2-OG, 1 mM NADH, 10 mM $MgCl_2$, 50mM $NaHCO_3$. The reaction was started with the addition of the NiHa OSR enzyme. The activity is measured following the oxidation of NADH (340 nm at RT).

NoFa ICL:

Reaction mixtures contained 30 mM imidazole (pH 6.8), 5 mM $MgCl_2$, 1 mM EDTA, 4 mM phenylhydrazine and 10 mM isocitrate. The reaction was performed at RT by adding purified protein or cell extracts and monitoring the absorbance of glyoxylate phenylhydrazone (324 nm) in the presence of phenylhydrazine (Chell et al., 1978).

Pyruvate Carboxylase:

This assay evaluates pyruvate carboxylase activity of MaFe OGC. It is a coupled assay, where oxaloacetate is first produced by pyruvate carboxylase. The oxaloacetate is then used by malate dehydrogenase to produce malate by the oxidation of NADH, measured by absorbance at 340 nm (Warren and Tipton, 1974).

Reaction mixtures contained 50 mM Tris-HCl (pH 8.0), 8 mM $MgCl_2$, 20 mM sodium pyruvate, 20 mM $NaHCO_3$, 8 mM ATP, 0.2 mM NADH, and 50 μM acetyl-CoA. The reaction was started by addition of 1 U of porcine heart malate dehydrogenase (Sigma, St. Louis, MO) and MaFe OGC. The production of NAD^+ was measured by absorbance at 340 nm at RT.

2.2.6 LC-MS Assay

LC-MS assays were developed for those enzymes that could not be assayed spectrophotometrically in the right direction of the crTCA cycle. Mass spectrometer (MS) analyses were performed on an Agilent LC-MS system comprised of an Agilent 1200 series HPLC with an Agilent 1260 Infinity micro degasser, binary pump, and standard auto-sampler, an Agilent 1290 Infinity diode-array detector and an Agilent 6520 Accurate-Mass Q-TOF spectrometer, equipped with an electrospray ionization interface. The condensed

rTCA cycle enzyme reaction samples were separated using a modified version of a published method (Lu et al., 2010). A Synergy Hydro-RP column (100 mm × 2 mm, 2.5 μm particle size, Phenomenex, Torrance, CA), was used for reversed phase chromatography. The total run time is 18 min with a flow rate of 0.200 ml/min. All solvents used for LC-MS were LC-MS grade. Solvent A was 0.1% formic acid in water; solvent B 0.1% formic acid in methanol. The gradient used was 0 min, 0% B; 10 min, 60% B; 11 min, 0% B; 17 min, 0% B. The MS was set in negative ion mode with spectra acquired over a mass range from m/z 50 to 1000. The optimum values of the ESI-MS parameters were: capillary voltage, +3.5 kV; drying gas temperature, 325 °C; drying gas flow, 10.0 L/min; nebulizing gas pressure, 35 psi; fragmentor voltage, 115V.

2.2.7 *In vitro* Demonstration of the crTCA Cycle

Reactions were stopped by addition of 50 μl methanol and processed by LC-MS as described above, unless otherwise stated.

OGC/OSR(step 3-4):

The OGC product, oxalosuccinate is labile, so the production of isocitrate for the OGC/OSR coupled reaction was tested by LC-MS. The reaction contained 50 mM Tris (pH 6.5), 5 mM $MgCl_2$, 20 mM 2-OG, 50 mM NH_4HCO_3, 5 mM ATP, 50 mM KCl, 2 mM β-NADPH and recombinant OGC and OSR enzymes. The reaction was initiated by adding the enzymes and held for 30 min at RT. The isocitrate product was analyzed by LC-MS.

Partial Function of crTCA Cycle (step 3-5):

The reaction mixture contained 50 mM Tris-HCl (pH 6.5), 5 mM $MgCl_2$, 20 mM 2-OG, 50 mM $NH_4H^{13}CO_3$, 5 mM ATP, 50 mM KCl, 2 mM β-NADPH and the recombinant

OGC, OSR and ICL enzymes. The reaction was initiated by adding the enzymes and incubated for 30 min at room temperature. The final products, glyoxylate and succinate, and intermediate product, isocitrate were analyzed by LC-MS.

Full Function of crTCACcycle:

To demonstrate *in vitro* function of the crTCA cycle, LC-MS samples were prepared (under anaerobic conditions) for all five crTCA cycle enzymes. In addition to the crTCA cycle enzymes, the reactions contained 50 mM Tris-HCl (pH 8.0), 4 mM NADH, 5 mM ATP, 5 mM $MgCl_2$, 10 mM $NaH^{13}CO_3$, 0.5 mM CoA, 100 µM succinyl-CoA, 1 mM 2-OG, and 60 µg HyTh ferredoxin, in 600 µL. The reactions were initiated by addition of HyTh KOR and HyTh Fd, and incubated for 0, 15, 30, 60, 90 and 120 minutes at 30°C. The ^{13}C-labeled crTCA cycle intermediates were analyzed by LC-MS, and quantification of the different labeled species of the crTCA cycle intermediates was performed using standards analyzed alongside the experimental samples.

crTCA Cycle Function Under Aerobic Conditions:

The *in vitro* crTCA cycle reactions were prepared (under aerobic conditions) to test cycle function when the crTCA cycle enzymes were exposed to air. The aerobic reactions were prepared on the bench top instead of in an anaerobic glovebox.

The Reversibility of the crTCA Cycle:

To test whether the crTCA cycle is reversible, the reactions contained 50 mM Tris-HCl (pH 8.0), 4 mM NAD^+, 5 mM ADP, 5 mM $MgCl_2$, 0.5 mM CoA, 500 µM succinate, 500 µM glyoxylate, and 60 µg HyTh ferredoxin, in 600 µl. The samples were prepared under anaerobic conditions. The reactions were initiated by addition of HyTh KOR and HyTh Fd, and incubated for 60 minutes at 30°C.

To further assess the reversibility of the ICL and OSR enzymes, a coupled assay was adapted from previous work (Pham et al., 2017). The assay couples ICL with OSR catalyzing the conversion of glyoxylate and succinate to isocitrate by ICL, and finally to 2-OG through the activity of OSR with the oxidation of NAD^+. The reactions contained 50 mM Tris-HCl (pH8), 5 mM $MgCl_2$, 1 mM NAD^+, 0.5 mM glyoxylate, and 0.5 mM succinate. The reaction was started with the addition of ICL and OSR in a 1:1 ratio and was monitored for NADH using a Shimadzu UV-2401PC UV-Visible spectrophotometer (340 nm).

2.2.8 Cloning of crTCA Genes for Transient Tobacco Expression

To validate the expression of the crTCA cyle enzymes in a plant, each enzyme was transiently expressed in tobacco. The selected crTCA cycle gene sequences for each step were synthesized using GenScript (Piscataway, NJ) with codon optimization for *Arabidopsis thaliana*. Each crTCA cycle gene was linked to a cauliflower mosaic virus (CaMV) 35S promoter, a chloroplast localization sequence (from tobacco), and the nopaline synthase (NOS) terminator. 6X-His tags were fused to the N terminus for NiHa OSR and NoFa ICL and the C terminus for the BrBT SCS and HyTh KOR coding sequences for the detection and purification of the proteins.

The inserts for each crTCA cycle enzyme were ligated to the multiple cloning sites of pCAMBIA-EGFP (Dalal et al., 2015b) using *Hind*III and *Bam*HI sites, and transformed into *E. coli* XL1-Blue. The clones were screened using restriction analysis and verified by sequencing (Eurofins Genomics, Louisville, KY). The verified constructs were transformed into competent *Agrobacterium tumefaciens* GV3101 by electroporation and selected using kanamycin.

2.2.9 Transient Tobacco Transformation

Each construct was transformed into 5-6 week old tobacco plants using *Agrobacterium* mediated transformation. BrBT-SCS, NiHa-OSR, and NoFa-ICL were all expressed in *Nicotiana tabacum*, while HyTh-KOR was expressed in *N. benthamiana* as expression with *N. tabacum* did not yield detectable protein. *A. tumefaciens* GV3101 harboring each crTCA cycle construct was grown in liquid yeast extract peptone (YEP) media with kanamycin, rifampicin, and gentamicin at 28°C until mid-log phase (OD_{600} 0.6-0.8). The cultures were centrifuged at 4,500 rpm for 30 min. The pellets were resuspended in sterile infiltration media (10 mM MES, 10mM $MgCl_2$, 0.5% glucose, 200 μM acetosyringone, at pH 5.6) to an OD600 between 0.2-0.5 in 1 L of infiltration media. Containers of *Agrobacterium* suspension media were placed inside a desiccator. The leaves of each plant were submerged in the suspension by placing the plant upside-down. For the infiltrations with *N. benthamiana*, additional *Agrobacterium* GV3101 cultures were prepared containing the p19 viral suppression plasmid (Lindbo, 2007) and a 1:1 mixture of p19 culture to crTCA construct culture were added to the desiccator. A vacuum of approximately 25 mm Hg was applied for 30 sec and released. The vacuum procedure was repeated for 3 cycles, after which the plants were allowed to dry and returned to the light shelf. The *N. tabacum* plants were grown with 12 h light and 12 h dark at 25°C , while *N. benthamiana* were grown with 16 h light (150 μmol m^{-2} s^{-1}) and 8 h dark at 25°C.

2.2.10 Western Blot Analysis and Enzyme Assays for Transient Tobacco Expression

A time course was conducted to determine the optimal day after transformation for harvesting tissue. Tobacco leaves were harvested 4 days post-transformation and the tissues

were ground in liquid nitrogen by mortar and pestle. Proteins were extracted from ground tissue in a buffer containing 50 mM Tris (pH 8), 150 mM NaCl, 10% (v/v) glycerol, 1% (v/v) Triton x-100, and 1:100 protease inhibitor cocktail for plant cells (Sigma). Either tissue lysate or an Ni-NTA Spin Kit (Qiagen) was used to prepare samples for Western blots. The extracts were mixed with Laemmli buffer containing 2-mercaptoethanol, boiled for 10 min, and fractionated by 12.5% SDS-PAGE. Proteins were transferred to a PVDF membrane (BioRad) using a Trans-blot Turbo System (BioRad). The membranes were blocked with 5% (w/v) non-fat dry milk in Tris-buffered saline and 0.1% (v/v) TWEEN 20 (TBST) overnight. The primary antibody used for BrBT-SCS, NiHa-OSR, and NoFa-ICL was the Penta-His antibody (Qiagen) at 1:4000 in TBST. Horseradish peroxidase (HRP)-conjugated goat anti-mouse (Seracare, Milford, MA) was used as the secondary antibody at 1:8,500. For the HyTh-KOR, the primary antibody used was a polyclonal antibody raised against a HyTh-KOR specific peptide epitope. The primary antibody was diluted 1:5,000 in TBST with 1% (v/v) casein (Sigma). The secondary antibody was the HRP-conjugated goat anti-rabbit (Seracare) diluted at 1:20,000 in TBST with 2.5% (w/v) dry milk. Blot immunoreactivity was visualized by Clarity Western ECL Substrate (BioRad) and exposure to X-ray film.

To demonstrate the activities of crTCA cycle enzymes in tobacco leaf cells, the cell extracts were prepared by adding the enzyme assay buffer to the ground tissue. 1% (v/v) Triton x-100 was also added to aid in chloroplast lysis, as enzymes were targeted to the chloroplast. Polyvinyl polypyrrolidone (PVPP) was added at 5% (w/v) to remove phenolic compounds. The lysate was centrifuged at 10,000 x g for 20 min, and supernatants were carefully collected. For preparation of cell extracts for HyTh-KOR, all steps and reagents were treated under anaerobic conditions. For the BrBt-SCS samples, the cell extracts were

applied to a Ni-NTA spin column (Qiagen) to concentrate the BrBt-SCS proteins and then dialyzed with the same buffer used in the SCS assay. Protein concentration was estimated using the Bradford reagent (BioRad). Enzyme activities were measured spectrophotometrically as described above. In all cases, tobacco transformed with pCAMBIA-EGFP alone was a control for assays and Western blots.

2.3 Results

2.3.1 Selection of the crTCA Cycle Enzymes

The crTCA cycle is composed of five enzymatic steps. The selection of candidate enzymes was based on the sequence alignment to functionally characterized enzymes, activity predictions from sequence, and the physiology of the source bacteria. After initial screening, four to seven enzyme candidates were selected for each of the crTCA cycle steps (Table 1). Candidate genes were codon optimized for recombinant expression in *E. coli* and cloned into either pQE1 or pET vectors for expression in M15 or BL21 (DE3) *E. coli* strains, respectively. Most of the protein candidates were successfully overexpressed using either the pQE1 – M15 or pET – BL21 (DE3) expression systems and were purified by immobilized nickel affinity chromatography (IMAC). Three out of 4 SCSs, 4 out of 6 KORs, 4 out of 7 OGCs, 3 out of 5 OSRs, and 4 out of 5 ICLs were purified with a yield of more than 5 mg per L of *E. coli* culture.

The best enzyme for each step was selected from the candidate enzymes, considering the specific activities and protein yields. The purified proteins were first tested using UV-Vis spectroscopy methods to screen for activity. For SCS, OGC, and ICL, UV-Vis

spectrophotometric methods measured the reaction rate in the forward direction. SCS from *Bradyrhizobium sp*.BTAi1 (BrBt SCS) and ICL from *Nocardia farcinica* IFM 10152 (NoFa ICL) were selected as the best enzymes for step 1 and step 5, respectively, based on their specific activities. While OGC from *Mariprofundus ferrooxydans* PV-1 (MaFe OGC) had a similar specific activity to other overexpressed OGC enzymes, its protein yield was much higher, and therefore, was selected. For the enzyme OSR, UV-Vis spectrophotometry was used to measure the reaction in the reverse direction of the crTCA cycle, due to the lability of the reactant metabolite, oxalosuccinate. Therefore, the recombinant OSRs were initially screened using UV-Vis spectrophotometry and then LC-MS was used to determine the best combination of OGC and OSR. OSR from *Nitrosococcus halophilus* Nc4 (NiHa OSR) coupled with MaFe OGC was the best choice for our crTCA cycle under our conditions.

KOR is the only enzyme of the crTCA cycle that required anaerobic conditions for recombinant protein purification. Experiments using KOR were done under anaerobic conditions unless otherwise specified. The KOR enzyme requires reduced ferredoxin for the carbon fixation reaction, which converts the four-carbon derivative, succinyl-CoA to the five-carbon product, 2-OG. The KOR from *Bacillus sp.* M3-13 (BaM3 KOR) showed the highest specific activity for the reverse reaction at RT. Attempts to run the full cycle with this enzyme did not succeed. Instead a combination of KOR and ferredoxin from *Hydrogenobacter thermophilus* TK-6 (HyTh) (Yamamoto et al., 2010) showed a greater preference for the forward reaction. Despite initial concerns about activity at mesophilic temperatures, the HyThKOR was evaluated for activity at lower temperatures and was found to have activity at ambient temperature. Thus, HyTh KOR and HyTh ferredoxin were selected as the best enzyme/coenzyme combination for step 2 of the crTCA cycle. The best

enzyme candidate for each step and the coenzyme ferredoxin for step 2 are listed in Table 2-2.

Table 2-2. Selected enzymes for crTCA cycle assays.

Enzyme/ coenzyme	Organism Source	Assay Method	Calc. Size (kDa)	Expression Conditions	Specific Activity (U/mg)[a]
Enzyme 1 Succinyl CoA Synthetase (SCS)	*Bradyrhizobium sp.*BTAi1 (BrBt)	UV-Vis	α: 43 β: 30	pET21b – BL21(DE3) 0.1 mM IPTG 18 ^{o}C for 18-24 hours	23.7 ± 0.5
Enzyme 2 2-oxoglutarate: Ferredoxin Oxidoreductase (KOR)	*Hydrogenobacter thermophilus* TK-6 (HyTh)	UV-Vis LC-MS	α: 65 β: 31	pET21b – BL21(DE3) 1 mM thiamine at inoculation 0.1 mM IPTG 0.5 mM $FeSO_4$ at induction 18 ^{o}C for 18-24 hours	0.22 ± 0.03
Coenzyme 2 Ferredoxin	*Hydrogenobacter thermophilus* TK-6 (HyTh)	LC-MS	7.9	pQE1 – M15 0.1 mM IPTG 37 ^{o}C for 3 hours	N/A
Enzyme 3 2-oxoglutarate Carboxylase (OGC)	*Mariprofundus ferrooxydans* PV-1 (MaFe)	UV-Vis LC-MS	α: 53 β: 68	pQE1 – M15 0.05 mM IPTG 18 ^{o}C for 18-20 hours	0.032 ± 0.002
Enzyme 4 Oxalosuccinate Reductase (OSR)	*Nitrosococcus halophilus* Nc4 (NiHa)	UV-Vis LC-MS	47	pQE1 – M15 0.05 mM IPTG 15 ^{o}C for 16-18 hours	19 ± 1
Enzyme 5 Isocitrate Lyase (ICL)	*Nocardia farcinica* IFM 10152 (NoFa)	UV-Vis LC-MS	48	pQE1 – M15 0.05 mM IPTG 15 ^{o}C for 16-18 hours	10.0 ± 0.3

[a] The results are an average of 3 replicates, and the error is reported as one standard deviation.

2.3.2 Demonstration of *in vitro* Carbon Fixation by the crTCA Cycle

To demonstrate carbon fixation by the crTCA cycle enzymes, partial function was evaluated for steps 3 to 5 (OGC, OSR, and ICL) of the crTCA cycle, which convert 2-OG to

succinate and glyoxylate with carbon fixation at step 3. Either carbon-13 labeled or unlabeled bicarbonate was used as the carbon source, with the expected production of ^{13}C labeled succinate and unlabeled succinate, respectively. The calculated molecular weight of the unlabeled succinic acid is 118 and its $[M-H]^-$ ion has an m/z ratio of 117 under the negative mode MS. One ^{13}C labeled succinic acid has a molecular weight of 119 and a $[M-H]^-$ ion with an m/z ratio of 118. The MS analysis of the OGC/OSR/ICL reaction showed a peak with an m/z ratio of 117 in the MS spectrum if unlabeled bicarbonate was used in the experiments (Supplemental Figure 2-1a). An m/z 118 peak was present when using $NaH^{13}CO_3$ (Supplemental Figure 2-1b). Therefore succinate was produced by the enzymes MaFe OGC, NiHa OSR and NoFa ICL, with 2-OG and $NaHCO_3$ as the starting reagents. Little isocitrate was detected by LC-MS. Isocitrate is an intermediate metabolite for steps 3 to 5 of the crTCA cycle and is produced by the OSR reaction. Isocitrate has been detected as the final product in similar experiments using only MaFe OGC and NiHa OSR (Supplemental Figure 2-2a & 2-2b). The failure to detect isocitrate as an intermediate suggests that the ICL reaction is not rate limiting among steps 3 to 5 of the crTCA cycle.

After confirming the partial function for steps 3 to 5 of the crTCA cycle, the presence of full cycle function was evaluated. 2-OG and succinyl-CoA were used as the starting metabolites instead of succinate to allow for the generation of a pool of reduced ferredoxin. As the cycle does not have a reductant replenishing system, starting with 2-OG generated the reductant pool needed for KOR carboxylation. $NaH^{13}CO_3$ was used as the carbon source. Multiple ^{13}C-labeled glyoxylic acid, succinic acid and 2-OG were detected (Figure 2-3), which provides direct evidence that the crTCA cycle fixes carbon under the current conditions. As expected, the amount of multiple labeled metabolites increases with longer

reaction times. The succinic acid detected by LC-MS in this experiment is the total amount of free succinic acid plus succinyl-CoA due to the difficulties in distinguishing the two in the LC-MS method used. The maximum production amounts of ^{13}C-labeled metabolites detected is summarized in Table 2-3.

Figure 2-3. *In vitro* activity of 5-step crTCA cycle and quantification. Reactions contained all 5 of the crTCA enzymes with the HyTh ferredoxin and were prepared under anaerobic conditions. Samples were taken at 0, 15, 30, 60, 90, and 120 min. The zero time point was subtracted from all other time points to account for background. Reactions were quantified through the use of standard curves analyzed at the same time as the reaction samples. Three replicates were conducted and the error bars represent the standard deviation. A.) Quantification of single ^{13}C-labeled succinate (118 m/z) and double ^{13}C-labeled succinate (119 m/z). B.) Quantification of single ^{13}C-labeled 2-OG (146 m/z), double ^{13}C-labeled 2-OG (147 m/z), and triple ^{13}C-labeled 2-OG (148 m/z). C.) Quantification of unlabeled glyoxylate (73 m/z), single ^{13}C-labeled glyoxylate (74 m/z), double ^{13}C-labeled glyoxylate (75 m/z).

A.

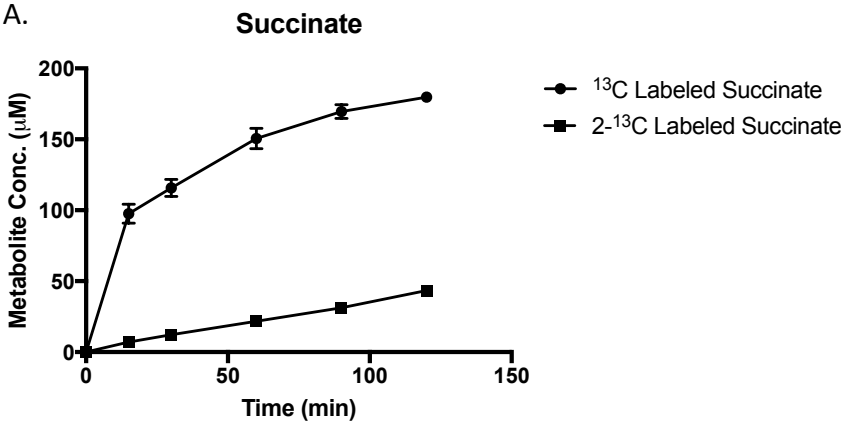
Succinate
Metabolite Conc. (μM)
200
150
100
50
0
0
50
100
150
Time (min)
13C Labeled Succinate
2-13C Labeled Succinate

B.

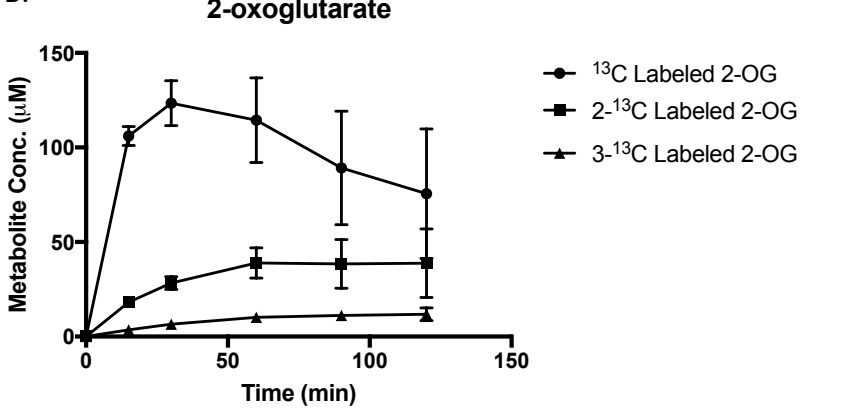
2-oxoglutarate
Metabolite Conc. (μM)
150
100
50
0
0
50
100
150
Time (min)
13C Labeled 2-OG
2-13C Labeled 2-OG
3-13C Labeled 2-OG

C.

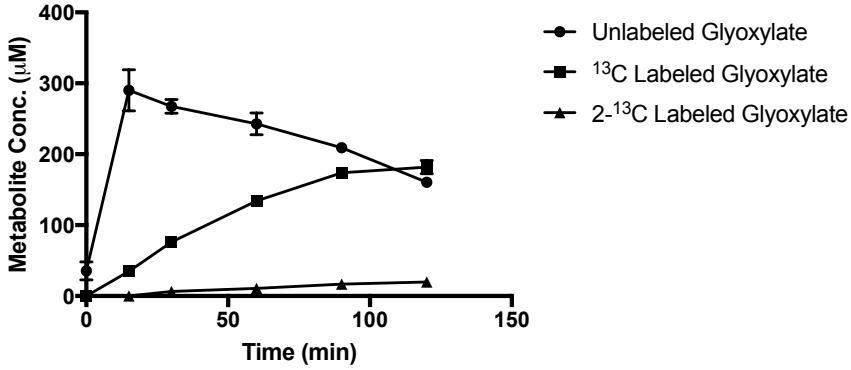
Glyoxylate
Metabolite Conc. (μM)
400
300
200
100
0
0
50
100
150
Time (min)
Unlabeled Glyoxylate
13C Labeled Glyoxylate
2-13C Labeled Glyoxylate

Table 2-3. crTCA cycle quantification under anaerobic conditions.

Metabolites		**Initial (μM)**	**Produced (μM) (anaerobic)[a]**
Glyoxylate	No ^{13}C-labeled	0	290.3 ± 29.2
	One ^{13}C-labeled	0	181.7 ± 9.5
	Two ^{13}C-labeled	0	19.8 ± 3.4
Succinate and Succinyl-CoA	No ^{13}C-labeled	100	N/A
	One ^{13}C-labeled	0	179.8 ± 3.9
	Two ^{13}C-labeled	0	43.4 ± 1.5
2-oxoglutarate	No ^{13}C-labeled	1000	N/A
	One ^{13}C-labeled	0	123.4 ± 11.9
	Two ^{13}C-labeled	0	38.9 ± 8.1
	Three ^{13}C-labeled	0	11.8 ± 3.4

[a] The results are an average of 3 replicates, and the error is reported as one standard deviation.

As the KOR is oxygen sensitive, it is important to demonstrate that the crTCA cycle can function under aerobic conditions, such as those present in the plant chloroplast. To test the full function of the crTCA cycle under aerobic conditions, an experiment similar to the one described for the full cycle was conducted except the reaction mixture was prepared aerobically. The production of labeled 2-OG was evaluated because KOR is responsible for the carboxylation of succinyl-CoA to produce 2-OG. From LC-MS, single, double, and triple ^{13}C-labeled 2-OG were detected (Figure 2-4.) The amount of these metabolites is less than that seen in the anaerobic samples; however, their detection confirms that the crTCA cycle functions in the presence of oxygen, though at lower efficiency.

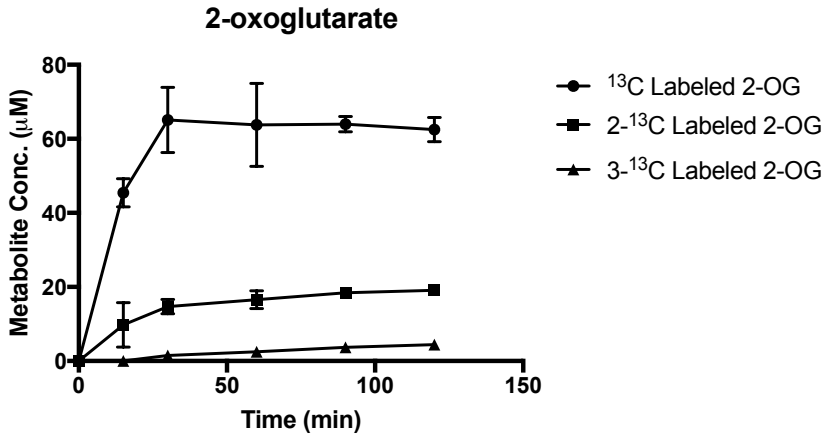

Figure 2-4. *In vitro* activity of 5-step crTCA cycle under aerobic conditions and quantification. Reactions contained all 5 of the crTCA enzymes with the HyTh ferredoxin. All reactions were prepared under aerobic conditions. Samples were taken at 0, 15, 30, 60, 90, and 120 min. The zero time point was subtracted from all other time points to account for background. Reactions were quantified through the use of standard curves analyzed at the same time as the reaction samples. Three replicates were conducted and the error bars represent one standard deviation.

2.3.3 The crTCA Cycle is Bidirectional

As shown above, the synthetic crTCA cycle functions *in vitro* in the carboxylating direction. Most crTCA cycle enzymes are theoretically capable of catalyzing the reverse reaction to their cycle activity. To evaluate this potential the last two enzymes of the cycle, the ICL and the OSR, were combined to create a coupled reaction. This reaction would evaluate the ability of ICL to utilize glyoxylate and succinate to produce isocitrate. The resulting isocitrate would be decarboxylated by OSR to produce 2-OG. The OSR reaction would also produce NADH, measured spectrophotometrically. The specific activity of this reaction was 0.07 ± 0.01 U mg^{-1} based on three replicates. While the measured activity is low compared to the activity of ICL in the production of glyoxylate and succinate (Table 2-2), this reaction demonstrates that the ICL and OSR can function together in the reverse reaction to produce 2-OG.

To test whether the full cycle can also proceed in the reverse direction, succinate and glyoxylate were used as the starting reagents with all of the crTCA cycle enzymes. The amount of glyoxylate decreases significantly after incubating 60 minutes at 30 ^{o}C, while little change was found for the control samples either with no succinate or no ICL (Figure 2-5). On the contrary, a large amount of 2-OG was detected in the full cycle reactions, suggesting 2-OG was produced under the experimental conditions. In summary, the consumption of glyoxylate and the production of 2-OG indicate that the crTCA cycle can proceed in the decarboxylation direction under certain conditions.

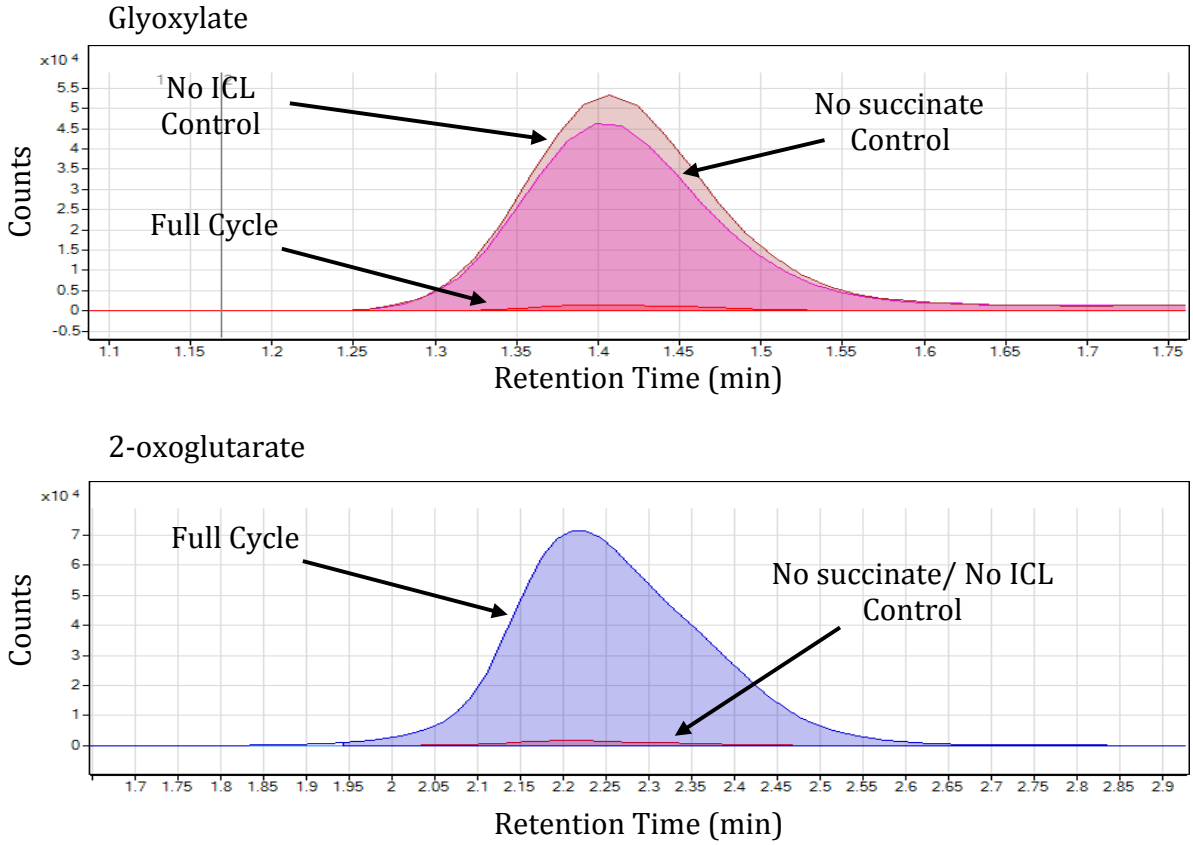

Figure 2-5. Reverse crTCA cycle activity. Reactions were prepared containing all 5 crTCA cycle enzymes and ferredoxin, but instead of feeding the cycle 2-OG, it was provided with succinate and glyoxylate. The reactions were prepared anaerobically and allowed to proceed for 60 min prior to analysis by LC-MS. Controls consist of a reaction containing all components except ICL, as well as a reaction without succinate.

2.3.4 The crTCA Cycle is Functional With Four Steps

It is well known that ICDH enzymes, such as the NiHa OSR, are often capable of catalyzing 2-OG carboxylation (Dean and Koshland, 1993). As such, NiHa OSR was evaluated for carboxylation activity using a UV-Vis assay measuring the oxidation of NAD^+ (Kanao et al., 2002). It was found that this enzyme could carboxylate 2-OG (Table 2-4). As this activity could be contributing to the full cycle activity, it was important to compare the crTCA cycle when it includes all five steps or only four steps. In the four-step cycle MaFe OGC was eliminated and NiHa OSR would be relied on to perform the carboxylation of 2-OG to produce isocitrate. The reactions were performed and analyzed by LC-MS. The peak areas were compared for the unlabeled and labeled metabolites and showed no statistically significant difference between the two reactions (Figure 2-6). Suggesting the crTCA cycle may actually perform primarily as a four-step cycle.

Figure 2-6. Comparison of 5-step crTCA cycle and 4-step crTCA cycle. Reactions were prepared in triplicate at the same time under the same conditions. The only difference was that the 4-step crTCA cycle omitted MaFe OGC. All reaction time points were run on LC-MS. The zero timepoint was subtracted from all samples to remove background. The peak areas of the relevant metabolites were measured using MassHunter software and compared. Statistical significance was determined using a two way ANOVA with a p-value <0.05. Only one point was statistically significant, and it is indicated with an asterisk (*). A.) Graphs representing the peak areas for unlabeled succinate (117 m/z), single ^{13}C-labeled succinate (118 m/z) double ^{13}C-labeled succinate (119 m/z).. B.) Graphs representing the peak areas for single ^{13}C-labeled 2-OG (146 m/z) and double ^{13}C-labeled 2-OG (147 m/z). C.) Graphs representing unlabeled glyoxylate (72 m/z) and single ^{13}C-abeled glyoxylate (73 m/z). Due to the low detection of the single labeled glyoxylate, duplicate samples were compared for the 4-step and 5-step cycle comparison instead of triplicate samples.

A.

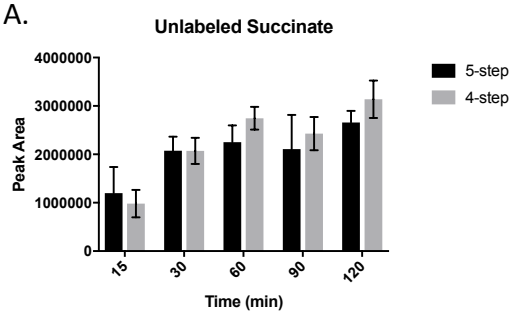
Unlabeled Succinate
Peak Area
4000000
3000000
2000000
1000000
0
15
30
60
90
120
Time (min)
5-step
4-step

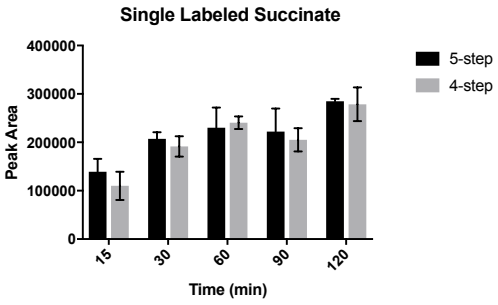
Single Labeled Succinate
Peak Area
400000
300000
200000
100000
0
15
30
60
90
120
Time (min)
5-step
4-step

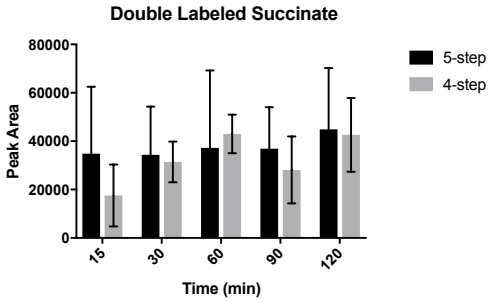
Double Labeled Succinate
Peak Area
80000
60000
40000
20000
0
15
30
60
90
120
Time (min)
5-step
4-step

B.

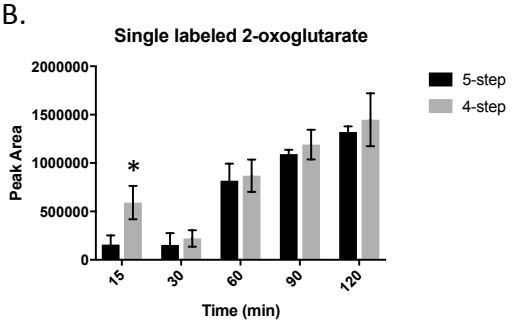
Single labeled 2-oxoglutarate
Peak Area
2000000
1500000
1000000
500000
0
*
15
30
60
90
120
Time (min)
5-step
4-step

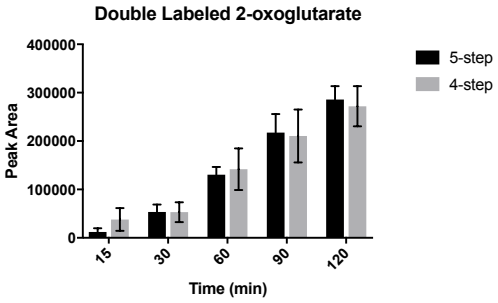
Double Labeled 2-oxoglutarate
Peak Area
400000
300000
200000
100000
0
15
30
60
90
120
Time (min)
5-step
4-step

C.

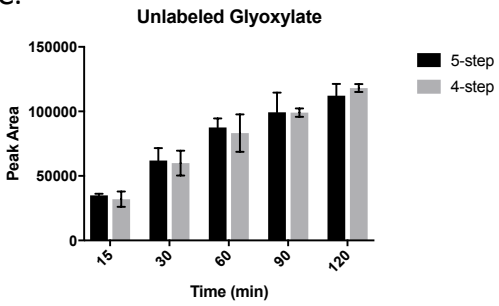
Unlabeled Glyoxylate
Peak Area
150000
100000
50000
0
15
30
60
90
120
Time (min)
5-step
4-step

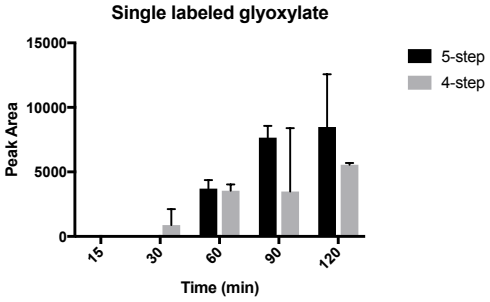
Single labeled glyoxylate
Peak Area
15000
10000
5000
0
15
30
60
90
120
Time (min)
5-step
4-step

The fact that the addition of the MaFe-OGC appeared to make no difference in cycle function raised questions about its activity. Further analysis of the enzyme with UV-Vis assays determined that MaFe-OGC is not an OGC, but is instead a pyruvate carboxylase (Table 2-4). Pyruvate carboxylase activity would not participate in the crTCA cycle as its substrates would not be present. Because of this finding, MaFe-OGC was not included in the transient tobacco experiments.

Table 2-4. NiHa OSR and MaFe OGC 4-step cycle activities.

Enzyme & assay	**Specific Activity (U/mg)** [a]
NiHa OSR **Carboxylation**	0.24 ± 0.01
MaFe OGC **Pyruvate Carboxylase**	0.11 ± 0.01

[a]The results are an average of 3 replicates, and the error reported as one standard deviation.

2.3.5 Transformation of tobacco for transient expression of the crTCA enzymes *in planta*

The target application of the synthetic crTCA cycle is to improve the carbon fixation efficiency of plants, especially C3 plants, by expression of the selected crTCA cycle enzymes in the plant chloroplast. To test if plants can produce active crTCA cycle enzymes, we transiently transformed either *N. tabacum* or *N. benthamiana* leaves with the individual crTCA cycle genes (Yang et al., 2000). For enzymes containing two subunits, both subunits with their individual promoters were incorporated onto one plasmid for transformation. All gene constructs were transformed first into *Agrobacterium tumefaciens* GV3101. Transformed *A. tumefaciens* cells were then used to transform tobacco plants by vacuum infiltration.

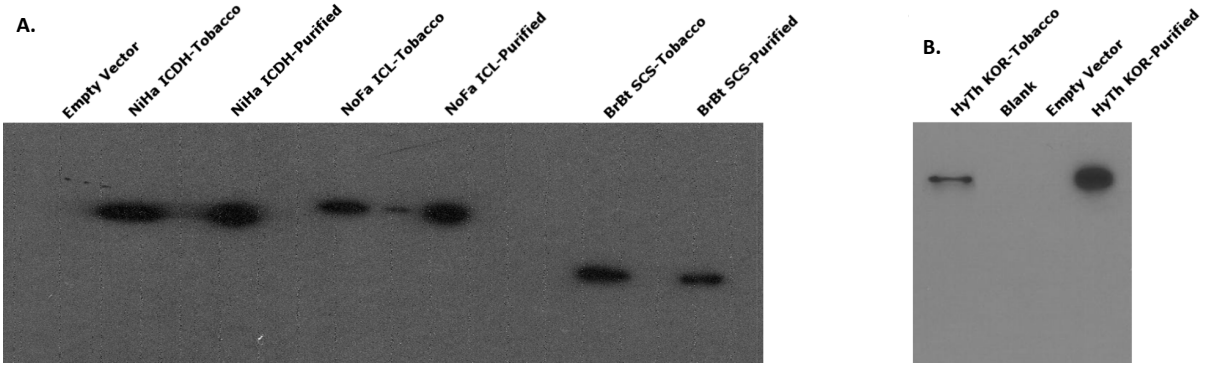

Figure 2-7. Transient tobacco expression western blots of crTCA cycle enzymes. Tobacco leaf tissue was harvested and ground in liquid nitrogen to produce extracts. Tobacco lysate was purified by nickel IMAC, prior to SDS-PAGE and transfer to PVDF. A.) NiHa OSR, NoFa ICL, and BrBT SCS were detected using a penta-his primary antibody. These expressions were conducted using *N. tabacum*. The empty vector transformed tobacco was used as a negative control, while purified recombinant enzymes were used as positive controls. B.) HyTh KOR expression was conducted using *N. benthamiana.* HyTh KOR was detected using an antibody specific for a peptide epitope for the large subunit of the HyTh KOR. Empty vector-transformed tobacco was used as a negative control and purified HyTh KOR was used as a positive control.

The expression of the crTCA cycle enzymes was detected using western blots (Figure 2-7). Detection of the HyTh-KOR required expression in *N. benthamiana* instead of *N. tabacum,* as no HyThKOR was detected using *N. tabacum*. To confirm functional expression, enzyme activity was measured in protein extracted from the tobacco leaf tissue. *In planta* activity was found for each of the four enzymes, confirming functional expression of each enzyme (Table 2-5).

Table 2-5. crTCA cylce enzyme activity from transient tobacco expression.

Enzyme	**Specific Activity, EV** [a] **(10^{-3} u/mg)**[b]	**Specific Activity, crTCA (10^{-3} u/mg)**[b]
Enzyme 1:BrBT SCS	133 ± 7	170 ± 5
Enzyme 2:HyTh KOR	0.02 ± 0.01	0.17 ± 0.06
Enzyme 4:NiHa OSR	2.7 ± 0.5	9.0 ± 0.4
Enzyme 5:NoFa ICL	1.9 ± 0.3	4.7 ± 0.3

[a]Empty Vector

[b] The results are an average of 3 replicates, and the error represented as one standard deviation.

2.4 Discussion

The increases in global population require higher agricultural productivity of crops to satisfy the growing demand for food, feed and fiber. One of the strategies is to improve the carbon fixation efficiency (Bar-Even et al., 2010; Ducat and Silver, 2012; Zhu et al., 2010). Several possible carbon fixation cycles have been proposed by Bar-Even et al., considering the kinetics, energetic cost, thermodynamics and topological compatibility with the endogenous metabolic network (Bar-Even et al., 2010). Although synthetic pathways can fix carbon based on computational models, no experimental evidence has verified their feasibility. Here we demonstrate the *in vitro* carbon fixation of a four-enzyme crTCA cycle

and the ability of plants to express functional enzymes with chloroplast targeting. This is the first demonstration of a reverse TCA cycle-based synthetic carbon fixation cycle *in vitro*, and the first demonstration of a functional four-step carbon fixation cycle.

The selection of the most suitable enzymes for the synthetic crTCA cycle in plants is one of the key steps in this work. The crTCA cycle has not been found in any one organism, but is composed of enzymes from several different bacteria (Table 2-1). Initially, several candidate enzymes were screened for each crTCA cycle step based on the physiology of source bacteria, and their predicted functions. The enzymatic activities were determined *in vitro* by spectrophotometry using recombinant enzymes produced in *E. coli.* Those enzymes with the most favorable performance were selected for assessment of the full crTCA cycle. Partial and full cycle function was detected *in vitro* using isotope based LC-MS. While initially designed to function with five enzymatic steps, it was demonstrated that this version of the cycle functions with only four steps. This does not mean that a five step crTCA cycle is not possible, but suggests that careful enzyme assessment and selection is required, particularly in identifying an OGC enzyme. Lastly, the four enzymes were evaluated for functional expression *in planta*.

One factor limiting the formation of the multiple labeled metabolites is the ability of the cycle to operate in the reverse direction. This reverse reaction was evaluated, and demonstrated that when the cycle is provided with glyoxylate and succinate as starting material, the amount of glyoxylate decreases rapidly (Figure 2-5). This creates a "see-saw" effect that limits the accumulation of multiple ^{13}C-labeled metabolites. Several strategies could be employed to limit this activity. The first is the incorporation of malate synthase, (MS), which is the endogenous partner of ICL in the glyoxylate pathway. This enzyme

condenses glyoxylate to malate with acetyl CoA. This method was employed in the *in vitro* demonstration of the carbon fixing crotonyl-CoA/ethylmolonyl-CoA/hydroxybutyryl-CoA (CETCH) cycle (Schwander et al., 2016). To ensure efficient coupling of the ICL and malate synthase activities, a bifunctional ICL/MS enzyme could be utilized (Nakazawa et al., 2011). Also, to limit reverse cycle activity and enhance crTCA cycle function, enzyme engineering could be employed. Particularly engineering of ICL could reduce reverse activity and of OSR to increase carboxylation activity and reduce affinity for isocitrate.

Additionally, while reduced ferredoxin is abundant in photosynthetically active plant chloroplasts in the light (Schürmann, 2003), it is a challenge to provide reduced ferredoxin for the *in vitro* carbon fixation of the crTCA cycle. Therefore we developed a reaction with ^{13}C-labeling for LC-MS detection and took advantage of the reversibility of the KOR reaction, the second step of the cycle. By initiating the full cycle reactions with 2-OG, KOR was able to decarboxylate 2-OG and reduce ferredoxin, thus building up a pool of reduced ferredoxin. This reduced ferredoxin was then able to be used again by KOR for carboxylation. In the full cycle reactions, the production of the multiple ^{13}C-labeled products supported the finding that the synthetic crTCA cycle can fix carbon as predicted. However, this remains a limiting factor for the cycle, which could be enhanced with the implementation of a reductant replenishing system. Such a system was implemented in the CETCH cycle for regeneration of NADPH and ATP (Schwander et al., 2016). A system to readily regenerate reduced ferredoxin would enhance cycle activity and help prevent cycle reversal. While the inclusion of these additional enzymes would be useful for further optimization and assessment *in vitro*, it is unlikely their inclusion would be beneficial *in vivo* or *in planta,*

particularly as plants have pathways for metabolism of glyoxylate and robust reductant metabolism (Dalal et al., 2015a; Hanke and Mulo, 2013; Kebeish et al., 2007).

The synthetic crTCA cycle consumes one molecule of ATP, two molecules of reduced ferredoxin and one molecule of NAD(P)H as the energetic cost, fixes two molecules of CO_2 and produces one molecule of glyoxylate. The energetic cost of fixation for one CO_2 by the crTCA cycle and conversion of glyoxylate into 3-phosphoglycerate is five ATPs and eight e- equivalents, compared to nine ATPs and six e- equivalents when one carbon is fixed by the Calvin-Benson cycle. While the four-step version of the cycle appears promising, Bar-Even, et al. raise concerns about the function of this cycle and others like it under physiological conditions due to thermodynamic bottlenecks (Bar-Even et al., 2010). Further evaluation of the crTCA cycle *in vivo* is required to assess function under physiological conditions. Analysis of the crTCA cycle activity *in vitro* will help in the feasibility analysis and implementation in plants.

In summary, we have successfully demonstrated the function of a short synthetic *in vitro* carbon fixation cycle. Each of these enzymes can be functionally expressed in a relevant plant host, supporting the feasibility for implementation of this technology for crop improvement.

References

Bainbridge, G., Madgwick, P., Parmar, S., Mitchell, R., Paul, M., Pitts, J., Keys, A.J., Parry, M.A.J., 1995. Engineering Rubisco to change its catalytic properties. J. Exp. Bot. 46, 1269–1276.

Bar-Even, A., Noor, E., Lewis, N.E., Milo, R., 2010. Design and analysis of synthetic carbon fixation pathways. Proc. Natl. Acad. Sci. U. S. A. 107, 8889–8894.

Borland, A.M., Hartwell, J., Weston, D.J., Schlauch, K.A., Tschaplinski, T.J., Tuskan, G.A., Yang, X., Cushman, J.C., 2014. Engineering crassulacean acid metabolism to improve water-use efficiency. Trends Plant Sci. 19, 327–338.

Bridger, W.A., Ramaley, R.F., Boyer, P.D., 1969. Succinyl coenzyme a synthetase from *Escherichia coli*. Methods Enzymol. 13, 70–75.

Chell, R.M., Sundaram, T.K., Wilkinson, A.E., 1978. Isolation and characterization of isocitrate lyase from a thermophilic *Bacillus* sp. Biochem. J. 173, 165–77.

Dalal, J., Lopez, H., Vasani, N.B., Hu, Z., Swift, J.E., Yalamanchili, R., Dvora, M., Lin, X., Xie, D., Qu, R., Sederoff, H.W., 2015a. A photorespiratory bypass increases plant growth and seed yield in biofuel crop *Camelina sativa*. Biotechnol. Biofuels 8, 175.

Dalal, J., Yalamanchili, R., La Hovary, C., Ji, M., Rodriguez-Welsh, M., Aslett, D., Ganapathy, S., Grunden, A., Sederoff, H., Qu, R., 2015b. A novel gateway-compatible binary vector series (PC-GW) for flexible cloning of multiple genes for genetic transformation of plants. Plasmid 81, 55–62.

Dean, A.M., Koshland, D.E., 1993. Kinetic mechanism of *Escherichia coli* isocitrate dehydrogenase. Biochemistry 32, 9302–9.

Ducat, D.C., Silver, P.A., 2012. Improving carbon fixation pathways. Curr. Opin. Chem. Biol. 16, 337–344.

Ellis, R.J., 1979. The most abundant protein in the world. Trends Biochem. Sci. 4, 241–244.

Eswar, N. *et al.* Comparative Protein Structure Modeling Using MODELLER. in *Current Protocols in Protein Science* Chapter 2**,** 2.9.1-2.9.31 (John Wiley & Sons, Inc., 2007).

Hanke, G., Mulo, P., 2013. Plant type ferredoxins and ferredoxin-dependent metabolism. Plant. Cell Environ. 36, 1071–1084.

Hanson, M.R., Lin, M.T., Carmo-Silva, A.E., Parry, M.A.J., 2016. Towards engineering carboxysomes into C3 plants. Plant J. 87, 38–50.

Hügler, M., Sievert, S.M., 2011. Beyond the Calvin Cycle: Autotrophic Carbon Fixation in the Ocean. Ann. Rev. Mar. Sci. 3, 261–289.

Jarvis, P., 2008. Targeting of nucleus-encoded proteins to chloroplasts in plants. New Phytol. 179, 257–85.

Kanao, T., Kawamura, M., Fukui, T., Atomi, H., Imanaka, T., 2002. Characterization of isocitrate dehydrogenase from the green sulfur bacterium *Chlorobium limicola*. A carbon dioxide-fixing enzyme in the reductive tricarboxylic acid cycle. Eur. J. Biochem. 269, 1926–31.

Kebeish, R., Niessen, M., Thiruveedhi, K., Bari, R., Hirsch, H.-J., Rosenkranz, R., Stäbler, N., Schönfeld, B., Kreuzaler, F., Peterhänsel, C., 2007. Chloroplastic photorespiratory bypass increases photosynthesis and biomass production in *Arabidopsis thaliana*. Nat. Biotechnol. 25, 593–599.

Kurek, I., Chang, T.K., Bertain, S.M., Madrigal, A., Liu, L., Lassner, M.W., Zhu, G., 2007. Enhanced Thermostability of *Arabidopsis* Rubisco Activase Improves Photosynthesis and Growth Rates under Moderate Heat Stress. Plant Cell 19, 3230–3241.

Leegood, R.C., 2013. Strategies for engineering C4 photosynthesis. J. Plant Physiol. 170, 378–388.

Lin, M.T., Occhialini, A., Andralojc, P.J., Parry, M.A.J., Hanson, M.R., 2014. A faster Rubisco with potential to increase photosynthesis in crops. Nature 513, 547–550.

Lindbo, J.A., 2007. High-efficiency protein expression in plants from agroinfection-compatible Tobacco mosaic virus expression vectors. BMC Biotechnol. 7, 52.

Lu, W., Clasquin, M.F., Melamud, E., Amador-Noguez, D., Caudy, A.A., Rabinowitz, J.D., 2010. Metabolomic Analysis via Reversed-Phase Ion-Pairing Liquid Chromatography Coupled to a Stand Alone Orbitrap Mass Spectrometer. Anal. Chem. 82, 3212–3221.

Nakazawa, M., Nishimura, M., Inoue, K., Ueda, M., Inui, H., Nakano, Y., Miyatake, K., 2011. Characterization of a Bifunctional Glyoxylate Cycle Enzyme, Malate Synthase/Isocitrate Lyase, of *Euglena gracilis*. J. Eukaryot. Microbiol. 58, 128–133.

Ogren, W.L., 1984. Photorespiration: Pathways, Regulation, and Modification. Annu. Rev. Plant Physiol. 35, 415–442.

Ogren, W.L., Bowes, G., 1971. Ribulose Diphosphate Carboxylase regulates Soybean Photorespiration. Nature 230, 159.

Pham, T. V, Murkin, A.S., Moynihan, M.M., Harris, L., Tyler, P.C., Shetty, N., Sacchettini, J.C., Huang, H.-L., Meek, T.D., 2017. Mechanism-based inactivator of isocitrate lyases 1 and 2 from *Mycobacterium tuberculosis*. Proc. Natl. Acad. Sci. U. S. A. 114, 7617–7622.

Schürmann, P., 2003. Redox Signaling in the Chloroplast: The Ferredoxin/Thioredoxin System. Antioxid. Redox Signal. 5, 69–78.

Schwander, T., Schada von Borzyskowski, L., Burgener, S., Cortina, N.S., Erb, T.J., 2016. A synthetic pathway for the fixation of carbon dioxide in vitro. Science. 354, 900–904.

Warren, G.B., Tipton, K.F., 1974. Pig liver pyruvate carboxylase. Purification, properties and cation specificity. Biochem. J. 139, 297–310.

Yamamoto, M., Ikeda, T., Arai, H., Ishii, M., Igarashi, Y., 2010. Carboxylation reaction catalyzed by 2-oxoglutarate : ferredoxin oxidoreductases from *Hydrogenobacter thermophilus*. Extremophiles 79–85.

Yang, Y., Li, R., Qi, M., 2000. In vivo analysis of plant promoters and transcription factors by agroinfiltration of tobacco leaves. Plant J. 22, 543–51.

Yoon, K.S., Ishii, M., Igarashi, Y., Kodama, T., 1996. Purification and characterization of 2-oxoglutarate:ferredoxin oxidoreductase from a thermophilic, obligately chemolithoautotrophic bacterium, *Hydrogenobacter thermophilus* TK-6. J. Bacteriol. 178, 3365–8.

Zhu, X.-G., Long, S.P., Ort, D.R., 2010. Improving Photosynthetic Efficiency for Greater Yield. Annu. Rev. Plant Biol. 61, 235–261.

Supplemental Data

Supplemental Table 2-1. Primers and expression vectors for crTCA cycle gene cloning.

Gene name	Organism source	Expression Vector	Forward primer (5'-3')	Reverse primer (5'-3')	Tm
AzB5 (SCS)	*Azospirillum* sp. B510	pQE1	ATGAACATCCATGAATACCAG	ACAATTTCACACAGGAAACAGCTA	65°C
AzVi (SCS)	*Azotobacter vinelandii* DJ	pQE1	ATGAATCTGCATGAATACCAGGGC	ACAATTTCACACAGGAAACAGCTA	65°C
BrBT (SCS)	*Bradyrhizobium* sp. BTAi1	pQE1	ATGAACATCCACGAATACCA	AACGACGGCCAGTGAATTCGAGC	65°C
BrBT (SCS)	*Bradyrhizobium* sp. BTAi1	pET21b	CCGATGACCCCATATGAACATCCACGAATACCA	CGAATGCATCTAGATGACTCGAGTCCGCTCTTCAGTTTTTCAACCAG	70°C
EsCo (SCS)	*Escherichia coli* K-12 substr. MG1655	pQE1	ATGAACCTGCACGAATACCAAG	AACGACGGCCAGTGAATTCGAGC	65°C
BaM3 (KOR)	*Bacillus* sp. M3-13	pQE1	ATGATTAACCAACTGTCCTGGAA	ACAATTTCACACAGGAAACAGCTA	65°C
BaM3 (KOR)	*Bacillus* sp. M3-13	pET21b	GCATCTAGATGACCCCATATGATTAAC	ATCCGATGACTCGAGTCCCATAAATTCC	65°C
BaM3 (KOR)	*Bacillus* sp. M3-13	pET28a	GCATCTAGATGACCCCATATGATTAAC	ATCCGATGACTCGAGTTACATAAATTCC	65°C
HaNR (KOR)	*Halobacterium* sp. NRC-1	pQE1	ATGCCGTACTGGAGCACCGCTGGCC	AACGACGGCCAGTGAATTCGAGC	65°C
HaPa (KOR)	*Haladaptatus paucihalophilus* DX253	pQE1	ATGCAGGATCTGAACTGGGC	ACAATTTCACACAGGAAACAGCTA	65°C
HyTh (KOR)	*Hydrogenobacter thermophilus* TK-6	pQE1	ATGGCGTTTGACCTGACGATTAAGATTG	AACGACGGCCAGTGAATTCGAGC	65°C
HyTh (KOR)	*Hydrogenobacter thermophilus* TK-6	pET21b	GGGATCCGATGTCTCATATGGCGTTT	TCGCGAATGACTCGAGATCACAAATTCCCA	70°C
HyTh (KOR)	*Hydrogenobacter thermophilus* TK-6	pET28a	GGGATCCGATGTCTCATATGGCGTTT	TCGCGAATGCCTCGAGATCCCAAATTTACA	65°C
MaMC (KOR)	*Magnetococcus* sp. MC-1	pQE1	ATGGAAAAGAAGGACCTGA	ACAATTTCACACAGGAAACAGCTA	65°C
PaLa (KOR)	*Paenibacillus larvae* subsp. larvae B-3650	pQE1	ATGATTAGCCAACTGAGCT	ACAATTTCACACAGGAAACAGCTA	65°C
PaLa (KOR)	*Paenibacillus larvae* subsp. larvae B-3650	pET21b	GCATCTAGATGACCCCATATGATTAGC	GGATCCGATGACTCGAGTGGCTTAAA	65°C
PaLa (KOR)	*Paenibacillus larvae* subsp. larvae B-3650	pET28a	GCATCTAGATGACCCCATATGATTAGC	GGGATCCGATGACTCGAGTTACTTA	60°C

Supplemental Table 2-1. (continued).

Gene name	Organism source	Expression Vector	Forward primer (5'-3')	Reverse primer (5'-3')	Tm
NiDe (OGC)	*Canditatus Nitrospira defluvii*	pQE1	ATGTTCCGTAAAATCCTGATCG	ACAATTTCACACAGGAAACAGCTATGAC	67°C
HyTh (OGC)	*Hydrogenobacter thermophilus TK-6*	pQE1	ATGTTCAAAAAAGTCCTGGTCGC	ACAATTTCACACAGGAAACAGCTATGAC	71.4°C
ThVi (OGC)	*Thiocystis violascens DSM198*	pQE1	ATGCTGCGTAAGATCCTGATTGCGAA	ACAATTTCACACAGGAAACAGCTATGAC	71.9°C
MaFe (OGC)	*Mariprofundus ferrooxydans PV-1*	pQE1	ATGTTTAAGCGTATCCTGGTGGC	ACAATTTCACACAGGAAACAGCTA	70°C
PsSt (OGC)	*Pseudomonas stutzeri ATCC14405*	pQE1	ATGCGTATCAATGACTTCCGTATCGTC	ACAATTTCACACAGGAAACAGCTATGAC	71.4°C
ChLi (OSR)	*Chlorobium limicola* DSM245	pQE1	ATGGCCTCCAAGTCCACGATTAT	AACGACGGCCAGTGAATTCGAGC	66°C
NiHa (OSR)	*Nitrosococcus halophilus* NC4	pQE1	ATGGCCTACGACAAGATTAGCCT	ACGACGGCCAGTGAATTCGAG	66°C
Gene name	Organism source	Expression Vector	Forward primer (5'-3')	Reverse primer (5'-3')	Tm
KoOl (OSR)	*Kosmotoga olearia TBF 19.5.1*	pQE1	ATGGAAGGTCAAAAGATTAAAGTG	ACGACGGCCAGTGAATTCGAG	66°C
MgPr (OSR)	Marine gamma proteobacterium HTCC2080	pQE1	ATGTCATACAAGCATATTAAAGTCC	ACAATTTCACACAGGAAACAGCTA	62°C
CoGl (ICL)	*Corynebacterium glutamicum* ATCC	pQE1	ATGTCAAATGTCGGCAAACC	ACGACGGCCAGTGAATTCGAG	64°C
GoAl (ICL)	*Gordonia alkanivorans* NBRC 16433	pQE1	ATGAGCAATGTGGGCAAACC	ACAATTTCACACAGGAAACAGCTA	62°C
NoFa (ICL)	*Nocardia farcinica* IFM 10152	pQE1	ATGAGCACCACCGGCACCCC	AACGACGGCCAGTGAATTCGAGC	66°C
RdPy (ICL)	*Rhodococcus pyridinivorans* AK37	pQE1	ATGAGCACGACCGGCACCCC	AACGACGGCCAGTGAATTCGAGC	66°C
HyTh-fdx	*Hydrogenobacter thermophilus* TK-6	pQE1	ATGGCTCTGCGCACGATG	ACAATTTCACACAGGAAACAGCTA	58°C

A.

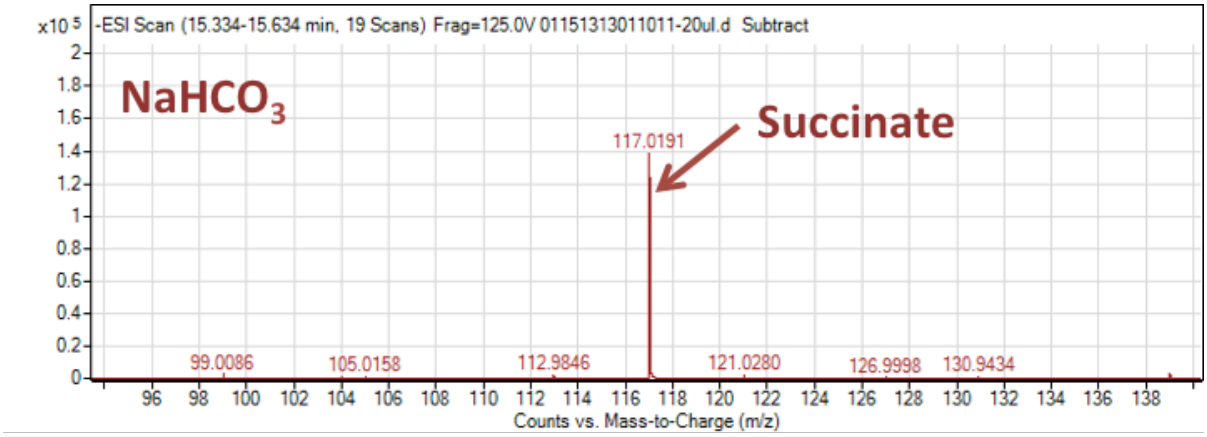

B.

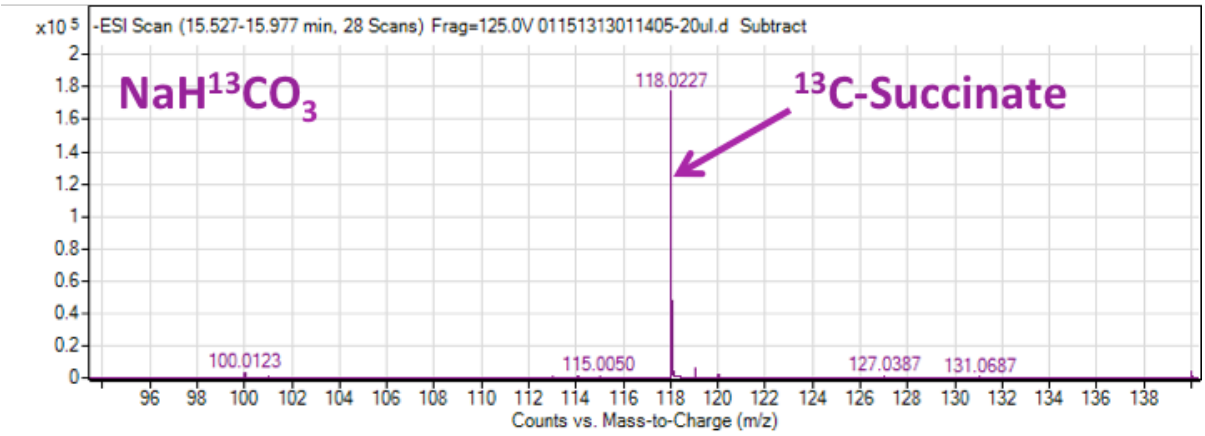

Supplemental Figure 2-1. Unlabeled and ^{13}C-labeled succinate produced by the OGC/OSR/ICL reaction. Reactions were prepared containing MaFe OGC, NiHa OSR, and NoFa ICL with the starting metabolite being 2-OG. Reactions incubated at room temperature for 30 min prior to analysis by LC-MS. Panel A shows the LC-MS detected succinate peak using unlabeled bircarbonate. Panel A shows the LC-MS detected succinate peak using ^{13}C-labeled bicarbonate.

A.

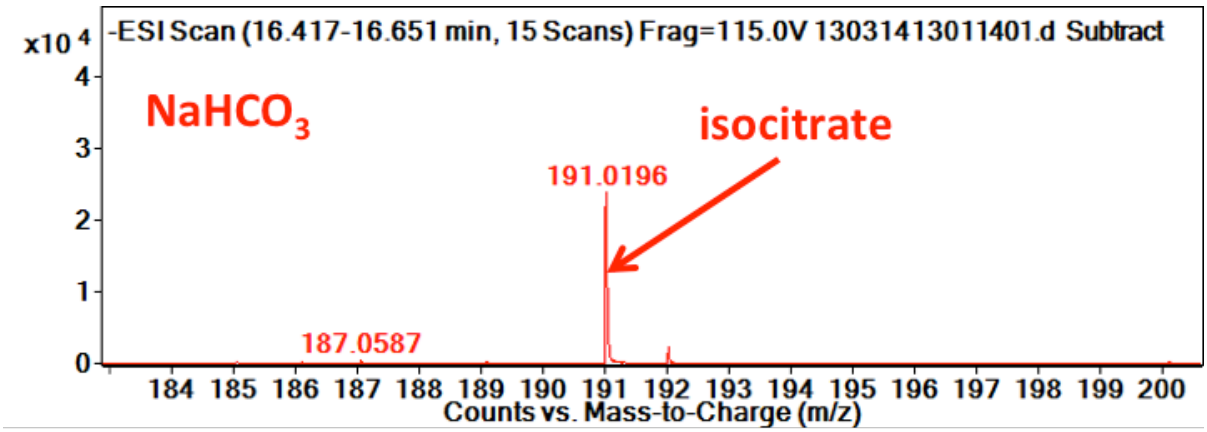

B.

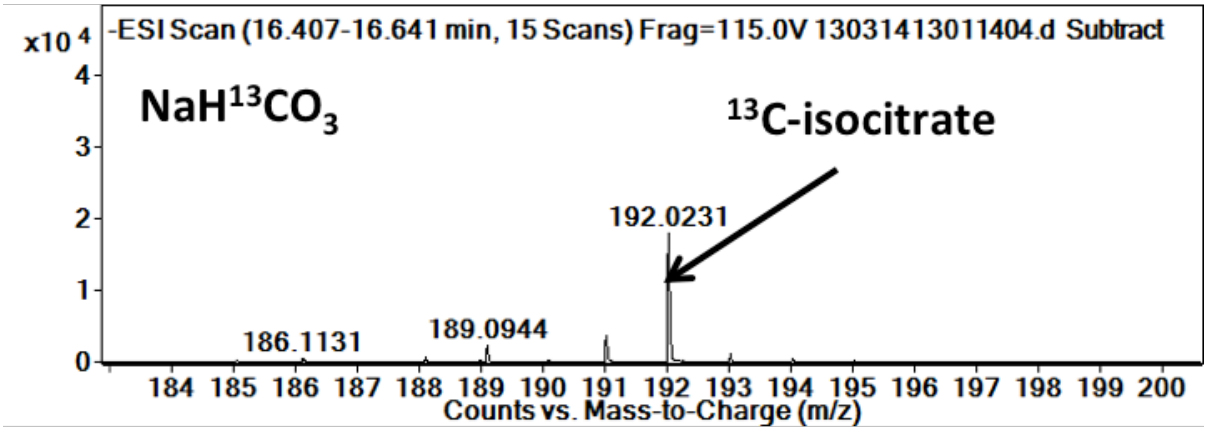

Supplemental Figure 2-2. Unlabeled and ^{13}C-labeled isocitrate produced by the OGC/OSR reaction. Reactions were prepared containing MaFe OGC and NiHa OSR with the starting metabolite being 2-OG. Reactions incubated at room temperature for 30 min prior to analysis by LC-MS. Panel A shows the LC-MS detected isocitrate peak using unlabeled bircarbonate. Panel A shows the LC-MS detected isocitrate peak using ^{13}C-labeled bicarbonate.

CHAPTER 3

Characterization of a 2-oxoglutarate:ferredoxin oxidoreductase from *Bacillus sp.* M3-13

Caroline M. Smith-Moore, Benjamin Bobay, and Amy Grunden

Abstract

The 2-oxoacid:ferredoxin oxidoreductase family enzymes are responsible for oxidative decarboxylation and carboxylation of 2-oxoacids in bacteria and archaea. These functions are essential for metabolism, particularly for energetically challenging reactions such as carboxylation reactions in the reverse TCA cycle and aromatic ring reduction. Despite their importance, this enzyme family has not been extensively studied. To generate increases in plant biomass, there is interest in incorporating alternative carbon fixation cycles into the plant chloroplast. Of particular interest is the enzyme 2-oxoglutarate:ferredoxin oxidoreductase (KOR) for its carboxylation activity in the reverse TCA cycle. However, the majority of characterized KOR enzymes are thermophilic and may not be active in the mesophilic conditions of the plant chloroplast. Using the KOR sequence from the thermophilic bacteria *Hydrogenobacter thermophilus* TK-6 shown to perform carboxylation, a homologous enzyme was identified from the mesophilic bacteria *Bacillus* sp. M3-13. The KOR from *Bacillus* sp. M3-13 was recombinantly expressed, characterized, and evaluated for carboxylation activity.

3.1 Introduction

2-oxoacid:ferredoxin oxidoreductase (OFOR) family enzymes play a pivotal role in bacterial and archaeal metabolism (Adams and Kletzin, 1996; Fuchs, 2011; Gibson et al., 2016; Ragsdale and Pierce, 2008). These enzymes are capable of oxidative decarboxylation and carboxylation of 2-oxoacids (Adams and Kletzin, 1996; Fuchs, 2011). OFOR enzymes perform a Coenzmye A (CoA)-dependent oxidative decarboxylation of 2-oxoacids (Adams and Kletzin, 1996). The electrons produced from this reaction reduce low potential ferredoxins (-500 mV) (Li and Elliott, 2016). These low potential ferredoxins are then capable of donating electrons for energetically challenging reactions such as aromatic ring reduction and carboxylation reactions (Dörner and Boll, 2002; Fuchs, 2011; Li and Elliott, 2016; Ragsdale and Pierce, 2008). OFOR enzymes are also capable of catalyzing carboxylation reactions as part of the reductive TCA cycle (Fuchs, 2011). Given the increased focus on the utilization of microbial enzymes to fix CO_2, produce valuable chemical building blocks, and breakdown complex aromatic structures, the identification and characterization of OFOR family enzymes potentially involved in these pathways is of great interest (Bar-Even et al., 2010; Dörner and Boll, 2002; Vuoristo et al., 2016).

OFOR enzymes are grouped by their 2-oxoacid substrate preference. Pyruvate ferredoxin oxidoreductase (POR) is the best characterized given its important role in linking glycolysis to the Wood-Ljundahl pathway (Furdui and Ragsdale, 2000; Ragsdale and Pierce, 2008). The 2-oxoglutarate/2-ketoglutarate ferredoxin oxidoreductase (KOR) has been shown to be an important enzyme in the rTCA cycle and for providing reduced ferredoxin for benzoyl-CoA reductase (Dörner and Boll, 2002; Ebenau-Jehle et al., 2003; Yamamoto et al., 2010). The least well characterized OFOR enzymes are the 2-ketoisovalerate oxidoreductase,

and the indolepyruvate oxidoreductase (Heider et al., 1996; Mai and Adams, 1996). A recently characterized addition to the OFOR enzyme family is the oxalate oxidoreductase, which does not utilize CoA unlike other OFOR enzymes (Pierce et al., 2010).

Enzymes of the OFOR family have a variety of subunit compositions (α_2, $(\alpha\beta)_2$, $(\alpha\beta\gamma)_2$, $(\alpha\beta\gamma\delta)_2$, and $(\alpha\beta\gamma\delta\varepsilon)_2$) (Gibson et al., 2016). The first structural characterization of an OFOR family enzyme was from the monomeric (α_2) POR of *Desulfovirbrio africanis* (Chabrière et al., 1999). Recently, structures have also been made available for the OOR ($(\alpha\beta\gamma)_2$) from *Moorella thermoacetica*, and a $(\alpha\beta)_2$ subunit type OFOR from *Sulfolobus tokodaii* which can catalyze reactions with both pyruvate and 2-oxoglutarate (Gibson et al., 2015; Yan et al., 2016). The structures and sequence analysis have shown that OFOR enzymes are multidomain, containing at least four domains (I, II, III, and VI; (Gibson et al., 2016). Domains I and VI coordinate the binding of the thiamine pyrophosphate (TPP) cofactor, and a [4Fe-4S] cluster (domain VI) (Gibson et al., 2016; Yan et al., 2016). Many OFOR enzymes also contain domain V, which possesses an additional 2 [4Fe-4S] clusters (Gibson et al., 2016). Despite the different substrate specificities and minimal sequence identity, the structure of these enzymes, their 2-oxoacid binding pockets, and position of other conserved motifs are markedly similar (Gibson et al., 2015; Yan et al., 2016).

To generate a synthetic rTCA cycle for implementation in the plant chloroplast, a KOR enzyme was sought, which would produce 2-oxoglutarate through the carboxylation of succinyl-CoA. The only KOR enzyme with characterized carboxylation activity is the heterodimeric KOR from *Hydrogenobacter thermophilus* TK-6 (Yamamoto et al., 2010, 2003). This enzyme has been shown to have a lower K_m for succinyl-CoA than 2-oxoglutarate, suggesting a preference for the carboxylation reaction (Yamamoto et al., 2010).

However, the thermoactive nature of this enzyme (optimal temperature for activity > 70°C) makes its use in a plant system problematic. To find a suitable KOR enzyme, the *H. thermophilus* TK-6 sequence was used to find a homologous sequence from a mesophillic organism. While many potential matches were found, the putative, heterodimeric KOR from *Bacillus* sp. M3-13 was chosen due to its sequence similarity to the *H. thermophilus* KOR, as well as the growth conditions of the organism. The bacteria *Bacillus* sp. M3-13 was isolated from a desiccation lagoon in Cuatro Cienegas, Coahuila, Mexico (Alcaraz et al., 2010). It is moderately halophillic, grows in the presence of oxygen, and at mesophillic temperatures (Alcaraz et al., 2010). Cuatro Cienegas is an oligotrophic environment unable to support the growth of algae that instead relies on sulfur redox reactions as the basis for most microbial metabolism that has been observed to date (Alcaraz et al., 2011). To ascertain whether the genes identified from *Bacillus* sp. M3-13 do encode a functional KOR, the genes were expressed in *E. coli*, and the resulting enzymes were purified, characterized, and evaluated for carboxylation activity.

3.2 Materials and Methods

3.2.1 Bacterial Strains, Plasmids, and Enzymes

The *E. coli* strain XL-1 blue (Novagen, EMD Bioscience, San Diego, CA) was used for cloning and plasmid storage and *E. coli* strain BL21(DE3) (Novagen, EMD Bioscience) was for overexpression and purification. The expression plasmids pET21b and pET28a were obtained from Novagen, EMD Bioscience. Restriction endonucleases and T4 DNA ligase were from New England Biolabs (Ipswich, MA). Primers were synthesized by Eurofins

MWG Operon (Huntsville, AL). Gene synthesis was conducted by Genscript (Piscataway, NJ).

3.2.2 Identification and Selection

The heterodimeric KOR subunits from the thermophillic bacterium (α and β) *Hydrogenobacter thermophilus* TK-6 were used as the query sequences for BLAST-p analysis. The resulting sequences were prioritized based on their similarity to the query and the growth conditions of the bacterial source organism (mesophilic and oxygen tolerant). The sequences, which came from appropriate organisms, were then analyzed for conserved residues indicated in the literature and in the Conserved Domains Database (CDD) to be associated with substrate and co-factor binding. The KOR from *Bacillus* sp. M3-13, from here on referred to as BaM3-KOR, was identified and used for all experiments.

3.2.3 Molecular Modeling and Simulations

PDBs of the α and β subunits were obtained through submission of the amino acid sequences in intensive mode to the Phyre 2 server (Kelley et al., 2015). The PDBs were duplicated and overlaid with the biologically active unit of 5b47 (Yan et al., 2016) within PyMol (The PyMOL Molecular Graphics System, version 1.7.4; Schrödinger, LLC). TPP, MG and SF4 from 5b47 were retained while PYR was removed and 2-oxoglutrate (created in ChemDraw (ChemDraw; PerkinElmer Informatics)) was placed in a similar conformation to that of the removed PYR.

The molecular dynamic (MD) simulations were performed with the GROMACS 5.0.1 software package utilizing 6 CPU cores and one NVIDIA Tesla K80 GPU to provide a

solution representation of the heterodimeric complex of 2- α /2- β:TPP, MG, and 2-oxoglutarate. MD simulations were performed with the AMBER 99sb-ildn force field and the flexible simple point-charge water model (Lindorff-Larsen et al., 2010). TPP and 2-oxoglutarate topology and parameter files were generated through the use of AMBER Antechamber (Wang et al., 2006). The initial structures (simple overlay with 5b47 without SF4 ligands) were immersed in a periodic water box with a dodecahedron shape that extended 1 nm beyond the protein in any dimension and neutralized with counterions. Energy minimization was accomplished through use of the steepest descent algorithm with a final maximum force below 100 kJ/mol/min (0.01 nm step size, cutoff of 1.2 nm for neighbor list, Coulomb interactions, and Van der Waals interactions). After energy minimization, the system was subjected to equilibration at 300 K and normal pressure for 1 ns. All bonds were constrained with the LINCS algorithm and virtual sites were used to allow a 4 fs time step (cutoff of 1.4 nm neighbor list, Coulomb interactions, and Van der Waals interactions). After temperature stabilization, pressure stabilization was obtained by utilizing the v-rescale thermostat to hold the temperature at 300K and the Berendsen barostat was used to bring the system to 1 bar pressure. Production MD calculations (500 ns) were performed under the same conditions, except that the position restraints were removed and the simulation was run for 100 ns (cutoff of 1.1, 0.9, and 0.9 nm for neighbor list, Coulomb interactions, and Van der Waals interactions). GROMACS built-in and homemade scripts were used to analyze the MD simulation results. In general, the last 100 ns of each simulation was used for analysis which included clustering of similar conformational states into an average structure defined as the middle structure of the r.m.s.d matrix. All images were produced with PyMOL (The PyMOL Molecular Graphics System, version 1.7.4; Schrödinger, LLC).

3.2.4 Cloning and Expression

As is commonly the case for heterodimer proteins, the genes encoding the KOR subunits are located adjacent to one another in the *Bacillus* sp. M3-13 genome with a single promoter driving their . For generating the recombinant expression vector, the intergenic space was preserved between the two KOR sunuit genes, and both subunit gene sequences were synthesized as one contiguous piece, allowing the genes to be expressed in *E. coli* as a cistron. The sequences were synthesized by Genscript with codon optimization for expression in *E. coli* and were ligated into the pUC57 vector at the EcoRV restriction site.

The pUC57 vector containing both of the KOR genes was used for PCR amplification with iProof High-fidelity DNA polymerase (Bio-Rad, Hercules, CA) according to the manufacturer instructions. Forward primers encoded an NdeI restriction site, and reverse primers included the XhoI restriction site for directional cloning into pET21b and pET28a (F: 5'-GCATCTAGATGACCCCATATGATTAAC-3'; R: 5'-ATCCGATGACTCGAGTCC CATAAATTCC-3'). The pET21b and pET28a vectors were chosen for the high level of expression and enabled in-frame fusion of C-or N-terminal His-tags, respectively. As the genes were encoded sequentially, the N-terminal His-tag is fused to the α subunit and the C-terminal His-tag is fused to the β subunit. A schematic of the expression cassettes is provided in Figure 3-1. The NdeI and XhoI digested PCR products were ligated into restriction enzyme-digested pET21b and pET28a using T4 DNA ligase overnight at 16°C. The ligation mix was used to transform *E. coli* strain XL-1 blue. Plasmid DNA was isolated and used for sequence confirmation. Confirmed constructs were used to transform the *E. coli* T7 expression strain BL21(DE3).

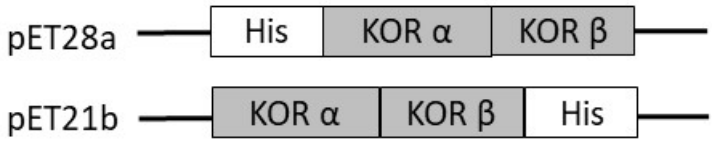

Figure 3-1. BaM3-KOR His-tag position. The BaM3-KOR gene was cloned into pET28a with an N-terminal his-tag on the α subunit, and into pET21b with a C-terminal his-tag on the β subunit. Both subunit genes were expressed as an operon under control of the T7 promoter of the vector.

Soluble *Bacillus* sp.M3-13 KOR expression was achieved by growing BL21(DE3) cells in Luria Bertani (LB) broth to exponential phase at 37 °C (OD_{600nm} 0.6-0.8), inducing them with 0.1 mM IPTG, and decreasing the temperature to 18 °C for expression for 16 h. In order to ensure that the KOR enzyme would contain the required Fe-S clusters and TPP, 1 mM thiamine was added upon culture inoculation and 0.1 mM $FeSO_4$ was added at the time of induction.

3.2.5 Purification

Microaerobic handling was required for KOR enzymes, which involved de-gassing and sparging with argon of all purification buffers, and anaerobic collection of elution fractions. 1 L cell cultures were pelleted by centrifugation, 4,780 rpm for 45 min at 4°C. The pellets were resuspended in 50 mM $NaPO_4$ (pH7.5), 30 mM imidazole, 500 mM NaCl, 1 mM benzamidine–HCl, and 0.01% Triton X100. The cells were lysed using a French pressure cell (1,100 lb/in^2). The lysed suspension was centrifuged at 14,000 x *g* for 40 min at 4°C to remove cell debris. The supernatant was filtered using a 0.45 µm syringe filter prior to loading on the column.

FPLC purification was conducted using a BioRad DuoFlow system. The filtered extract was applied to a 5 ml HisTrap HP Nickel Sepharose™ affinity column (GE Healthcare Life Sciences) and washed with five column volumes of binding buffer (50 mM $NaPO_4$, 500 mM NaCl, 30 mM imidazole, 0.01% Triton x 100, pH 7.5). The elution buffer was 50 mM $NaPO_4$, 500 mM NaCl, 250 mM imidazole, 0.01% Triton X100, pH 7.5. Protein was eluted using a linear gradient with 0% to 100% elution buffer over a 40 ml elution volume. All fractions were analyzed on 12.5% SDS-PAGE.

Fractions containing the BaM3-KOR protein were either desalted into buffer containing 20 mM Tris-HCl, 0.01% Triton x-100, pH 8, using centrifugation filters with a 30 kDa MWCO (Millipore), or combined and stored without desalting as further manipulation caused a reduction in enzyme activity. The enzymes were stored under Argon in stoppered vials with 10% glycerol at -80°C.

3.2.6 Size Exclusion HPLC

BaM3-KOR protein was purified by nickel affinity chromatography as described previously. To prepare the protein for size-exclusion chromatography (SEC), the protein was desalted on a Hiprep 26/10 desalting column (GE Healthcare Life Sciences) into 20 mM Tris (pH 8), 150 mM NaCl, and 0.01% Triton x-100. The desalted BaM3-KOR was then run on a Hiprep 16/60 Sephacryl S-200 HR SEC column (GE Healthcare Life Sciences). Both purification steps were conducted on a BioRad Duoflow system using anaerobic buffers and sample collection.

The purified sample was analyzed by SEC HPLC on a Shimadzu (Columbia, MD) Prominence HPLC system with an Agilent (Santa Clara, CA) Advance Bio SEC 300 column (250 mm x 2.6 mm). The injection volume was 10 µL at 0.35 mL/min. The mobile phase was

phosphate buffered saline (pH 7.4), with a column temperature of 30 °C. Elution was monitored with a photodiode array detector at 280 nm. The molecular weight standard was the Aqueous SEC 1 standard from Phenomenex (Torrance, CA).

3.2.7 Spectrophotometric Analysis

Purified BaM3-KOR was analyzed by UV spectrophotometry for the presence of [4Fe-4S] clusters, which have an absorbance at approximately 410 nm. The absorbance spectrum of 0.5 mg/mL BaM3-KOR samples in 100 µL was analyzed with a spectral scan measuring in 1 nm increments from 255-500 nm using a Thermo Scientific BioMate 3S, UV-Vis spectrophotometer.

3.2.8 Activity Assays

KOR activity was detected in a continuous spectrophotometric assay following the enzyme-, substrate-, and time-dependent reduction of oxidized benzyl viologen at 600 nm. The assay measures the ability of KOR to donate an electron to benzyl viologen, indicating its decarboxylation of 2-oxoglutarate. The reaction mix contained 50 mM Tris (pH 8), 1 mM benzyl viologen, 2.5 mM 2-oxoglutarate, 0.5 mM coenzyme A, 4 mM $MgCl_2$, and 0.025 mM sodium dithionite. Optimal reaction conditions were determined empirically by varying pH and temperature. The following buffers were used for pH evaluation: MES (pH 6), $NaPO_4$ (pH 7-7.5), Tris (pH 8-8.5), and CAPS (pH 9). For kinetic measurements, the substrate amounts were varied (CoA: 0.5mM – 5 µM and 2-oxoglutarate: 3mM – 10 µM). The reaction mixture was prepared without the 2-oxoglutarate, de-gassed, and sparged with argon. The assay was performed in anaerobic gas-tight glass cuvettes. The KOR enzyme was treated with 5 mM DTT for 15 min prior to adding the enzyme to the reaction mix. The

reaction was started by the addition of 2-oxoglutarate using gas-tight glass syringes. Activity was read continuously at 600 nm on a Shimadzu UV-2401PC UV-visible spectrophotometer with a thermostatted cuvette holder. An extinction coefficient for reduced benzyl viologen of 8.3 mM^{-1} cm^{-1} was used for calculating the activity, and the activity unit is defined as μmol min^{-1} (Adams and Hall, 1979).

In addition to oxidative decarboxylation activity, some KOR enzymes have carboxylation activity leading to the synthesis of 2-oxoglutarate. To evaluate the activity of BaM3-KOR for this reverse reaction, assays were conducted measuring the oxidation of benzyl viologen. The reaction mixture contained 50 mM Tris (pH 8), 4 mM $MgCl_2$, 1 mM benzyl viologen, 100 mM $NaHCO_3$, and 0.5 mM succinyl CoA. Prior to the addition of the enzyme, the benzyl viologen was reduced by the addition of dithionite until an A_{600} of 0.5-0.6 was reached. The approximate final concentration of dithionite in the reaction was 6 mM. The reaction was started with the addition of 6 μg of KOR enzyme through a gas tight syringe. Due to the sensitivity of benzyl viologen to oxidation, all reaction components were maintained under anaerobic conditions by sparging with argon. Reactions were performed in glass cuvettes with rubber stoppers. The reaction was monitored continuously on a Shimadzu UV-2401PC UV-visible spectrophotometer with a thermostatted cuvette holder maintaining a temperature of 35 °C.

3.2.9 Genbank Accession Numbers

The nucleotide sequence for the *Hydrogenobacter thermophilus* TK-6 KOR is available through Genbank, with accession number AB046568.1. The *E. coli* codon

optimized *Bacillus* sp.M3-13 KOR nucleotide sequence is available through Genbank as well with the accession number MG552118.

3.3 Results and Discussion

3.3.1 Sequence Selection/Alignment

The *Hydrogenobacter thermophilus* TK-6 KOR amino acid sequences for the α and β subunits were used to identify candidate KOR proteins using BLAST-p. The *H. thermophilus* TK-6 KOR was chosen as the template due to its increased affinity for succinyl-CoA, which drives the reaction toward carboxylation to produce 2-oxoglutarate (Yamamoto et al., 2010). While the BLAST-p analysis yielded a large number of potential KOR enzymes, the list was further refined to organisms which preferred mesophilic growth conditions and were able to tolerate oxygen. These characteristics were desirable in a host organism to ensure that the chosen enzymes would be functional in a mesophilic, aerobic system, such as the plant chloroplast.

Once the host organism growth conditions were met, the sequences were evaluated for sequence identity and the presence of conserved motifs. The sequence identity between the *H. thermophilus* TK-6 sequences and those for the candidate genes were fairly low, between 31-48%. Low sequence identity among OFOR family enzymes is common, though structure is more conserved (Gibson et al., 2016, 2015; Yan et al., 2016). The *Bacillus* sp. M3-13 KOR was identified with approximately 38% identity for the α subunit, and 43% identity for the β subunit. As mentioned previously, *Bacillus* sp. M3-13 was isolated from a desiccation lagoon in Cuatro Cienegas, Coahuila, Mexico and is mesophilic, oxygen tolerant, and moderately halophilic (Alcaraz et al., 2010). While this organism has been isolated, its

growth and metabolism have not been characterized in depth outside of genomic annotation (Alcaraz et al., 2011).

In addition to sequence identity, there are several conserved motifs, which were evaluated. Of structurally characterized OFOR enzymes, the most similar to BaM3-KOR is the $(\alpha\beta)_2$ POR/KOR from *Sulfolobus tokodaii* (Yan et al., 2016). Alignments of the amino acid sequences of the *S. tokodaii, H. thermophilus* TK-6, and BaM3-KOR subunits can be seen in Figure 3-2. The YPITP motif located on the α subunit is highly conserved in the OFOR family and is involved in 2-oxoacid and TPP binding (Chabrière et al., 1999; Gibson et al., 2015; Yan et al., 2016). Additional residues associated with 2-oxoacid binding are found in both the α and β subunits, indicated with asterisks in Figure 3-2 (Yan et al., 2016). Interestingly, the BaM3-KOR has 100% identity for the active site residues identified for the *S. tokodaii* POR/KOR, but has low activity with pyruvate as the substrate (Figure 3-11). This may suggest that there are additional residues responsible for this shift in substrate preference. Despite attempts at structural characterization of OFORs, there is still little information known about the binding site for CoA in OFOR enzymes (Chabrière et al., 1999; Gibson et al., 2016; Yan et al., 2016). Other important residues are the four cysteine residues in the β subunit responsible for Fe-S cluster binding, indicated with diamonds in Figure 3-2. The presence of the four cysteine residues, suggests that BaM3-KOR maintains one [4Fe-4S] cluster, similar to other $(\alpha\beta)_2$ OFOR enzymes.

Figure 3-2. Alignment of $(\alpha\beta)_2$ OFOR amino acid sequences. Alignment of OFOR amino acid sequences for the α subunit (A.) and the β subunit (B.) from *Bacillus* sp. M3-13, *Hydrogenobacter thermophilus* TK-6, and *Sulfolobus tokodaii*. Amino acid sequences were obtained from NCBI. Active site residues based on the *S. tokodaii* structure are indicated with a (*), and cysteine residues responsible for binding the 4Fe-4S cluster are indicated (w). Alignments were created using T-Coffee (Notredame et al., 2000).

A.

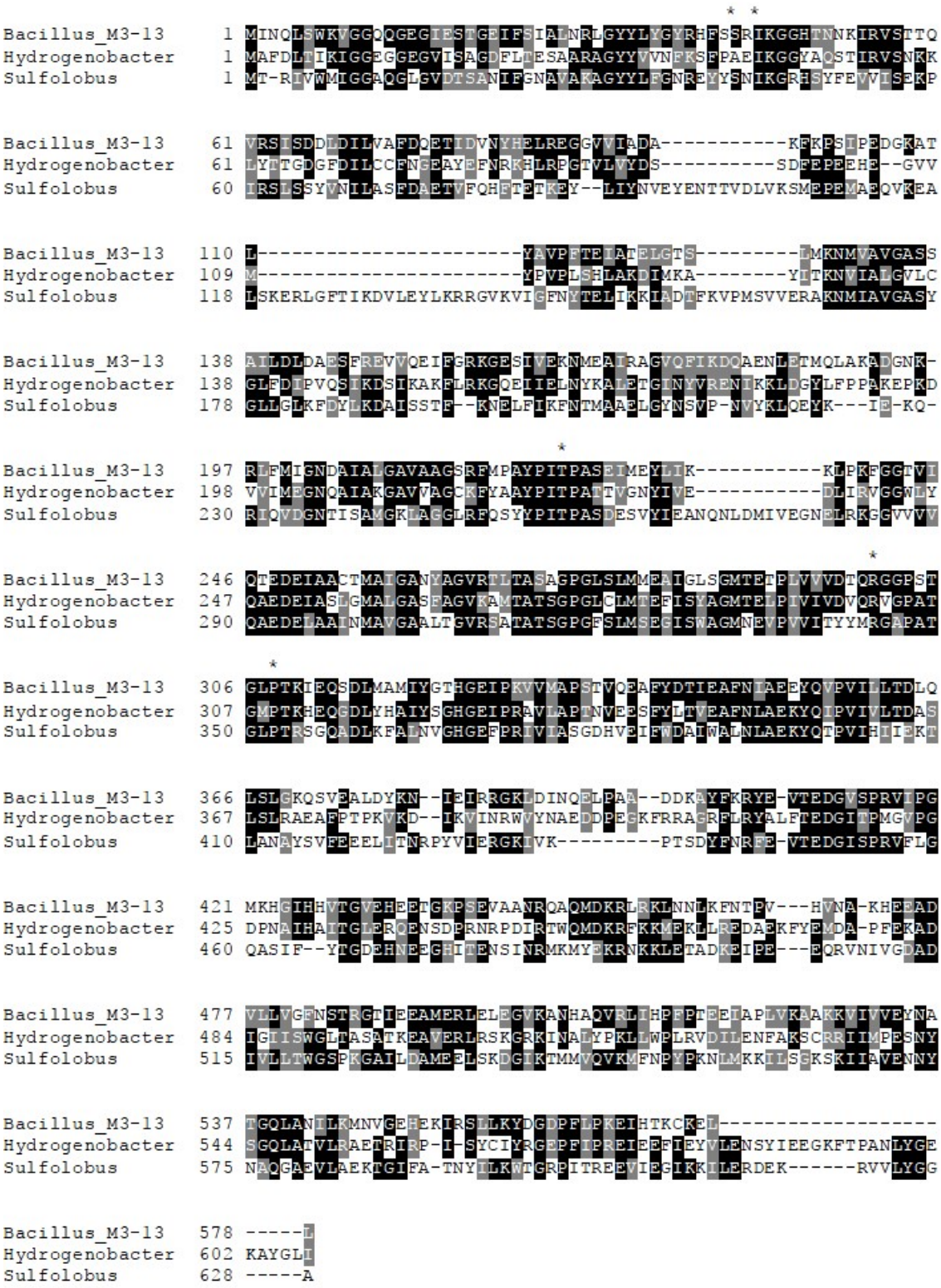

B.

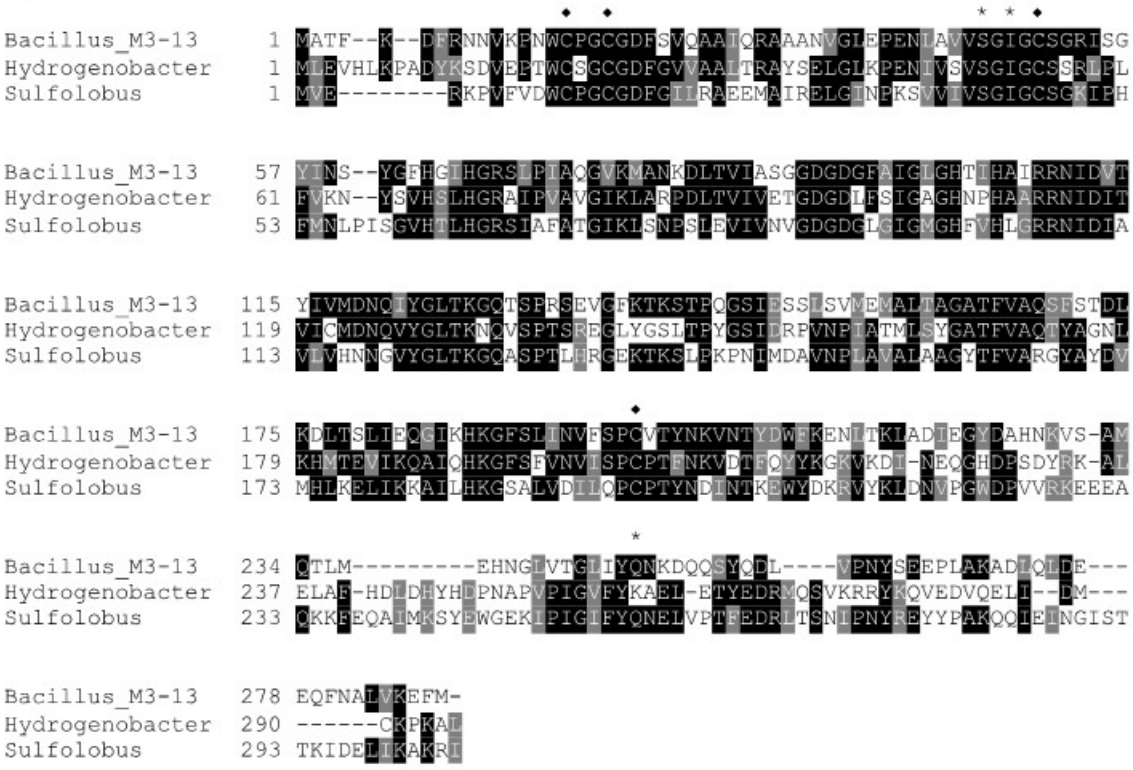
Bacillus_M3-13 1 MATF--K--DFRNNVKPNWCPGCGDFSVQAAIQRAAANVGLEPENLAVVSGIGCSGRISG
Hydrogenobacter 1 MLEVHLKPADYKSDVEPTWCSGCGDFGVVAALTRAYSELGLKPENIVSVSGIGCSSRLPL
Sulfolobus 1 MVE--------RKPVFVDWCPGCGDFGILRAEEMAIRELGTNPKSVVTVSGIGCSGKIPH
Bacillus_M3-13 57 YINS--YGFHGIHGRSLPIAQGVKMANKDLTVIASGGDGDGFAIGLGHTIHAIRRNIDVT
Hydrogenobacter 61 FVKN--YSVHSLHGRAIPVAVGIKLARPDLTVIVETGDGDLFSIGAGHNPHAARRNIDIT
Sulfolobus 53 FMNLPISGVHTLHGRSIAFATGIKLSNPSLEVIVNVGDGDGLGIGMGHFVHLGRRNIDIA
Bacillus_M3-13 115 YIVMDNQIYGLTKGQTSPRSEVGFKTKSTPQGSIPSSLSVVEMALTAGATFVAQSFSTDL
Hydrogenobacter 119 VICMDNQVYGLTKNQVSPTSREGLYGSLTPYGSIDRPVNPLATMLSYGATFVAQTYAGNL
Sulfolobus 113 VLVHNNGVYGLTKGQASPTLLRGEKTKSLPKPNIMDAVNPLAVALAAGYTFVARGYAYDV
Bacillus_M3-13 175 KDLTSLIEQGIKHKGFSLINVFSPCVTYNKVNTYDWFKENLTKLADIEGYDAHNKVS-AM
Hydrogenobacter 179 KHMTEVIKQAIQHKGFSFVNVISPCPTFNKVDTFQYYKGKVKDI-NEQGHDPSDYFK-AL
Sulfolobus 173 MHLKELIKKAILHKGSALVDILQPCPTYNDINTKEWYDKRVYKLDNVPGWDPVVRKEEEA
Bacillus_M3-13 234 QTLM----------EHNGLVTGLIYQNKDQQSYQDL----VPNYSEEPLAKADLQLDE---
Hydrogenobacter 237 ELAF-HDLDHYHDPNAPVPIGVFYKAEL-ETYEDRMQSVKRRYKQVEDVQELI--DM---
Sulfolobus 233 QKKFEQAIMKSYEWGEKIPIGIFYQNELVPTFEDRLTSNIPNYREYYPAKQQIEINGIST
Bacillus_M3-13 278 EQFNALVKEFM-
Hydrogenobacter 290 ------CKPKAL
Sulfolobus 293 TKIDELIKAKRI

3.3.2 Structural Comparison of BaM3-KOR and *S. tokodaii*

To further evaluate the structural differences between BaM3-KOR and the *S. tokadaii* POR/KOR, molecular modeling and molecular dynamic simulations were conducted. The Phyre 2 server was utilized in intensive mode to obtain homology modeled PDB files for the α and β subunits of the BaM3-KOR. The structure with the highest scoring alignment in Phyre 2 to BaM3-KOR was the structure from *S. tokodaii* (PDB: 5b47) (Yan et al., 2016). The *S. tokodaii* structure was then used as a model for the construction of the BaM3-KOR heterodimer complex containing Mg, TPP and replacing pyruvate with 2-oxoglutarate. In order to generate a more accurate model for the BaM3-KOR in solution, molecular dynamic (MD) simulations were conducted to find the minimal energy state. These simulations also enabled analysis of the KOR structure in the presence of the larger 2-oxoglutarate substrate. The full MD modeled BaM3-KOR complex can be seen in Figure 3-3.

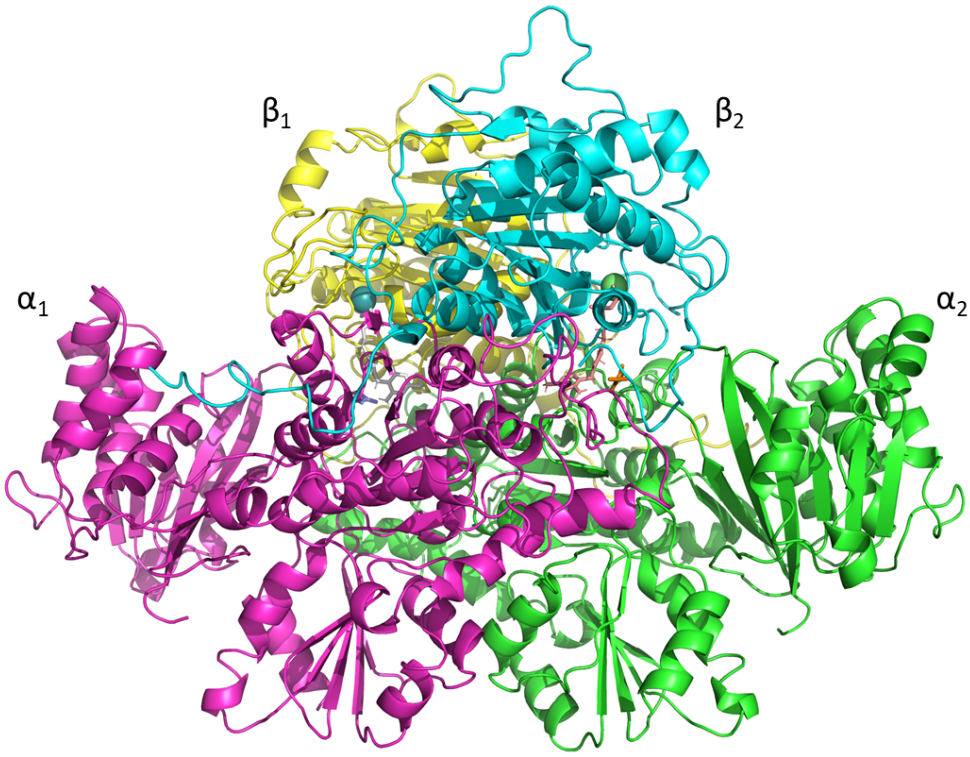

Figure 3-3. Molecular dynamics modeled BaM3-KOR complex structure. The structure was modeled using the *S. tokodaii* crystal structure containing pyruvate (PDB:5b47). The pyruvate was replaced with 2-oxoglutarate for the BaM3-KOR, and molecular dynamic simulations were conducted to allow the structure to relax to the lowest energy state around the new substrate. The chains in yellow and cyan each represent one β subunit, and the chains in magenta and green each represent one α subunit. The α_1 and the β_1 form one of the two heterodimers with the α_2 and β_2 forming the second one. The binding pocket is located between the α and β subunits.

As mentioned previously, it was noted that despite having different substrate preferences, that the BaM3-KOR sequence had 100% identity for the substrate (pyruvate) binding residues identified in *S. tokodaii* (Yan et al., 2016). DoGSiteScorer (Volkamer et al., 2012) was used to characterize the binding pockets for the BaM3-KOR model and the *S. tokodaii* structure. This analysis provides a predicted measure of the volume ($Å^3$), surface area ($Å^2$), and depth (Å) of the binding pocket. The average pocket (A and B) volume for the *S. tokodaii* structure is 1526.1 $Å^3$ with an average surface area of 1334.7 $Å^2$ and a depth of 27.3 Å. The BaM3-KOR MD model has an average binding pocket volume of 2511.57 $Å^3$, a surface area of 2360.5 $Å^2$, and a depth of 36.1 Å. The difference between these values for the two structures likely stems from the comparison of an X-ray crystal structure and a MD simulation model. MD simulations remove crystal contacts, allowing for dynamic conformational changes of the subunits under solution like conditions. The added volume, surface area, and depth found in the BaM3-KOR MD model is likely due to the "tunnels" leading to the TPP/pyruvate/2-oxoglutarate binding pocket. An example of a "tunnel" leading to the 2-oxoglutarate can be seen in Figure 3-4. The dynamics of these "tunnels" could serve as gates, determining which ligands can enter, playing a vital role in substrate specificity for these enzymes. A visual comparison of the two binding pockets can be seen in Figure 3-5.

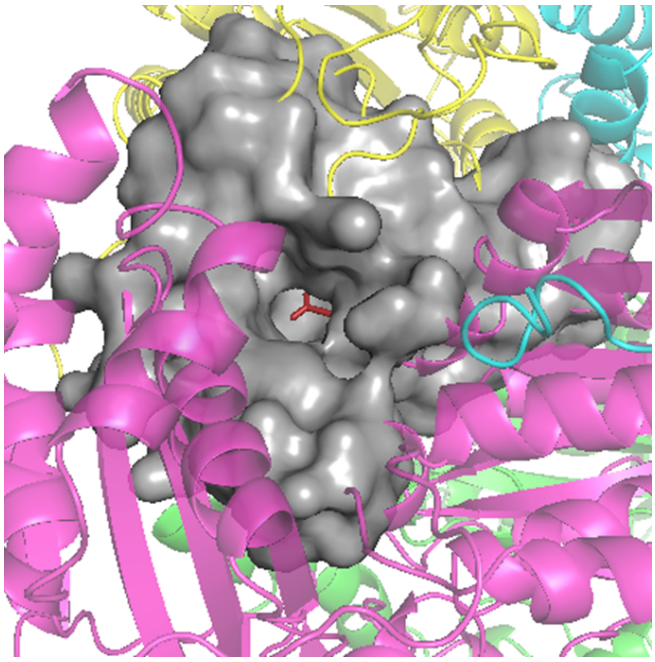

Figure 3-4. BaM3-KOR MD model binding pocket "tunnel." The binding pocket is depicted as a grey surface. The "tunnel" is located at the center of the image with the 2-oxoglutarate in red at the end of the "tunnel." The coloring scheme for the subunits is consistent with that used in Figure 3-3.

Figure 3-5. Analysis of TPP and pyruvate/2-oxoglutarate binding pockets of *S. tokodaii* and BaM3. Panel A and panel B are cartoon depictions of the *S. tokodaii* structure and the BaM3 average MD structure, respectively. The coloring scheme is the same as used in Figures 3-3 and 3-4. The binding pockets are shown as a white surface. On the right are zoomed in images of the binding pockets with the subunits labeled and the residues involved shown in stick format and colored according to the subunit. Panel C shows a sequence alignment of the residues that comprise the binding pocket. The top sequence is the BaM3 KOR, and the bottom sequence is for the *S. tokodaii* enzyme. The colored residues denote the following: red = identical residues, green = strongly similar residues, blue = somewhat similar residues, and black = dissimilar residues. The (•) symbol denotes residues within 5 Å of the TPP, the (‡) symbol denotes residues within 5 Å of pyruvate/2-oxoglutarate, and the □ denotes residues within 5 Å of the Mg^{2+} ion. Lastly, the residues shown in reduced font are residues involved in the creation of the "tunnel" to the binding pocket.

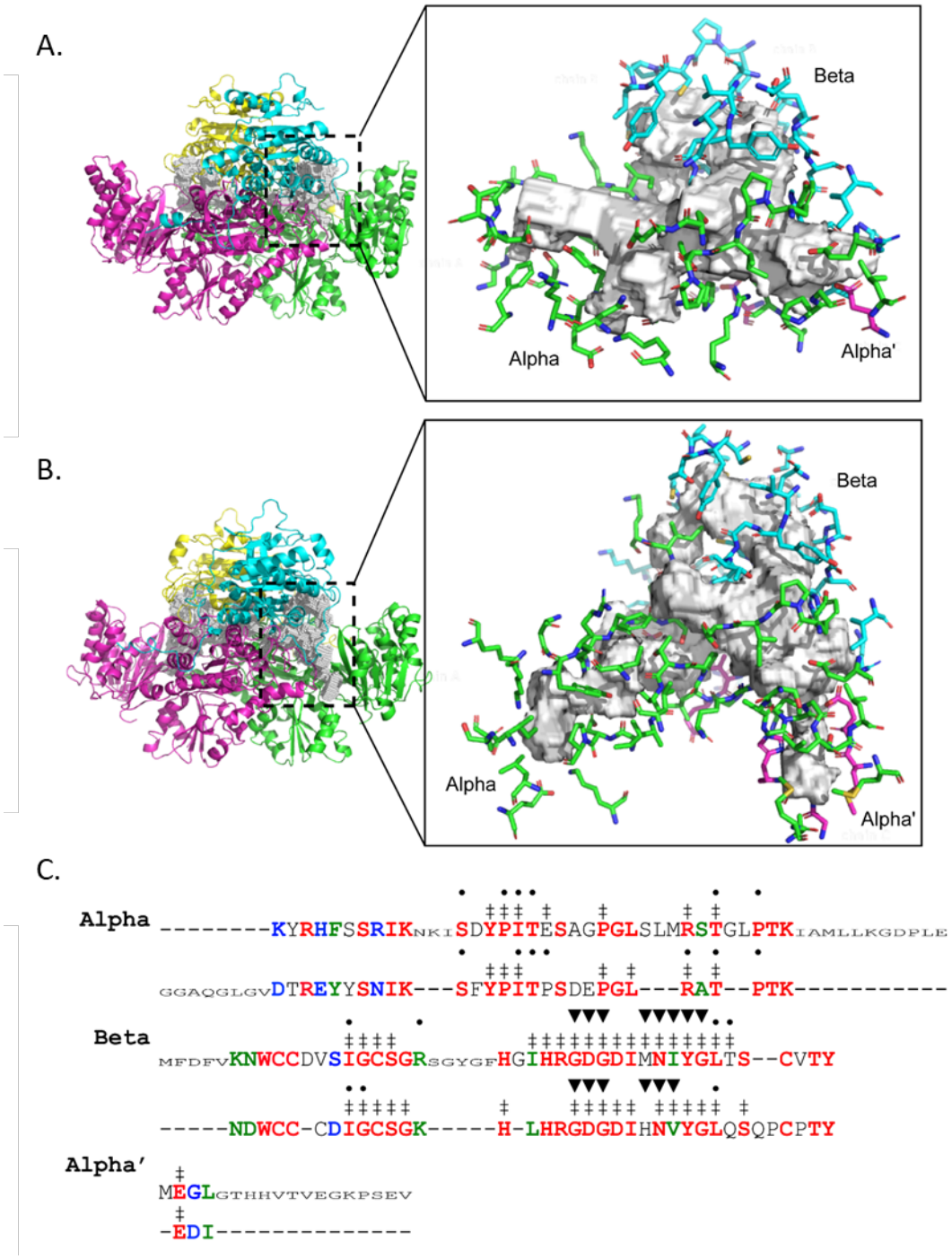
A.
Beta
Alpha
Alpha'
B.
Beta
Alpha
Alpha'
C.
Alpha
Beta
Alpha'

Additionally, the binding pockets for *S. tokodaii* and BaM3 have a similar amino acid composition: apolar ratio of 0.28 and 0.31, polar ratio of 0.41 and 0.39, positive ratio of 0.15 and .018, and a negative ratio of 0.16 and 0.12, respectively. Alignments of the binding pocket resides are presented in Figure 3-5. From the alignments, it can be seen that the binding pockets between the two structures are quite similar with identical residues at a majority of the positions. This similarity likely accounts for the ability of the *S. tokodaii* POR/KOR, and to a smaller extent the BaM3-KOR, to use both pyruvate and 2-oxoglutarate as substrate. However, there are a number of residue differences which likely account for the specificity shown, particularly for the BaM3-KOR. A particularly interesting residue difference in the β subunit is the difference from the Arg residue in BaM3-KOR and the Lys residue in *S. tokodaii* (Figure 3-5 C). In the *S. tokodaii* structure this residue is located near the methyl group of the pyruvate and near the TPP (Yan et al., 2016). Mutation of this Lys residue to Arg in *S. tokodaii* led to an increase in activity with pyruvate as substrate and a coordinate decrease in activity with 2-oxoglutarate (Fukuda and Wakagi, 2002). It is interesting that in BaM3-KOR an Arg exists in the same position, but the enzyme has high affinity for 2-oxoglutarate not pyruvate. Additionally, the Met to His residue mutation between BaM3-KOR and *S. tokodaii* β subunits is interesting. His residues are common catalytic residues as they are capable of carrying out a number of roles due to their ability to be charged or neutral at physiologically relevant pHs, while Met is not commonly associated with active sites (Bartlett et al., 2002). It is possible this change could be affecting the catalytic activity of the BaM3-KOR. Further analysis and mutational studies could help in determining which residues are vital for substrate specificity.

3.3.3 Cloning, Expression, and Purification of Recombinant BaM3-KOR

After selection of the BaM3-KOR enzyme, the *korA* and *korB* genes from *Bacillus* sp. M3-13 were codon optimized for expression in *E. coli* and synthesized. The *korA* and *korB* genes were adjacent in the genome, with the stop codon of *korA* immediately followed by the ATG of the *korB* gene. Upstream of the *korA* stop codon is a potential ribosome binding site for *korB*. As it appeared that the genes are expressed as an operon in *Bacillus* sp. M3-13, the same strategy was used for their expression in *E. coli*, and both genes were synthesized as a contiguous DNA piece. The synthesized DNA encoding the *korA/korB* genes was amplified using PCR and inserted into the expression vectors pET21b and pET28a under the control of the T7 promoter. The pET21b vector allowed for the fusion of a C-terminal 6x His-tag on the β subunit, while the pET28a vector fused an N-terminal 6x His-tag on the α subunit. A diagram of the vector design is provided in Figure 3-1.

Recombinant expression was conducted using *E.coli* BL21(DE3) transformed with pET21b:BaM3-KOR (B21p-KOR) or pET28a:BaM3-KOR (B28p-KOR). Cells were grown in LB media supplemented with 1 mM thiamine and appropriate antibiotic (100 µg/mL ampicillin for pET21b; 50 µg/mL kanamycin for pET28a) at 37 °C until mid-log (OD_{600nm} 0.6-0.8). Once the cells reached mid-log phase the temperature was reduced to 18 °C to enhance soluble protein expression. To induce expression 0.1 mM IPTG was added, and the media was further supplemented with 0.1 mM $FeSO_4$ to provide sufficient iron for Fe-S cluster formation. The expression was allowed to continue for 16 h. Despite the anaerobic nature of the KOR enzyme, anaerobic expression was not necessary, suggesting that the protein is stable in the reducing intracellular environment.

Recombinant expression of B21p-KOR or B28p-KOR was conducted in a 1 L volume for purification. After expression, the cells were pelleted by centrifugation and lysed 3 times using a French pressure cell. The lysate was then centrifuged to separate soluble protein from debris and filtered prior to FPLC purification. In order to limit KOR enzyme contact with oxygen, all buffers used for purification were degassed and sparged with argon. B21p-KOR and B28p-KOR were purified using nickel affinity chromatography. Additionally, all fractions were collected in gas tight serum bottles containing 90% nitrogen, 10% hydrogen. After fraction collection, all fractions were sparged with argon immediately. Fractions containing the BaM3-KOR were yellow/brown in color. The purity of the enzyme was confirmed by SDS-PAGE (Figure 3-6). A slight shift in size of the α subunit for B28p-KOR and the β subunit for B21p-KOR is seen as a result of the location of the His-tag. The enzyme was desalted using centrifugation filters, but was found to result in decreased KOR activity, likely due to increased oxygen contamination. The presence of similar amounts of the α and β subunits for the BaM3-KOR suggests that *E. coli* was able to successfully express both genes from the bicistronic sequence.

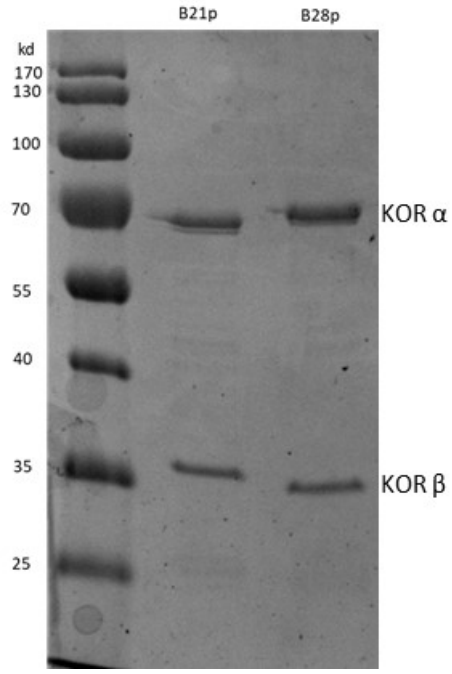

Figure 3-6. SDS-PAGE analysis of purified, recombinant KOR enzymes. 1 μg of each purified BaM3-KOR protein was loaded per well. The expected size for the B21p α BaM3-KOR subunit is 63.4 kDa, and B21p β subunit is 32.5 kDa. The expected size for the B28p α subunit is 65.6 kDa, and the B28p β subunit is 31.4 kDa. Enzymes are estimated to be >90% pure.

To confirm the subunit composition of the KOR holoenzyme, the B21p-KOR protein was evaluated by SEC HPLC. Prior to conducting the HPLC analysis, the B21p-KOR protein was purified as described above with an additional FPLC SEC step. HPLC SEC was able to confirm that the B21p-KOR is a dimer of heterodimers, $(\alpha\beta)_2$ (Figure 3-7). This is the same subunit structure as the *S. tokadaii* POR/KOR (Yan et al., 2016).

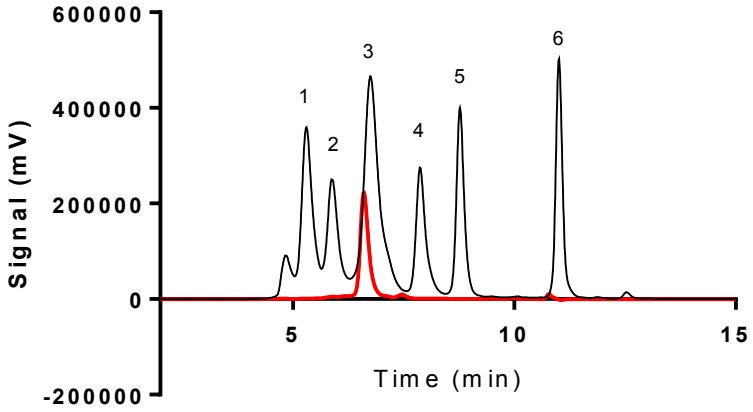

Figure 3-7. Chromatograph showing BaM3-KOR subunit composition. The BaM3-KOR was confirmed to have an $(\alpha\beta)_2$ subunit composition by SEC HPLC. The red line is the BaM3-KOR sample, and the black line is the molecular weight standard. MW standard sizes are 670 kDa (1), 300 kDa (2), 150 kDa (3), 44 kDa (4), 17 kDa (5), and 0.244 kDa (6).

3.3.4 Comparison of B21p-KOR and B28p-KOR Enzyme Properties

Enzymes containing iron-sulfur clusters display characteristic UV/Vis absorption spectra (Kerscher and Oesterhelt, 1981). In order to determine whether the clusters were successfully incorporated into the recombinant BaM3-KORs, the spectrum of each of the BaM3-KOR proteins was evaluated after purification. In addition to the A_{280} peak, the spectra showed a shoulder at 410 nm. This shoulder is characteristic for [4Fe-4S] cluster containing proteins, and is a noted feature of OFOR enzymes (Yan et al., 2014). The shoulder at 410nm is smaller for the B28p-KOR, which could suggest that the B28p-KOR contains fewer bound [4Fe-4S] clusters than the B21p-KOR enzyme (Figure 3-8).

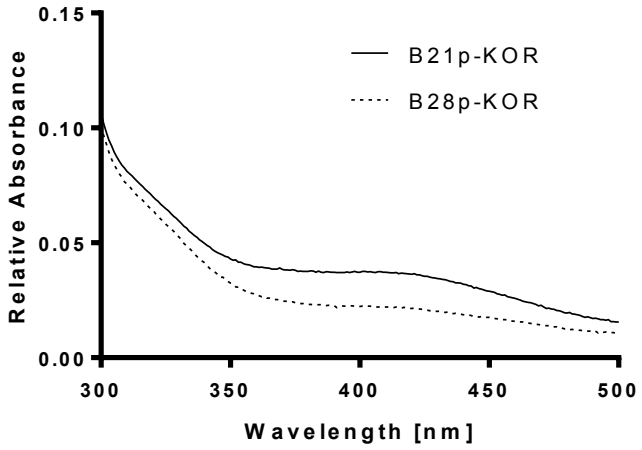

Figure 3-8. Absorption spectra of B21p-KOR and B28p-KOR. Protein concentration was normalized to 0.5 mg/mL for both B21p-KOR and B28p-KOR.

B21p-KOR and B28p-KOR oxidoreductase activities were evaluated using a benzyl viologen reduction assay. It was found that the B21p-KOR had nearly 3-fold higher activity than the B28p-KOR (Figure 3-9). Given the decreased absorbance at 410 nm in the spectrum (Figure 3-8), it is possible that the His-tag position (Figure 3-1) may have affected the activity of the B28p-KOR. From the *S. tokadaii* structure, the C-terminus of the β subunit wraps around the protein surface, whereas the N-terminus of the α subunit is more buried (Yan et al., 2016). Additionally, the N-terminus of the α subunit is in close proximity to residues responsible for interactions with TPP and ferredoxin, which are vital for activity (Yan et al., 2016). This is supported in the BaM3-KOR model. Figure 3-10 depicts the heterodimer highlighting the location of the C-terminus of the β subunit as well as the N-terminus of the α subunit. Due to the increased activity, the B21p-KOR was utilized for further characterization.

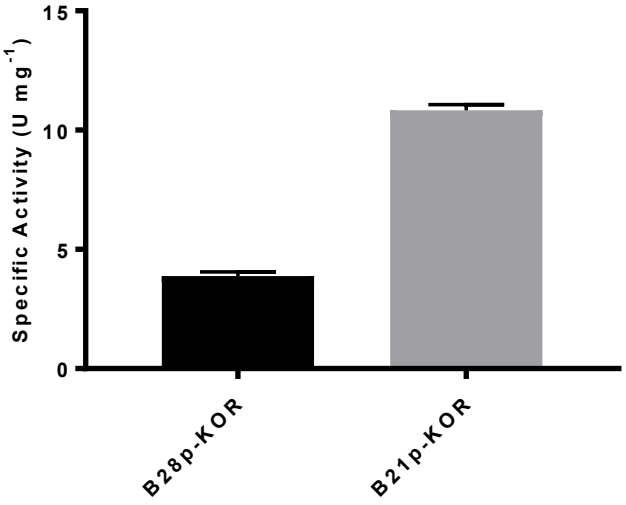

Figure 3-9. Comparison of benzyl viologen reduction activity. Activity was evaluated by measuring benzyl viologen reduction at 600 nm at 35°C and pH 8 to compare the activity of B28p-KOR and B21p-KOR. Reactions were started with the addition of 3 mM 2-oxoglutarate. Data represent an average of three replicates; error bars indicate the standard error.

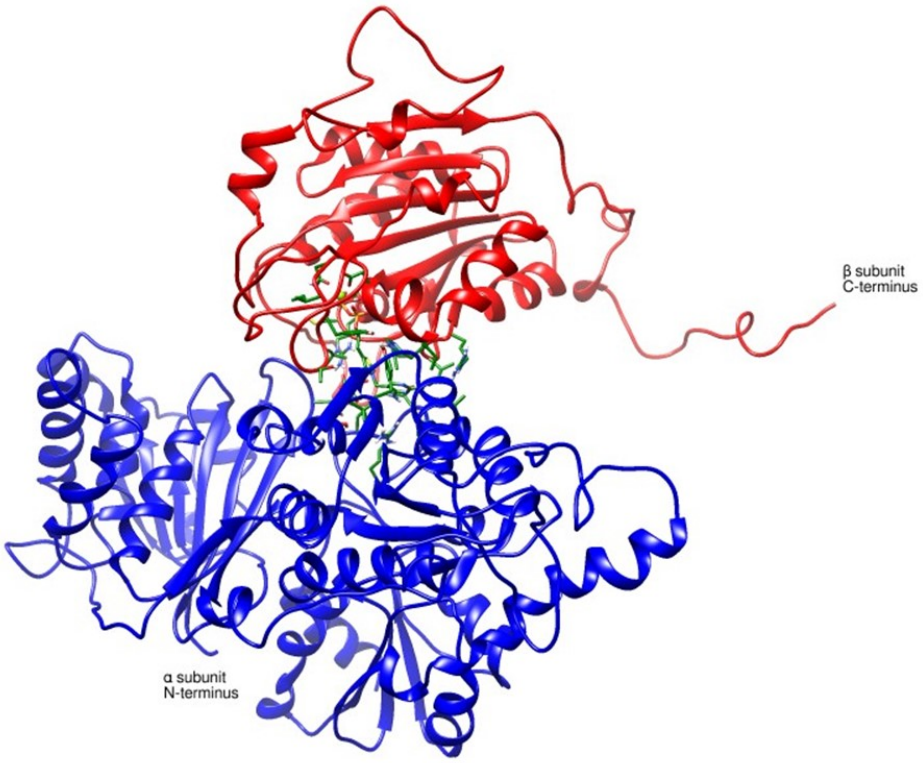

Figure 3-10. Ribbon diagram highlighting the location of the BaM3-KOR termini for accessibility. The C-terminus of the β subunit is extended around the outside of the structure, whereas the N-terminus of the α subunit is less accessible. Structure images were created using Chimera (Pettersen et al., 2004).

3.3.5 B21p-KOR Substrate Specificity and Kinetics

Most OFOR enzymes have high specificity for a particular substrate, 2-oxoacid. The *Hydrogenobacter thermophilus* TK-6 KOR has been shown to have a high specificity for 2-oxoglutarate (Yamamoto et al., 2003). However, other heterodimeric OFOR enzymes have been characterized, which can decarboxylate 2-oxoglutarate and pyruvate (Fukuda and Wakagi, 2002). To evaluate the specificity of B21p-KOR, benzyl viologen reduction assays were conducted utilizing either 2-oxoglutarate or pyruvate as the 2-oxoacid substrate. B21p-KOR was found to be 100-fold more active with 2-oxoglutarate than pyruvate, confirming B21p-KOR is a 2-oxoglutarate ferredoxin oxidoreductase (Figure 3-11).

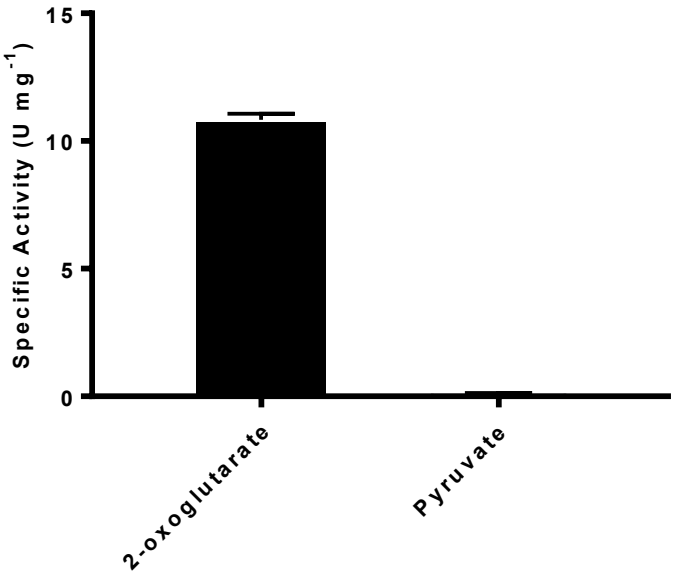

Figure 3-11. 2-Oxoacid substrate preference of B21p-KOR. Substrate preference was evaluated by measuring the reduction of benzyl viologen at 600 nm with either 3 mM 2-oxoglutarate or 3 mM pyruvate at 35°C and pH 8. The specific activity for 2-oxoglutarate is 10.8 ± 0.243 U mg^{-1}, and the specific activity for pyruvate is 0.107 ± 0.029 U mg^{-1}. Data represent an average of three replicates; error bars indicate the standard error.

The ability of B21p-KOR to reduce benzyl viologen was dependent on the presence of CoA and 2-oxoglutarate. The K_m and V_{max} values for 2-oxoglutarate at 35°C and pH 8 were 29.4 μM and 11.29 μmol min^{-1} mg^{-1}, respectively. For CoA, the K_m and V_{max} were found to be 17.8 μM and 11.14 μmol min^{-1} mg^{-1}, respectively. The K_m values show an extremely high affinity for these two substrates compared to the *H. thermophilus* TK-6 KOR (2-oxoglutarate K_m 1.4 mM, and CoA K_m 80 μM) (Yamamoto et al., 2003). The K_m for 2-oxoglutarate is the lowest reported for KOR enzymes (Table 3-1).

Table 3-1. Comparison of K_m values for 2-oxoglutarate and CoA for KOR enzymes.

Organism	2-oxoglutarate, K_m	CoA, K_m	Citation
Bacillus sp. M3-13 KOR	29.4 μM	17.8 μM	This work.
Hydrogenobacter thermophilus TK-6, KOR and FOR	1.4 mM	80 μM	(Yamamoto et al., 2003)
	2.9 mM	26 μM	(Yamamoto et al., 2003)
Thauera aromatica	110 μM	290 μM	(Dörner and Boll, 2002)
Azoarcus evansii	1.2 mM	32 μM	(Ebenau-Jehle et al., 2003)
Sulfolobus tokadaii	720 μM	17 μM	(Fukuda et al., 2001)
Thermococcus litoralis	250 μM	40 μM	(Mai and Adams, 1996)

3.3.6 Effects of pH and Temperature on BaM3-KOR Activity

The effect of temperature was evaluated using the benzyl viologen reduction assay where the temperature was varied between 25 °C and 55 °C. The highest specific activity was found at 35 °C, 10.8 μmol mg^{-1}, while B21p-KOR had approximately 100-fold less activity at 55 °C (Figure 3-12A). The lower relative activity at higher temperatures demonstrates that the enzyme selection strategy was successful in identifying a mesophilic KOR enzyme.

The effect of pH was also evaluated using the benzyl viologen reduction assay. The pH was evaluated within a range of 6 to 9. Optimal pH was determined to be 8-8.5, which had very similar specific activities, 10.8 U mg^{-1} and 10.6 U mg^{-1}, respectively (Figure 3-12B). This pH optimum is similar to the *H. thermophilus* TK-6 KOR (Yamamoto et al., 2003). B21p-KOR has a fairly narrow pH range, between 7-8.5, with little to no activity being detected at pH 6 or pH 9 (Figure 3-12B).

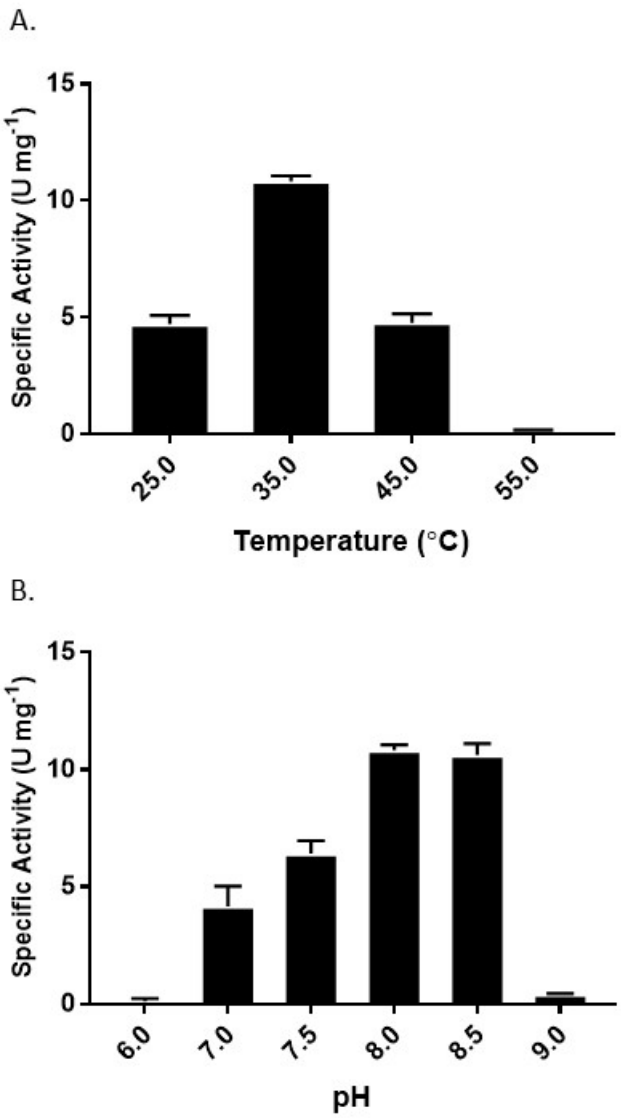

Figure 3-12. Effect of temperature (A) and pH (B) on recombinant B21p-KOR activity. Oxidoreductase activity was evaluated by the reduction of benzyl viologen at 600 nm. Data represent an average of three replicates; error bars indicate the standard error.

3.3.7 Evaluation of Carboxylation Activity

Many OFOR enzymes are hypothesized to possess carboxylation activity for the synthesis of their respective 2-oxoacids, though few have been characterized (Yamamoto et al., 2010). For KOR, this carboxylation activity would lead to the production of 2-

oxoglutarate. This reaction is key for the function of the rTCA cycle (Fuchs, 2011). Carboxylation activity was evaluated for B21p-KOR by measuring the oxidation of benzyl viologen. An evaluation of the rate of oxidation between reactions containing the B21p-KOR enzyme and negative control reactions containing no enzyme revealed that B21p-KOR was not capable of oxidizing benzyl viologen sufficiently under the reaction conditions. The oxidation of the negative control exceeded that of the reactions containing B21p-KOR.

There are a number of potential reasons for these results. Due to the high affinity of B21p-KOR for 2-oxoglutarate, in the reaction as 2-oxoglutarate is produced it may be rapidly converted back into succinyl CoA. This would further reduce benzyl viologen, leading to a perceived decrease in benzyl viologen oxidation. Additionally, the high amount of dithionite required for this reaction may also be inhibitory of B21p-KOR carboxylation activity. Further evaluation with more sensitive assay methods is required for more effective characterization of carboxylation activity.

3.4 Conclusion

KOR enzymes play a vital role in metabolism as participants in the rTCA cycle, and as a source of reduced ferredoxin for energetically challenging reactions (Dörner and Boll, 2002; Ebenau-Jehle et al., 2003; Yamamoto et al., 2010). While the OFOR enzyme family has been discussed in the literature for many years, only a few KOR enzymes have been characterized, with the vast majority of these enzymes coming from extremophilic sources (Dörner and Boll, 2002; Ebenau-Jehle et al., 2003; Mai and Adams, 1996; Tersteegen et al., 1997; Yamamoto et al., 2003). As interest increases in metabolic engineering of alternative

carbon fixation pathways in photosynthetic and other organisms, the characterization of enzymes capable of performing these reactions grows (Bar-Even et al., 2010).

In this work, a thermophilic KOR amino acid sequence from *H. thermophilus* TK-6 was used to perform a BLAST-p search to identify a mesophilic KOR enzyme. The KOR from *Bacillus* sp. M3-13 was identified, cloned, and recombinantly expressed in *E. coli*. The structure of the enzyme was evaluated using molecular modeling and molecular dynamic simulations. The binding pocket was identified and analysis suggests that both difference in residue composition and dynamics likely account for the substrate preferences for the BaM3-KOR. BaM3-KOR showed the greatest activity at pH 8 and 35 °C. This enzyme had a very high affinity for its substrates, particularly 2-oxoglutarate, which has the lowest K_m reported to date. The mesophilic activity observed for BaM3-KOR suggests that it could be a good candidate for metabolic engineering in plants and bacteria. Further characterization and mutational studies of the KOR to enhance carboxylation function, would enable to BaM3-KOR to be utilized in synthetic CO_2 fixation cycles in plants (Bar-Even et al., 2010). Additionally, the ability of KOR enzymes, like BaM3-KOR, to provide reduced ferredoxin is useful in the metabolic engineering of bacteria for bioremediation of aromatic compounds (Carmona et al., 2009).

References

Adams, M.W.W., Hall, D. 0, 1979. Properties of the Solubilized Membrane-Bound Hydrogenase from the Photosynthetic Bacterium *Rhodospirillum rubrum*. Arch. Biochem. Biophys. 195, 288–299.

Adams, M.W.W., Kletzin, A., 1996. Oxidoreductase-type Enzymes and Redox Proteins Involved in Fermentative Metabolisms of Hyperthermophilic Archaea. Adv. Protein Chem. 48, 101–180.

Alcaraz, L., Moreno-Hagelsieb, G., Eguiarte, L.E., Souza, V., Herrera-Estrella, L., Olmedo, G., 2010. Understanding the evolutionary relationships and major traits of *Bacillus* through comparative genomics. BMC Genomics 11, 332.

Alcaraz, L.D., Lopez-Ramirez, V., Moreno-Letelier, A., Herrera-Estrella, L., Souza, V., Olmedo-Alvarez, G., 2011. Genomics of Bacteria from an Ancient Marine Origin: Clues to Survival in an Oligotrophic Environment, in: Dar, I.A. (Ed.), Earth and Environmental Sciences. InTech.

Bar-Even, A., Noor, E., Lewis, N.E., Milo, R., 2010. Design and analysis of synthetic carbon fixation pathways. Proc. Natl. Acad. Sci. U. S. A. 107, 8889–8894.

Bartlett, G.J., Porter, C.T., Borkakoti, N., Thornton, J.M., 2002. Analysis of Catalytic Residues in Enzyme Active Sites. J. Mol. Biol. 324, 105–121.

Carmona, M., Zamarro, M.T., Blázquez, B., Durante-Rodríguez, G., Juárez, J.F., Valderrama, J.A., Barragán, M.J.L., García, J.L., Díaz, E., 2009. Anaerobic catabolism of aromatic compounds: a genetic and genomic view. Microbiol. Mol. Biol. Rev. 73, 71–133.

Chabrière, E., Charon, M.H., Volbeda, a, Pieulle, L., Hatchikian, E.C., Fontecilla-Camps, J.C., 1999. Crystal structures of the key anaerobic enzyme pyruvate:ferredoxin oxidoreductase, free and in complex with pyruvate. Nat. Struct. Biol. 6, 182–90.

Dörner, E., Boll, M., 2002. Properties of 2-oxoglutarate:ferredoxin oxidoreductase from *Thauera aromatica* and its role in enzymatic reduction of the aromatic ring. J. Bacteriol. 184, 3975–83.

Ebenau-Jehle, C., Boll, M., Fuchs, G., 2003. 2-Oxoglutarate:NADP(+) oxidoreductase in *Azoarcus evansii*: properties and function in electron transfer reactions in aromatic ring reduction. J. Bacteriol. 185, 6119–29.

Fuchs, G., 2011. Alternative Pathways of Carbon Dioxide Fixation: Insights into the Early Evolution of Life? Annu. Rev. Microbiol. 65, 631–658.

Fukuda, E., Kino, H., Matsuzawa, H., Wakagi, T., 2001. Role of a highly conserved YPITP motif in 2-oxoacid:ferredoxin oxidoreductase: heterologous expression of the gene from *Sulfolobus* sp.strain 7, and characterization of the recombinant and variant enzymes.

Eur. J. Biochem. 268, 5639–46.

Fukuda, E., Wakagi, T., 2002. Substrate recognition by 2-oxoacid:ferredoxin oxidoreductase from *Sulfolobus* sp. strain 7. Biochim. Biophys. Acta 1597, 74–80.

Furdui, C., Ragsdale, S.W., 2000. The role of pyruvate ferredoxin oxidoreductase in pyruvate synthesis during autotrophic growth by the Wood-Ljungdahl pathway. J. Biol. Chem. 275, 28494–9.

Gibson, M.I., Brignole, E.J., Pierce, E., Can, M., Ragsdale, S.W., Drennan, C.L., 2015. The Structure of an Oxalate Oxidoreductase Provides Insight into Microbial 2-Oxoacid Metabolism. Biochemistry 54, 4112–4120.

Gibson, M.I., Chen, P.Y.T., Drennan, C.L., 2016. A structural phylogeny for understanding 2-oxoacid oxidoreductase function. Curr. Opin. Struct. Biol. 41, 54–61.

Heider, J., Mai, X., Adams, M.W.W., 1996. Characterization of 2-Ketoisovalerate Ferredoxin Oxidoreductase, a New and Reversible Coenzyme A-Dependent Enzyme Involved in Peptide Fermentation by Hyperthermophilic Archaea. J. Bacteriol. 178, 780–787.

Kelley, L.A., Mezulis, S., Yates, C.M., Wass, M.N., Sternberg, M.J.E., 2015. The Phyre2 web portal for protein modeling, prediction and analysis. Nat. Protoc. 10, 845–858.

Kerscher, L., Oesterhelt, D., 1981. The Catalytic Mechanism of 2-Oxoacid : Ferredoxin Oxidoreductases from *Halobacterium halobium* One-Electron Transfer at Two Distinct Steps of the Catalytic Cycle. Eur. J. Biochem 116, 595–600.

Li, B., Elliott, S.J., 2016. The Catalytic Bias of 2-Oxoacid:ferredoxin Oxidoreductase in CO2: Evolution and reduction through a ferredoxin-mediated electrocatalytic assay. Electrochim. Acta 199, 349–356.

Lindorff-Larsen, K., Piana, S., Palmo, K., Maragakis, P., Klepeis, J.L., Dror, R.O., Shaw, D.E., 2010. Improved side-chain torsion potentials for the Amber ff99SB protein force field. Proteins Struct. Funct. Bioinforma. 78, 1950-8.

Mai, X., Adams, M.W.W., 1996. Characterization of a fourth type of 2-keto acid-oxidizing enzyme from a hyperthermophilic archaeon: 2-Ketoglutarate ferredoxin oxidoreductase from *Thermococcus litoralis*. J. Bacteriol. 178, 5890–5896.

Notredame, C., Higgins, D.G., Heringa, J., 2000. T-Coffee: A Novel Method for Fast and Accurate Multiple Sequence Alignment. J. Mol. Biol. 302, 205–217.

Pettersen, E.F., Goddard, T.D., Huang, C.C., Couch, G.S., Greenblatt, D.M., Meng, E.C., Ferrin, T.E., 2004. UCSF Chimera-A visualization system for exploratory research and analysis. J. Comput. Chem. 25, 1605–1612.

Pierce, E., Becker, D.F., Ragsdale, S.W., 2010. Identification and characterization of oxalate oxidoreductase, a novel thiamine pyrophosphate-dependent 2-oxoacid oxidoreductase

that enables anaerobic growth on oxalate. J. Biol. Chem. 285, 40515–24.

Ragsdale, S.W., Pierce, E., 2008. Acetogenesis and the Wood–Ljungdahl pathway of CO2 fixation. Biochim. Biophys. Acta - Proteins Proteomics 1784, 1873–1898.

Tersteegen, A., Linder, D., Thauer, R.K., Hedderich, R., 1997. Structures and Functions of Four Anabolic 2-Oxoacid Oxidoreductases in *Methanobacterium Thermoautotrophicum*. Eur. J. Biochem. 244, 862–868.

Volkamer, A., Kuhn, D., Grombacher, T., Rippmann, F., Rarey, M., 2012. Combining Global and Local Measures for Structure-Based Druggability Predictions. J. Chem. Inf. Model. 52, 360–372.

Vuoristo, K.S., Mars, A.E., Sanders, J.P.M., Eggink, G., Weusthuis, R.A., 2016. Metabolic Engineering of TCA Cycle for Production of Chemicals. Trends Biotechnol. 34, 191–197.

Wang, J., Wang, W., Kollman, P.A., Case, D.A., 2006. Automatic atom type and bond type perception in molecular mechanical calculations. J. Mol. Graph. Model. 25, 247–60.

Yamamoto, M., Arai, H., Ishii, M., Igarashi, Y., 2003. Characterization of two different 2-oxoglutarate:ferredoxin oxidoreductases from *Hydrogenobacter thermophilus* TK-6. Biochem. Biophys. Res. Commun. 312, 1297–1302.

Yamamoto, M., Ikeda, T., Arai, H., Ishii, M., Igarashi, Y., 2010. Carboxylation reaction catalyzed by 2-oxoglutarate : ferredoxin oxidoreductases from *Hydrogenobacter thermophilus*. Extremophiles 79–85.

Yan, Z., Fushinobu, S., Wakagi, T., 2014. Four Cys residues in heterodimeric 2-oxoacid:ferredoxin oxidoreductase are required for CoA-dependent oxidative decarboxylation but not for a non-oxidative decarboxylation. Biochim. Biophys. Acta - Proteins Proteomics 1844, 736–43.

Yan, Z., Maruyama, A., Arakawa, T., Fushinobu, S., Wakagi, T., 2016. Crystal structures of archaeal 2-oxoacid:ferredoxin oxidoreductases from *Sulfolobus tokodaii*. Sci. Rep. 6, 33061.

CHAPTER 4

Phenotypic Evaluation of *Arabidopsis thaliana* Expressing *E. coli* Biotin Protein Ligase and *Hydrogenobacter thermophilus* TK-6 Ferredoxin

Caroline M. Smith-Moore, Denise Aslett, and Amy Grunden

Abstract

Expression of the crTCA cycle in plants requires the addition of a biotin protein ligase for efficient biotinylation of the 2-oxoglutarate carboxylase and a ferredoxin to act as the electron donor for the 2-oxoglutarate:ferredoxin oxidoreductase. In order to ensure that phenotypes ascribed to the function of the crTCA cycle are not due to the expression of these accessory proteins, transgenic lines expressing *Escherichia coli* biotin protein ligase (*birA)*, *Hydrogenobacter thermophilus* TK-6 ferredoxin (*fdx)*, or both genes were created. These transgenic lines were evaluated for changes in morphology, biotinylation, and resistance to methyl viologen-induced oxidative stress. While no differences in growth and morphology were noted, preliminary data suggest potential differences in biotinylation for plants expressing *birA* and in oxidative stress under certain conditions for plants expressing *fdx*.

4.1 Introduction

Plant biomass and productivity are limited by the amount of carbon the plant is capable of incorporating through the Calvin Benson-Bassham cycle (Bar-Even et al., 2010; Long et al., 2015). To augment carbon fixation in the chloroplast, it has been suggested that alternative carbon fixation cycles could be employed (Bar-Even et al., 2010). A promising cycle for this application is the condensed, reverse tricarboxylic acid (crTCA) cycle. This cycle is a shortened version of the reverse TCA cycle and consists of 4-5 enzymatic steps. The cycle begins with succinate, which is converted to succinyl-CoA by succinyl-CoA synthetase. The succinyl-CoA is then converted to 2-oxoglutarate with the fixation of CO_2 and the oxidation of a ferredoxin by the enzyme 2-oxoglutarate:ferredoxin oxidoreductase (KOR). The 2-oxoglutarate is then carboxylated by either 2-oxoglutarate carboxylase or isocitrate dehydrogenase to form oxalosuccinate or isocitrate, respectively. The isocitrate is then cleaved by isocitrate lyase into succinate to continue the cycle and glyoxylate, which exits the cycle. The crTCA cycle was demonstrated *in vitro*, and the individual enzymes have been functionally expressed in plants.

To ensure efficient function of the crTCA cycle in plants, additional genes are required for two of the steps. Specifically, a 4Fe-4S ferredoxin from *Hydrogenobacter thermophilus* TK-6 and a biotin protein ligase (BirA) from *Escherichia coli* (Ikeda et al. 2005, Barker and Campbell 1981). The *H. thermophilus* TK-6 ferredoxin (HyTh-FDX) is important as the selected KOR is also from *H. thermophilus* TK-6 and has been shown to have some specificity for its endogenous ferredoxin (Yoon et al., 1996). The BirA is used to enhance biotinylation of the 2-oxoglutarate carboxylase, which is a necessary post-translational modification required for enzyme activity. While the introduction of these

additional genes was not intended to directly affect plant phenotypes in the absence of the crTCA cycle, both could influence the function of important plant metabolic pathways.

Ferredoxins are key iron sulfur (Fe-S) proteins responsible for electron transfer reactions. Depending on their structure and Fe-S cluster, ferredoxins have different redox potentials (Meyer, 2008). The redox potential of a ferredoxin influences which proteins and reactions it can participate in due to its ability to donate or accept electrons. Bacterial-type ferredoxins contain one or two 4Fe-4S clusters. These ferredoxins have particularly low redox potentials between -150 and -700 mV (Meyer, 2008). This low potential allows them to play critical roles in anaerobic metabolism and reducing reactions of the electron transport chain. The ferredoxin from *H. thermophilus* TK-6 contains a single 4Fe-4S cluster and has the lowest reduction potential of any reported single cluster ferredoxin at -485 mV (Ikeda et al., 2005; Li and Elliott, 2016). This ferredoxin is the endogenous ferredoxin which participates in electron transfer with *H. thermophilus* TK-6 KOR (Yoon et al., 1996).

Plant-type ferredoxins have a 2Fe-2S cluster with a redox potential between -350 and -450 mV (Hanke et al., 2004). These ferredoxins can be subdivided into root and shoot-type ferredoxins, which participate in different reactions depending on their location. While these proteins may be expressed in different tissues, the ferredoxins are all expressed in plastids (Hanke et al., 2004). The most well characterized role for ferredoxin is in the leaf chloroplast. Here ferredoxins accept electrons from photosystem I (PSI) and transfer them to ferredoxin:$NADP^+$ reductase (FNR), which produces NADPH for the Calvin Benson-Bassham cycle (Hanke and Mulo, 2013; Hase et al., 2006). While this activity is essential to plant survival, ferredoxin also engages in electron transfer with enzymes involved in lipid

metabolism, reactive oxygen species (ROS) detoxification, and nitrogen and sulfur metabolism, among others (Hase et al., 2006; Zurbriggen et al., 2008).

Ferredoxin plays a role in a number of vital metabolic reactions; however, under stress conditions ferredoxin is down regulated (Tognetti et al., 2006). The decrease in the amount of ferredoxin present in the chloroplast to accept electrons from PSI, allows PSI to instead transfer those electrons to oxygen and create ROS (Allen, 1995; Apel and Hirt, 2004). Previous work has attempted to alleviate this problem through the expression of a cyanobacterial flavodoxin (Blanco et al., 2011; Giró et al., 2011; Tognetti et al., 2007, 2006). This strategy created plants with broad stress tolerance and a reduction in ROS build up under stressed conditions (Tognetti et al., 2006). Another attempted strategy was to express a cyanobacterial 2Fe-2S ferredoxin in the chloroplast (Ceccoli et al., 2011). However, this strategy failed to elicit stress tolerance from the plants, potentially due to the ability of the plant to regulate the cyanobacterial ferredoxin (Ceccoli et al., 2011). While the expression of the cyanobacterial ferredoxin was not successful, it is possible that the expression of a ferredoxin that is unregulated by the plant, such as a bacterial-type ferredoxin, would increase stress tolerance. Expression of the HyTh-FDX in the plant chloroplast could increase plant stress tolerance, particularly tolerance of oxidative stress.

Enzymatic biotinylation is a vital post-translational modification, primarily for carboxylase enzymes. In *E.coli*, BirA only biotinylates the enzyme acetyl-CoA carboxylase (ACCase), more specifically the biotin carboxyl carrier protein (BCCP) subunit of the ACCase (Barker and Campbell, 1981; Chapman-Smith and Cronan, 1999). BirA biotinylates BCCP by covalently attaching a biotin moiety to a specific lysine residue with an amide bond (Chapman-Smith and Cronan, 1999). This biotin binds bicarbonate, which is then transferred

onto an acetyl-CoA, allowing the ACCase to produce malonyl-CoA, which is an essential building block for fatty acids (Polakis et al., 1974).

In *Arabidopsis thaliana*, the protein responsible for biotinylation is holocarboxylase synthetase (HCS). While there are two HCS proteins described in the literature, HCS1 and HCS2, it has been shown that HCS1 is responsible for biotinylation in *Arabidopsis thaliana* (Puyaubert et al., 2008). Unlike *E. coli*, plants have several biotinylated carboxylase enzymes including heteromeric ACCase in plastids, monomeric ACCase in the cytosol, methylcrotonyl-CoA carboxylase (MCCase) in mitochondria, and geranoyl-CoA carboxylase in plastids (Puyaubert et al., 2008). In addition to organellar specificity, the expression of these carboxylase enzymes is also tissue and developmentally specific (Puyaubert et al., 2008). In *Arabidopsis* there are two BCCP proteins, BCCP1 and BCCP2, with BCCP1 being widely expressed in most plant tissues, whereas BCCP2 is primarily expressed in developing seed (Thelen et al., 2001). Both BCCP proteins fulfill a role as the biotin-containing subunit of the heteromeric ACCase in plastids. Recombinant expression of *Arabidopsis* BCCP1 and BCCP2 in *E. coli* demonstrated that the endogenous *E. coli* BirA is also capable of biotinylating these proteins (Thelen et al., 2001). It is hypothesized that transgenic plants expressing *E. coli* BirA in the chloroplast could have increased biotinylation of BCCP.

As mentioned, the expression of HyTh-FDX and BirA could lead to changes in plant phenotype. It is important to evaluate the effect these genes have when expressed alone or in combination in plants to achieve a better understanding of the phenotypes displayed by crTCA expressing plants. *Arabidopsis thaliana* was used as the model plant to evaluate the effect of expression of BirA, HyTh-FDX, and BirA/HyTh-FDX. Transgenic *Arabidopsis* lines were generated and evaluated for differences in growth. Additionally, the plants were

evaluated for specific phenotypes hypothesized for each gene. For BirA, biotinylation patterns were evaluated, and for ferredoxin, response to oxidative stress was studied.

4.2 Materials and Methods

4.2.1 Plant Growth Conditions and Measurement

Arabidopsis thaliana (Columbia ecotype) plants were grown in Pro-Mix PGX soil and received Miracle-GRO nutrient once a week. The plants were grown with a 12 h photoperiod at 23 °C and approximately 80 μmol m^{-2} s^{-1} of PAR light as measured by the MultispeQ Beta and PhotosynQ (Kuhlgert et al., 2016). Rosette leaf area from 5 week old plants was measured using Image J with the measure rosette area tool (http://dev.mri.cnrs.fr/projects/imagej-macros/wiki/Measure_Rosette_Area_Tool).

4.2.2 Gene Synthesis and Cloning

The *E. coli birA* and *H. thermophilus* TK-6 *fdx* genes were synthesized by GenScript (Piscataway, NJ) with codon optimization for *Arabidopsis thaliana*. In addition to the coding sequence, each gene was synthesized with a promoter, a chloroplast targeting sequence, terminator, and restriction digestion sites for cloning. The synthesized *birA* gene was fused to the constitutive *EntCUP4* promoter (Malik et al., 2002), an *OCS* terminator (De Greve et al., 1982), and the restriction digestion sites for EcoRI and KpnI were encoded on the ends. The synthesized *HyTh-fdx* gene was fused to the constitutive *Actin2* promoter (An and Meagher, 2010), a *NOS* terminator (Bevan et al., 1983), and the restriction digestions sites for *Bam*HI and *Hind*III were included. Both genes were also fused to the RuBisCO small subunit (*rbcs*) transit peptide sequence for targeting of the proteins to the chloroplast (Lee et al., 2008) and

contained a Kozak consensus sequence. The synthesized genes were ligated into separate pUC57 vectors by GenScript.

Synthesized genes were utilized to create three different constructs containing either the *birA* gene (pCAMBIA2300-BAR:birA), the *fdx* gene (pCAMBIA2300-BAR:HyTh-fdx), or both genes (pCAMBIA2300-BAR:birA:HyTh-fdx). The vector constructs can be seen in Figure 4-1. These constructs were generated using the pCAMBIA2300-BAR plasmid as a backbone allowing for selection with the herbicide BASTA (Dalal et al., 2015). The synthesized genes in pUC57 were digested with restriction enzymes (New England Biolabs, Ipswich, MA, USA) corresponding to the synthesized restriction sites (*Eco*RI and *Kpn*I for *birA* and *Bam*HI and *HindI*II for *fdx*), and gel extracted using the QIAquick Gel Extraction Kit (Qiagen, Frederick, MD, USA). T4 DNA ligase (New England Biolabs) was used for ligation reactions between digested vector and insert. The ligation reactions were used to transform *E. coli* XL-1 Blue (Novagen; EMD Biosciences, San Diego, CA, USA) and plated on media containing kanamycin for selection. The dual gene construct was created by sequentially cloning first the *birA* gene and then the *HyTh-fdx* gene into pCAMBIA-BAR. Constructs were confirmed using DNA sequencing (Eurofins MWG Operon, Huntsville, AL, USA).

Figure 4-1. Plasmid map of pCAMBIA-BAR constructs. All constructs were cloned using the pCAMBIA2300-BAR binary vector, which contained a kanamycin selectable marker (Kan) for bacterial selection as well as the Basta selectable marker (BAR) under the control of the CaMV 35s promoter for selection in plants. A.) The pCAMBIA2300-BAR:birA:HyTh-fdx vector contains both the *birA* and *HyTh-fdx* genes. The *birA* gene is under the control of the *Entcup4* constitutive promoter and uses the *OCS* terminator. The *HyTh-fdx* gene is under the control of the *Actin2* (Act2) promoter and uses the *NOS* terminator. Both genes are fused to the RuBisCO small subunit transit peptide for chloroplast expression and have Kozak consensus sequences (not pictured). B.) pCAMBIA2300-BAR:HyTh-fdx contains the *HyTh-fdx* gene for individual expression. All additional elements for expression are as described for pCAMBIA2300-BAR:birA:HyTh-fdx. C.) pCAMBIA2300-BAR:birA contains the *birA* gene for individual expression. All additional elements for expression are as described for pCAMBIA2300-BAR:birA:HyTh-fdx.

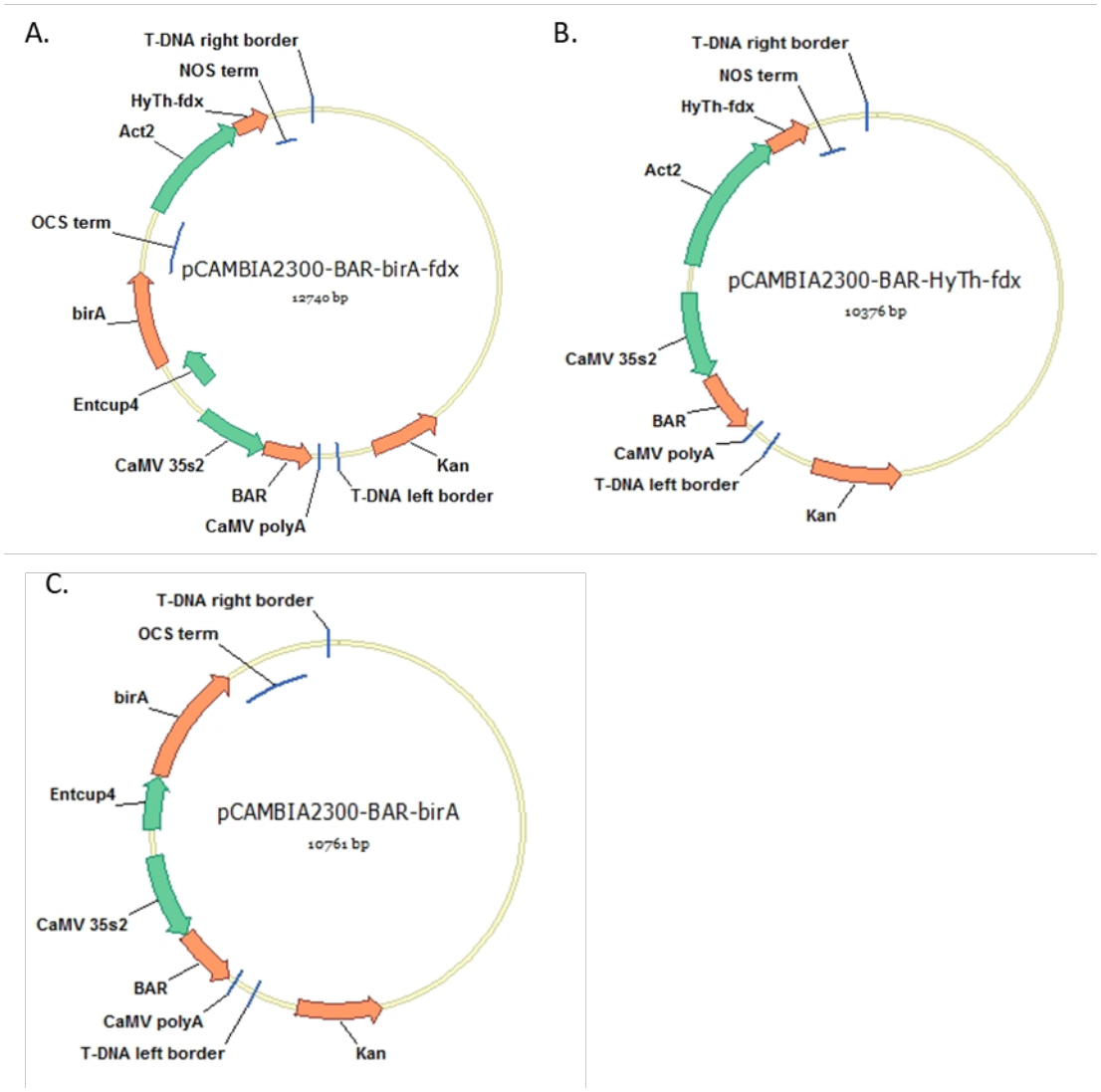
A.
T-DNA right border
NOS term
HyTh-fdx
Act2
OCS term
pCAMBIA2300-BAR-birA-fdx
12740 bp
birA
Entcup4
CaMV 35s2
BAR
CaMV polyA
T-DNA left border
Kan
B.
T-DNA right border
NOS term
HyTh-fdx
Act2
pCAMBIA2300-BAR-HyTh-fdx
10376 bp
CaMV 35s2
BAR
CaMV polyA
T-DNA left border
Kan
C.
T-DNA right border
OCS term
birA
Entcup4
pCAMBIA2300-BAR-birA
10761 bp
CaMV 35s2
BAR
CaMV polyA
T-DNA left border
Kan

4.2.3 *Arabidopsis thaliana* Transformation and Selection

The sequence verified constructs and an empty vector control were transformed into *Agrobacterium tumefaciens* GV3101 using the freeze-thaw method (Chen et al., 1994). Transformed *Agrobacterium* was used to transform *Arabidopsis thaliana* (ecotype Columbia) by floral dip (Clough and Bent, 1998). Briefly, a culture of *A. tumefaciens* GV3101 was grown to an optical density of 1 in YEP, and then pelleted by centrifugation. The pellet was resuspended in 5% sucrose, with 0.01% Silwet L-77 (Phytotechnology Laboratories, Lenexa, KS, USA). *Arabidopsis thaliana* flowers from approximately 6-week old plants were dipped in the *A. tumefaciens* solution for approximately 1 min. Plants were then laid horizontally and covered in plastic in the dark overnight. Plants were returned to the growth chamber and continued to grow until seed was set.

Seed harvested from the transformed plants was plated on 1X Murashige and Skoog basal salts media (MP Biomedicals, Solon, OH, USA) containing 1% sucrose, 0.8% plant cell culture tested agar (Sigma Aldrich, St. Louis, MO, USA), and 15 μg ml^{-1} DL-Phosphinothricin (BASTA) (Phytotechnology Laboratories) for selection. To obtain homozygous *Arabidopsis* transgenic lines, successive generations of plants were grown and segregation ratios were calculated. Homozygous parental plants at the T2 generation were considered to be those that produced 100% BASTA resistant seed.

4.2.4 PCR Analysis of Transgenic Plants

To isolate crude genomic DNA, *Arabidopsis* leaf tissue was excised and ground in buffer composed of 200 mM Tris-HCl (pH 8), 400 mM LiCl, 25 mM EDTA, and 1% SDS. Samples were then subjected to centrifugation at 14,000 rpm, and the resultant supernatant

was mixed 1:1 with isopropanol. This mixture was subjected to centrifugation again at 14,000 rpm. The supernatant was removed and the pellet containing the DNA was allowed to air dry before being resuspended in molecular biology grade water.

DNA samples were used as the template for PCR using Qiagen TopTaq Master Mix to confirm transgene insertion. The primers used for each gene are as follows: *birA* (*Entcup4* F:5'-CAGCCTCTCATCATCCTCAC-3'; *birA* R:5'-ATTCAGCGATACACGCATCTC-3'); *fdx* (*Actin2* F:5'-GGATTTGTAGTGTCGTACGTTG-3'; *fdx* R:5'-GGAAGGACACTCATC-AGTAAC-3'). Insertion for the empty vector control was confirmed using primers for the *35S* promoter (5'-CTATCCTTCGCAAGACCTTC-3') and *bar* gene (5'-GAAGTCCAGCTGCCAGAAAC-3'). PCR reactions were run on a Bio-Rad C1000 Touch Thermalcycler. The following PCR conditions were used: 95 °C, 3 min; 2. 95 °C, 30 sec; 3. 55 °C, 1 min; 4. 72 °C, 1 min; 5. Repeat steps 2-4 30x; and 6. 72 °C, 10 min. Following PCR, all samples were separated on 1% agarose gels and visualized with ethidium bromide staining on a BioRad GelDoc.

4.2.5 Reverse Transcription PCR Analysis

Harvested tissue was ground in liquid nitrogen to a fine powder. Aliquots of 100 mg were made for RNA isolation. RNA was isolated using the Qiagen RNeasy Plant Mini Kit. Isolated RNA was treated to remove contaminating DNA using the TURBO DNA-free Kit (Thermo Fisher Scientific). RNA was quantified using a Nanodrop (Thermo Fisher Scientific), and the concentration was normalized so that the same amount of starting material was added to each cDNA synthesis reaction. cDNA synthesis was conducted using the Qiagen Omniscript RT kit with Random Primers (Invitrogen; Thermo Fisher Scientific)

and RNase Inhibitor (Thermo Fisher Scientific). The reaction was incubated at 37 °C for 1 h followed by 2 min at 93 °C in a Bio-Rad C1000 Touch Thermal Cycler.

The synthesized cDNA was used as the template for PCR using Qiagen TopTaq Master Mix. The gene specific primers used for each gene are as follows: *birA* F (5'-CTTGGAATGTCTAGGGCTGC-3'); *birA* R (5'-ATTCAGCGATACACGCATCTC-3'); *fdx* F (5'-TGGCTCTTAGGACGATGGTC-3'); and *fdx* R (5'-GGAAGGACACTCATCAG-TAAC-3'). Actin 2 was used as a positive control with the following primers; *act2* F (5'-GCAAGTCATCACGATTGGTGC-3') and *act2* R (5'-GCAACGACCTTAATCTTCAT-GCTG-3'). PCR was conducted in a Bio-Rad C1000 Touch Thermalcycler with the following cycles: 1. 95 °C, 3 min; 2. 95 °C, 30 sec; 3. 50 °C, 1 min; 4. 72 °C, 1 min; 5. Repeat steps 2-4 30x; and 6. 72 °C, 10 min. After PCR all samples were evaluated on 1% agarose gel electrophoresis.

4.2.6 Western Blot Analysis

Plant tissue was ground in liquid nitrogen to a fine powder and 200 mg aliquots were made. The 200 mg of tissue was resuspended in buffer containing 50 mM Tris-HCl (pH 7.5), 150 mM NaCl, 10% (v/v) glycerol, 1% (v/v) Triton X-100, 2.5 mM DTT, and 1:100 Protease Inhibitor Cocktail (Sigma Aldrich). As the proteins were targeted to the chloroplast, the increased Triton X-100 was necessary for chloroplast lysis. The tissue and buffer were vortexed vigorously, and subjected to centrifugation at 14,000 rpm to remove debris. Centrifugation was repeated until all debris was removed. The protein concentration of the lysate was determined using the Bradford Assay reagent (Bio-Rad) and a BSA standard curve.

The lysate was mixed with 4X Laemmli buffer (with 2-mercaptoethanol) 3:1. Samples containing equal amounts of total protein were separated on 4-15% gradient SDS-PAGE (Bio-Rad, Hercules, CA, USA) and transferred onto 0.2 μm PVDF membrane using the Bio-Rad Transblot Turbo Transfer system. Membranes were blocked overnight in TBS-T with 2.5% (w/v) nonfat dry milk. For detection of BirA and HyTh-FDX, rabbit polyclonal peptide antibodies were prepared by GenScript using protein specific peptide sequences (BirA: CQQAGRGRRGRKWFS; HyTh-FDX: NRGDGIAEVVSPGPC) as the antigens. After blocking, membranes were washed and incubated in TBS-T with 1% casein and the appropriate primary antibody (1:5,000) for at least 1 hour. The secondary antibody was a goat anti-rabbit antibody conjugated with horseradish peroxidase (Thermo Fisher Scientific, Waltham, MA, USA) diluted at 1:20,000 in TBS-T with 2.5% nonfat dry milk. The blot was visualized by chemiluminescence using the Bio-Rad Clarity Western ECL Substrate and exposure to X-ray film.

4.2.7 Streptavidin-HRP Western Blot

Arabidopsis lysates were prepared and separated by SDS-PAGE as described above. Proteins were then transferred to 0.2 PVDF membrane using the Bio-Rad Transblot Turbo Transfer system. Membranes were blocked overnight in TBS-T with 5% (w/v) nonfat dry milk. After blocking, membranes were washed and incubated for 1 hour in HRP conjugated streptavidin (Thermo Fisher Scientific) at a dilution of 1:20,000 in TBS-T with 2.5% (w/v) nonfat dry milk. The blot was washed in TBS-T prior to visualization by chemiluminescence as described previously.

4.2.8 Methyl Viologen Plate Assay

Seeds were surface sterilized by treatment with 70% EtOH for 30 s, followed by a 12 min incubation in 40% (v/v) commercial bleach with periodic agitation, and washed with sterile deionized water seven times. Sterilized seeds were kept for 48 h at 4 °C to stratify. Seeds were plated aseptically on 1X Murashige and Skoog basal salts media (MP Biomedicals) with 1% sucrose and 0.8% plant cell culture tested agar (Sigma). Media were made to contain 0, 0.25, 0.5, or 1 μM methyl viologen. Sterile transgenic seeds were plated individually onto the different media, and incubated horizontally on a light shelf at approximately 23 °C. For the first experiment, the plants were exposed to continuous light at 45 μmol m^{-2} s^{-1}. For the second experiment, the plants were exposed to 80 μmol m^{-2} s^{-1} light with a 12 hour photoperiod. Surviving seedlings were classified as green seedlings, and were counted on days 4, 7, and 11 post plating.

4.3 Results

4.3.1 Generation of Transgenic *Arabidopsis thaliana*

Arabidopsis thaliana plants were transformed by *Agrobacterium tumefaciens* mediated floral dip. Plants were transformed with each construct pCAMBIA2300-BAR:birA (*birA*), pCAMBIA2300-BAR:HyTh-fdx (*HyTh-fdx)*, and pCAMBIA2300-BAR:birA:HyTh-fdx (*birA/HyTh-fdx*) and with pCAMBIA2300-BAR alone (EV) to be used as a control. The plants were selected on MS media containing the herbicide Basta. Three independent homozygous transgenic lines were maintained for each construct with one EV line. Integration of the DNA was confirmed first by genotyping using forward primers specific for the promoter and reverse primers internal to the gene, either *birA*, *HyTh-fdx*, or *bar* (for EV).

The presence of the transcript was confirmed using RT-PCR. These reactions used primers internal to either *birA* or *HyTh-fdx*, and the EV was used as a negative control. The *Actin2* gene was used as a positive control as well as a loading control. The expression level of the transcript is similar for the independent lines. An agarose gel image can be seen in Figure 4-2, depicting the RT-PCR results.

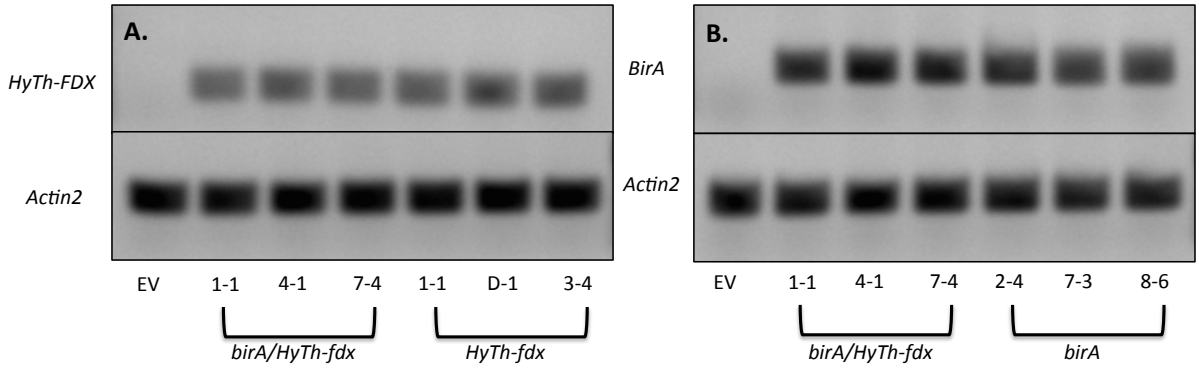

Figure 4-2. RT-PCR of independent *HyTh-fdx*, *birA*, and *birA/HyTh-fdx* transgenic lines. RNA was isolated from 2 week old seedlings and DNase treated prior to cDNA synthesis. After cDNA synthesis, PCR was conducted using gene specific internal primers. EV was used as a negative control for gene specific reactions. *Actin2* was used as a positive control as well as a loading control. Images are of 5 µL of each reaction run on a 1% agarose gel and stained with ethidium bromide. A.) RT-PCR reactions for *HyTh-fdx* and *birA/HyTh-fdx,* the transcript was detected in all lines at similar levels. B.) RT-PCR reactions for *birA* and *birA/HyTh-fdx*; the transcripts were detected in all lines at similar levels.

Confirmation of protein expression was sought next through the use of Western blots. As these proteins should have been localized to the chloroplast, an increased amount of Triton X-100 was used to aid in chloroplast lysis and membrane solubilization. Lysates prepared with the additional Triton X-100 had a bright green color, whereas lysates without Triton X-100 appeared faintly green to clear. The Triton X-100 lysates were separated by SDS-PAGE and transferred to PVDF membranes for western blotting. The primary

antibodies for the western blots were designed to be specific for a particular peptide epitope of either BirA or HyTh-FDX. Prior to their use on plant lysates, the ability of these antibodies to bind to their antigens was confirmed using purified polyhistidine tagged HyTh-FDX and *E. coli* lysates for BirA. BirA was readily detected by western blot in all *birA* and *birA/HyTh-fdx* plants, while no band was seen in EV plants (Figure 4-3). However, despite numerous attempts, the HyTh-FDX could not be identified in either the *HyTh-fdx* plants or the *birA/HyTh-fdx* plants.

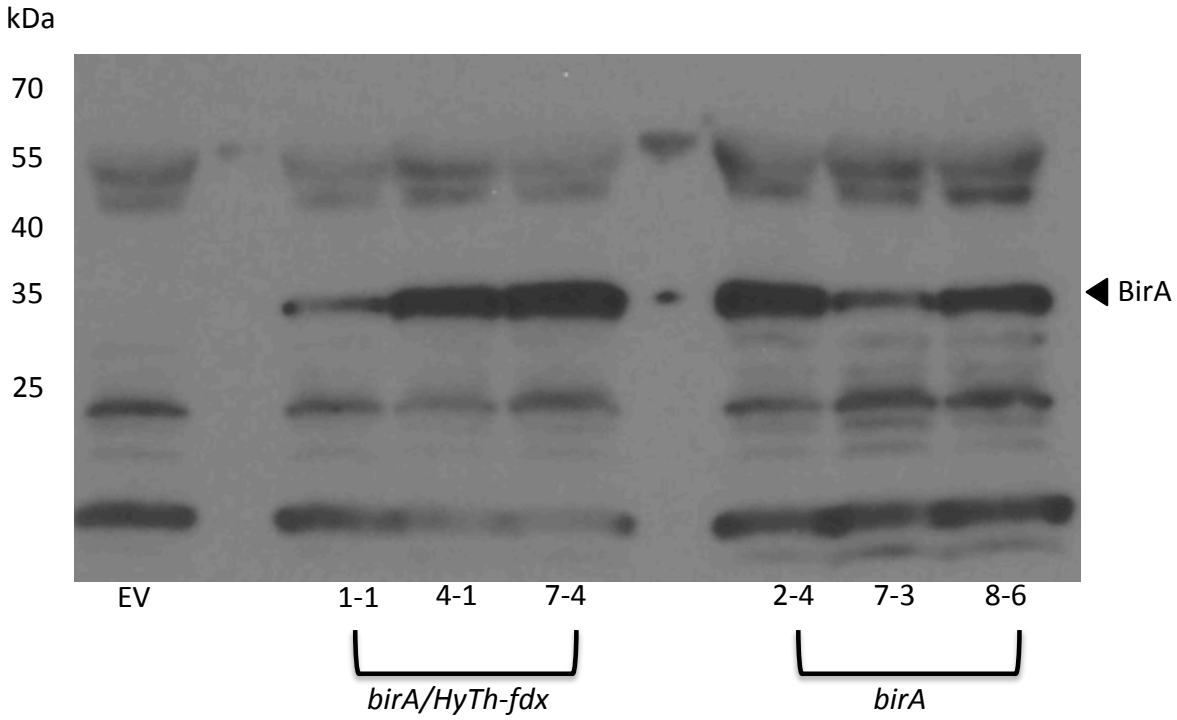

Figure 4-3. BirA Western blot. Western blot analysis confirms that BirA is expressed in transgenic *Arabidopsis* and is not present in EV. BirA was detected with a primary antibody raised against a BirA peptide epitope. Equal amounts of total soluble protein were added per lane (50 μg). The molecular weight for BirA is approximately 33 kDa. Additional bands are non-specific interactions with plant lysate proteins.

4.3.2 Growth Characteristics

All lines were grown to evaluate any morphological differences. Seeds were started on MS plates and transplanted into soil after 1 week. At 5 weeks, the plants were evaluated for differences in rosette area. The rosette area was measured using the measure rosette area tool in Image J. It was found that there were no statistically significant differences between EV and transgenic lines. Figure 4-4 summarizes these data. Additionally, throughout the growth cycle the plants were observed for any differences in morphology. No obvious morphological differences were observed. Figure 4-5 is an image of the plants at 5 weeks.

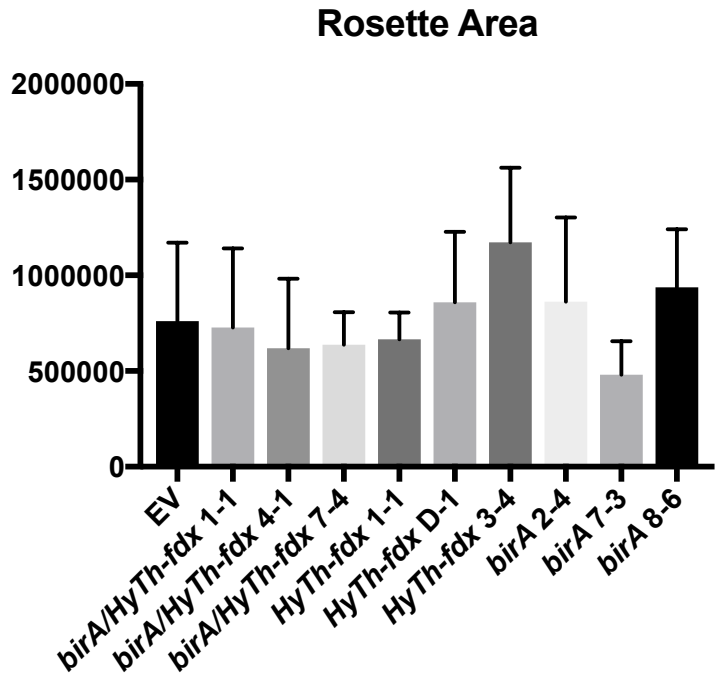

Figure 4-4. Rosette area of transgenic lines compared to EV. 5 week old plants were photographed individually, and the images were analyzed using the measure rosette tool in Image J. The area is measured in pixels and thus is unitless. Each bar represents the average area for 4 plants (5 plants for EV). No statistically significant differences were found as analyzed by t-test. Error bars represent one standard deviation.

Figure 4-5. Morphology of 5-week old transgenic *Arabidopsis thaliana* lines. Plants were grown on a light shelf at 23°C with 80 μmol m^{-2} s^{-1} light and a 12 h photoperiod. Plants were rotated during growth to minimize positional effects. Plants display normal growth and phenotype comparable to the EV transformed plants. A.) *birA/HyTh-fdx* and EV *Arabidopsis* lines; B.) *birA* and EV *Arabidopsis* lines; C.) *HyTh-fdx* and EV *Arabidopsis* lines.

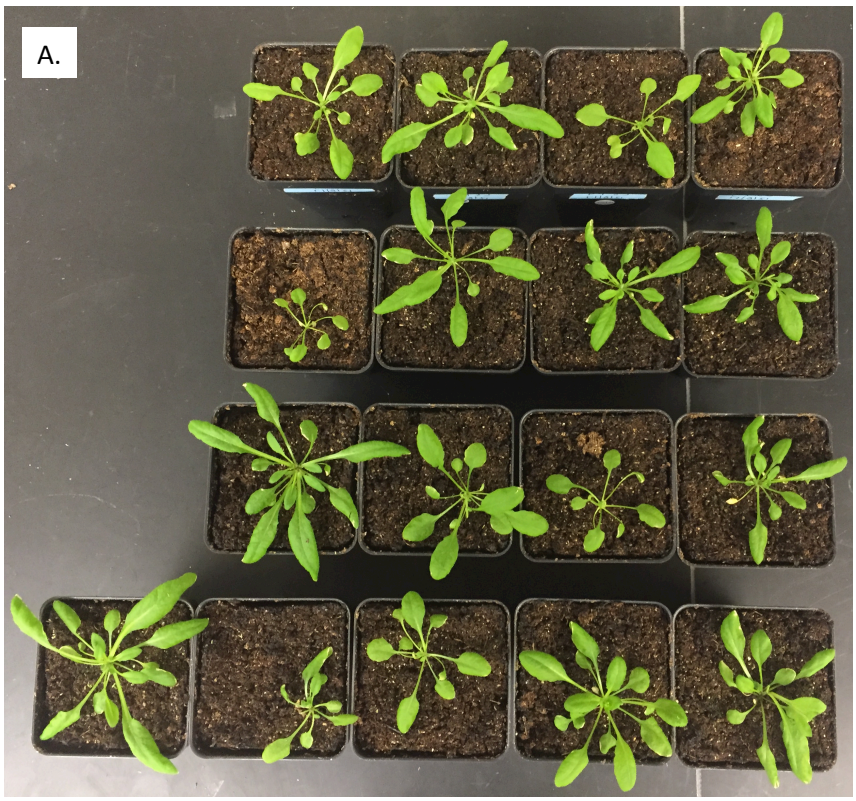
A.
birA/HyTh-fdx
7-4
birA/HyTh-fdx
4-1
birA/HyTh-fdx
1-1
EV


B.
birA 8-6
birA 7-3
birA 2-4
EV


C.
HyTh-fdx 3-4
HyTh-fdx D-1
HyTh-fdx 1-1
EV

4.3.3 Biontinylation Comparison

Evaluation of the biotinylation profile of *birA* expressing plants was conducted using HRP-conjugated streptavidin. The EV plants were used as a negative control. As described in the introduction, *Arabidopsis* has a number of biotinylated carboxylases which could be detected by a streptavidin blot. As expected due to abundance and tissue specificity, the proteins detected in the Western blot are MCCase and BCCP1 of the heteromeric ACCase (Figure 4-6). BirA was targeted to chloroplasts, making the BCCP1 of particular interest as it is localized to the chloroplast as well. *Arabidopsis* BCCP1 has also been shown previously to be biotinylated by *E. coli* BirA when expressed recombinantly (Thelen et al., 2001). From the Western blot image in Figure 4-6, BCCP1 appears to have increased biotinylation in some lines compared to the EV control.

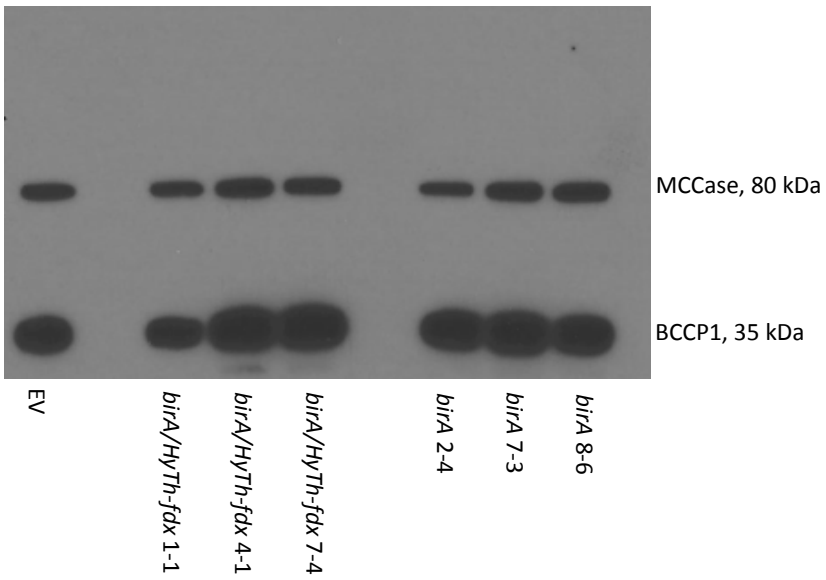

Figure 4-6. Biotinylation of *birA/HyTh-fdx* and *birA*. Lysate samples prepared from 2-week old seedlings were separated by 4-15% gradient SDS-PAGE. The blot was probed with HRP-conjugated streptavidin to detect biotinylated proteins. An equivalent amount of total soluble protein (75 μg) was added per lane. The blot detected the presence of MCCase at approximately 80 kDa and BCCP1 at approximately 35 kDa. Some samples appear to have increased biotinylation of BCCP1 relative to the EV control.

4.3.4 Response to Oxidative Stress

The expression of HyTh-FDX in the chloroplast was hypothesized to increase *Arabidopsis* stress tolerance by allowing metabolic processes to continue when endogenous ferredoxin is downregulated by stress, and inhibiting the generation of ROS. Given its low redox potential, the HyTh-FDX could accept electrons from PSI fulfilling the role of chloroplastic ferredoxin in the transfer of electrons from PSI to FNR (Hanke et al., 2004). Methyl viologen (MV) was selected as the best stress to evaluate the function of the HyTh-FDX. MV will accept electrons from PSI, which it then passes on to oxygen, generating superoxide, a harmful ROS molecule in the chloroplast (Scarpeci et al., 2008). The presence

of HyTh-FDX could limit this activity and reduce damage to plant macromolecules from ROS.

Seeds from *HyTh-fdx* and *birA/HyTh-fdx Arabidopsis* plants were plated on MS media containing 0, 0.25, 0.5, or 1 μM MV. The plates were maintained under continuous light and the number of surviving seedlings was counted at days 4 and 7. While plant growth was inhibited with increasing amounts of MV in all lines, as seen in Figure 4-7, seedling survival and germination were not significantly inhibited until 1 μM MV. The survival data for 1 μM MV can be seen in Figure 4-8; no significant differences were found with the other concentrations of MV. At the day 4 time point, *HyTh-fdx* lines 1-1 and 3-4 show a statistically significant increase in percent survival compared to EV (Figure 4-8C). However, line D-1 has a significant decrease in survival compared to EV and the other two *HyTh-fdx* lines. It is hypothesized that this difference is likely due to a positional effect of gene insertion in the genome. The early difference seen for the *HyTh-fdx* plants is no longer observed by day 7 (Figure 4-8D). The *birA/HyTh-fdx* lines displayed a different pattern where at day 4 there was no significant difference between EV and *birA/HyTh-fdx* lines (Figure 4-8A). However, by day 7 all *birA/HyTh-fdx* lines showed a statistically significant decrease in percent survival compared to EV as determined using a one-way ANOVA (Figure 4-8B). This difference was not anticipated and could signify a decrease in oxidative stress tolerance as a result of the *birA*. It is important to note that the HyTh-FDX protein was not detected by Western blot for any of the transgenic lines.

Figure 4-7. Methyl viologen plate assay images. Sterilized seeds were sown on MS media plates containing 0, 0.25, 0.5, and 1 μM MV. While growth was inhibited with increasing MV, germination was not inhibited until 1 μM MV. 20 seeds were plated of each line per plate. Three replicates were conducted for each condition. Images were taken on day 7. A.) Images are of representative plates containing EV, and the three independent lines of *bira/HyTh-fdx Arabidopsis* seedlings. B.) Images are of representative plates containing EV, and the three independent lines of *HyTh-fdx Arabidopsis* seedlings.

A.

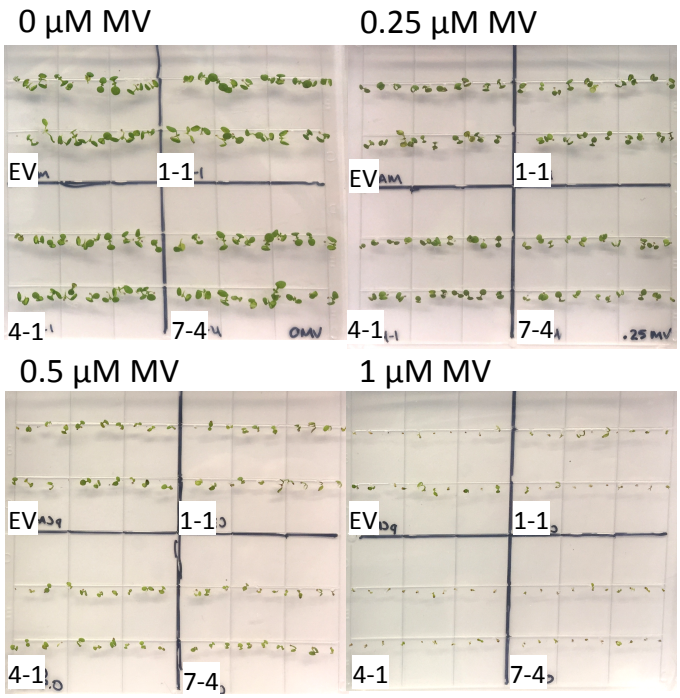
0 µM MV
0.25 µM MV
EV
1-1
4-1
7-4
0.5 µM MV
1 µM MV
EV
1-1
4-1
7-4

B.

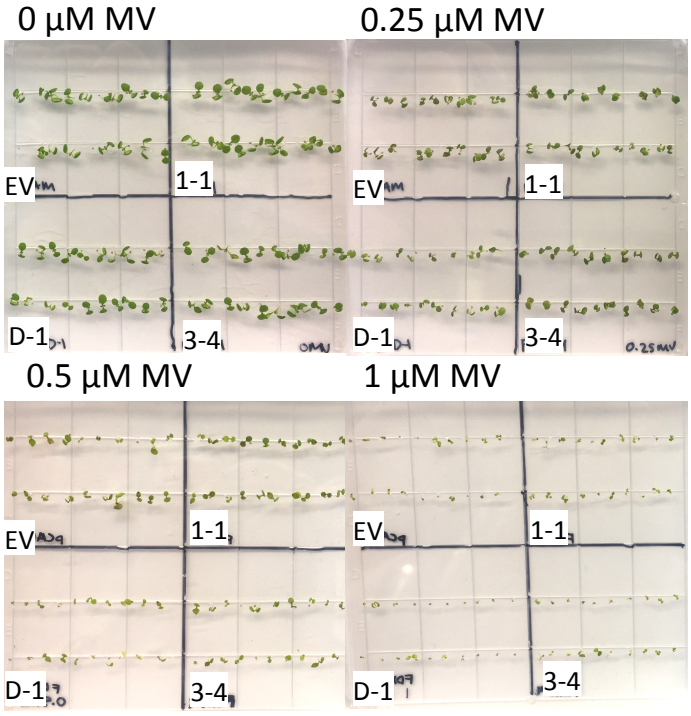
0 µM MV
0.25 µM MV
EV
1-1
D-1
3-4
0.5 µM MV
1 µM MV
EV
1-1
D-1
3-4

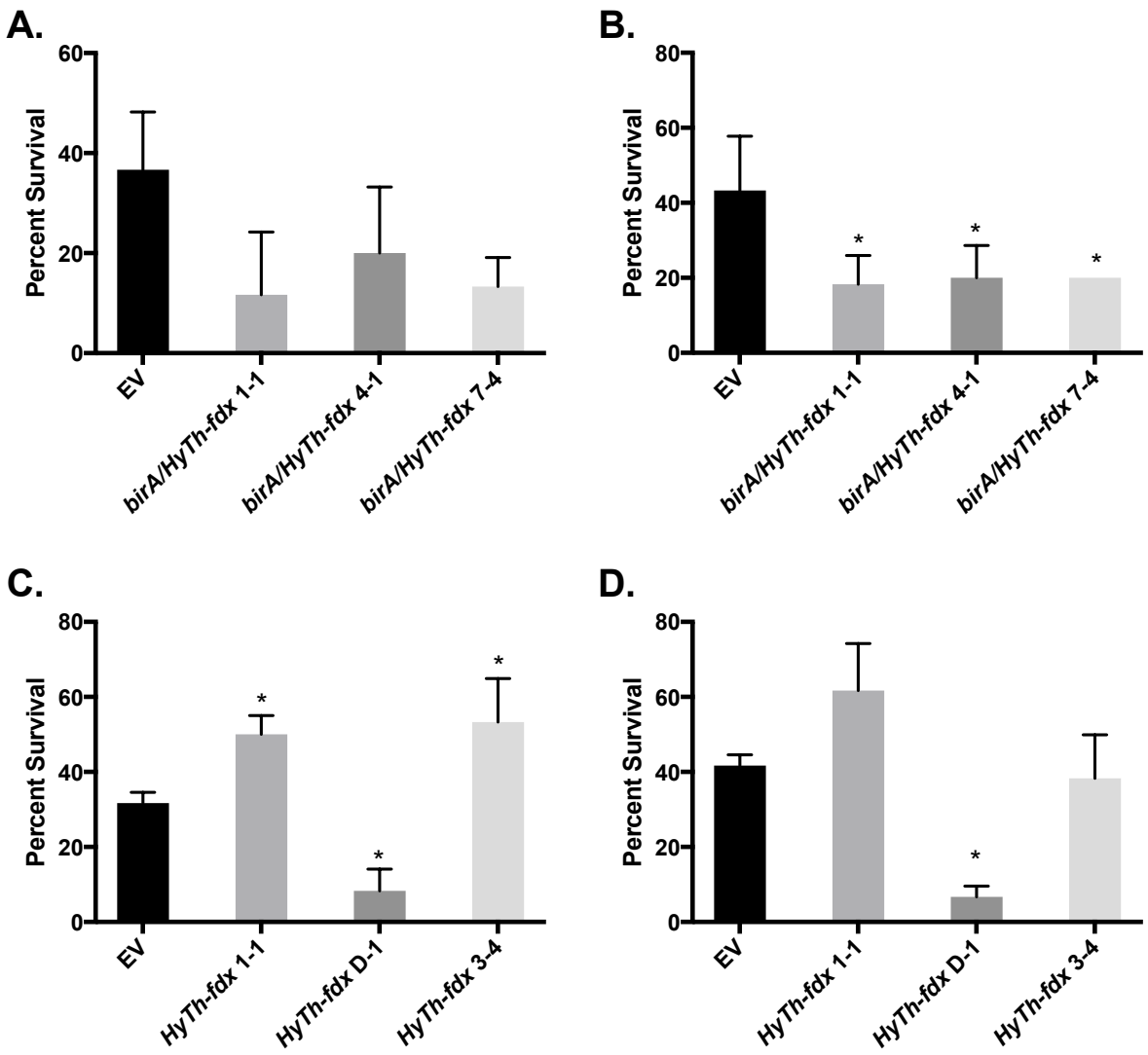

Figure 4-8. Percent survival of transgenic lines on 1 μM MV plates. Seeds of transgenic *birA/HyTh-fdx* and *HyTh-fdx Arabidopsis* were plated on MS media containing 1 μM MV. The number of seedlings surviving, those that were green, were counted at day 4 and day 7. The percent survival was calculated by dividing the number of surviving seedlings by the total number of seeds plated (20). Three biological replicates were conducted. Differences of statistical significance ($p<0.05$) are indicated with an asterisk as calculated using a one-way ANOVA. Error bars represent one standard deviation. A.) Day 4 counts for EV and *birA/HyTh-fdx* (1-1, 4-1, and 7-4). B.) Day 7 counts for EV and *birA/HyTh-fdx* (1-1, 4-1, and 7-4). C.) Day 4 counts for EV and *HyTh-fdx* (1-1, D-1, and 3-4). D.) Day 7 counts for EV and *HyTh-fdx* (1-1, D-1, and 3-4).

To further evaluate this phenotype, this experiment was conducted a second time to include all of the transgenic lines, *birA*, *HyTh-fdx*, and *birA/HyTh-fdx*. In this second experiment, all of the previous conditions were the same, except that the light intensity was increased from 45 μmol m^{-2} s^{-1} to 80 μmol m^{-2} s^{-1}, and the duration of light was changed from continuous to a 12 h photoperiod. Unlike the previous experiment, in this experiment no clear trends were seen. The only significant differences were for *birA* lines 2-4 and 8-6 at 1 μM on day 4, and *HyTh-fdx* 1-1 at 0.5 μM on day 7. The data are shown in Figure 4-9.

Figure 4-9. Percent survival of transgenic lines on various concentrations of MV with a 12 hour photoperiod. Seeds of transgenic *birA/HyTh-fdx, HyTh-fdx*, and *birA Arabidopsis* were plated on MS media containing 0, 0.25, 0.5, and 1 μM MV. The plants were grown with 80 μmol m^{-2} s^{-1} light with a 12 h photoperiod. The number of seedlings surviving, those that were green, were counted at days 4 and 7. The percent survival was calculated by dividing the number of surviving seedlings by the total number of seeds plated (20). Three biological replicates were conducted. Differences of statistical significance ($p<0.05$) are indicated with an asterisk as calculated using a one-way ANOVA. Error bars represent one standard deviation. A.) Day 4 and 7 counts for EV and *birA/HyTh-fdx* (1-1, 4-1, and 7-4). B.) Day 4 and 7 counts for EV and *HyTh-fdx* (1-1, D-1, and 3-4). C.) Day 4 and 7 counts for EV and *birA* (2-4, 7-3, and 8-6).

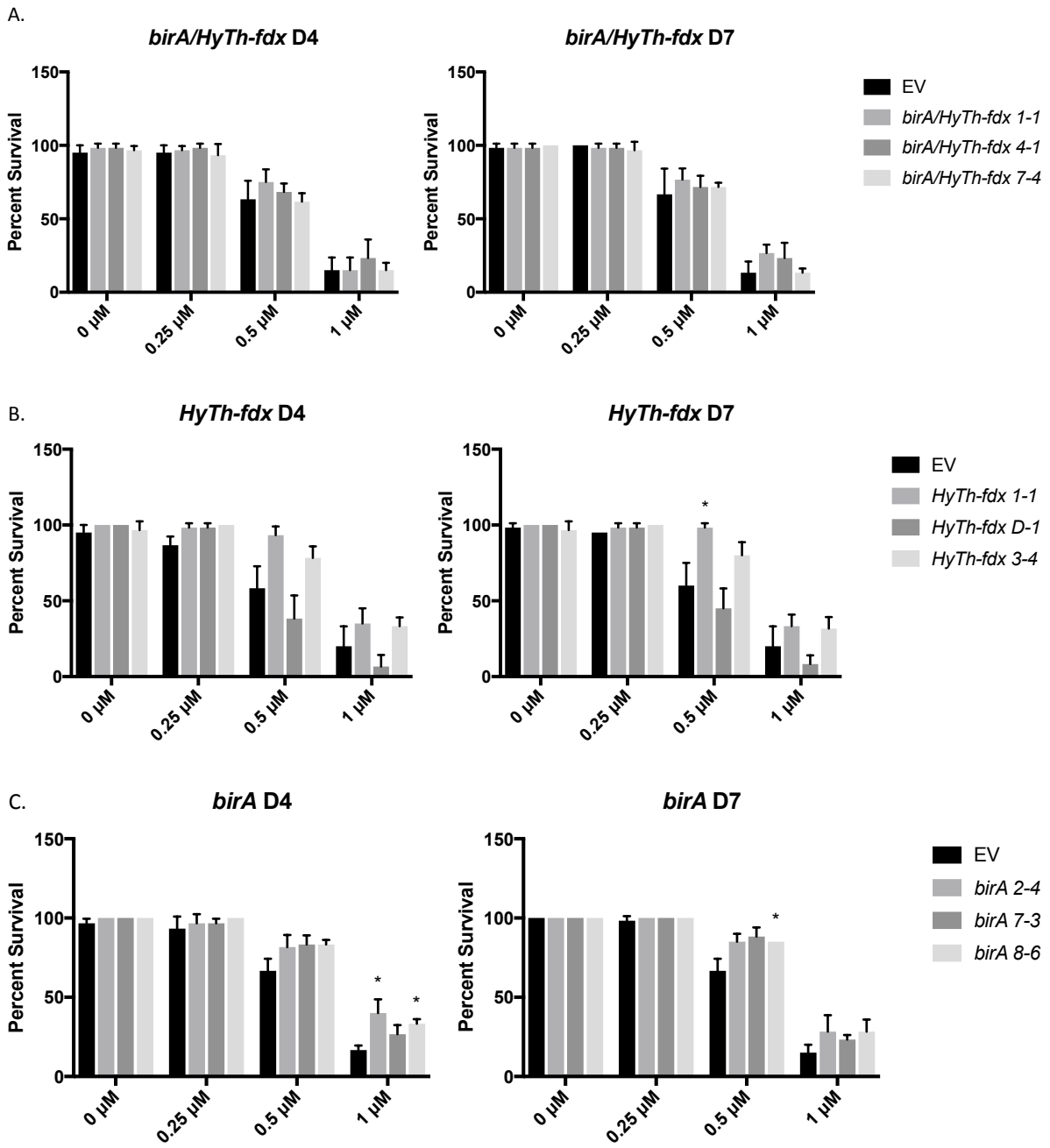
A.
birA/HyTh-fdx D4
birA/HyTh-fdx D7
Percent Survival
150
100
50
0
0 µM
0.25 µM
0.5 µM
1 µM
EV
birA/HyTh-fdx 1-1
birA/HyTh-fdx 4-1
birA/HyTh-fdx 7-4
B.
HyTh-fdx D4
HyTh-fdx D7
*
EV
HyTh-fdx 1-1
HyTh-fdx D-1
HyTh-fdx 3-4
C.
birA D4
birA D7
*
EV
birA 2-4
birA 7-3
birA 8-6

4.4 Discussion

The transformation of any gene into another organism has the potential to have unpredicted effects. For efficient function of the crTCA cycle in plants, additional genes were needed. In order to evaluate the effect that expression of *H. thermophilus* TK-6 ferredoxin or *E. coli* biotin protein ligase may have on *Arabidopsis thaliana* plants, transgenic lines expressing each of these genes individually or together were created. After transformation, the plants were selected and underwent segregation to obtain three independent, homozygous transgenic lines expressing either *birA*, *HyTh-fdx,* or *birA/HyTh-fdx*. Expression of the transcripts were confirmed by RT-PCR (Figure 4-2). However, only the expression of BirA could be confirmed by Western blot.

Multiple attempts were made to identify the HyTh-fdx protein in the plants. Detection of the HyTh-fdx is complicated by the fact that the protein is very small, approximately 8 kDa, and is very acidic (pI 4). The detection of the protein was attempted using both the soluble and insoluble fraction plant tissue extract fractions, and numerous technical optimizations were performed, including heat treatment of the lysate (Ikeda et al., 2005), membrane fixation with paraformaldehyde (Suzuki et al., 2008), and various optimizations of transfer and blotting conditions. However, no expression of the transgenic ferredoxin was detected using any of the methods. As transcript was detected by RT-PCR (Figure 4-2), it is possible that the HyTh-fdx was subjected to proteolysis after translation. Despite the inability to detect the HyTh-fdx protein, the plants were still evaluated for phenotypic differences.

Plants were grown for 5 weeks and during that time observed for morphological and phenotypic differences. All plants appeared to grow normally, with no clear differences (Figure 4-5). Additionally, the rosette areas for the plants were measured, and no significant

differences were found. These data suggest that the expression of the genes alone or in combination does not produce significant changes in plant growth that would interfere with observation of phenotypes resulting from *in planta* function of the crTCA cycle.

Alterations in biotinylation in *birA/HyTh*-f*dx* and *birA* plants were evaluated using western blotting with HRP-conjugated streptavidin. The results suggest that mild increases in biotinylation of the *Arabidopsis thaliana* BCCP1 in 2-week old seedlings (Figure 4-6). The data demonstrate that the BirA was successfully transported to the chloroplast and is active *in vivo*. In order to quantify and assess this difference further assays are needed. Increases in biotinylation of BCCP1 could lead to changes in fatty acid metabolism in the chloroplast. Evaluation of the amount of malonyl-CoA would enable a better understanding of the effect *birA* expression has on *Arabidopsis* ACCase activity in the chloroplast.

The different results seen for the two methyl viologen assays raise some questions. These data clearly show that the difference in lighting and photoperiod led to different phenotypes. As MV stress is less effective in the dark (Scarpeci et al., 2008), it is possible that the continuous light experiment provided a more chronic stress condition despite the lower light intensity. Under this more chronic, and presumably strenuous stress, phenotypic differences were observed. The *HyTh-fdx* lines 1-1 and 3-4 demonstrated increased survival at 1 μM MV in the continuous light experiment at Day 4. This result is particularly interesting as no HyTh-fdx protein was detected in these plants. It is possible that despite the failure to detect the protein by western blot, a small amount of expression may be occurring or the detection is being impeded by the small size and acidic nature of the protein. Additionally, the *birA/HyTh-fdx* plants were more effected by the 1 μM MV at Day 7. This could suggest that the expression of BirA may cause sensitivity to oxidative stress. The

mechanism for this sensitivity is unclear. Additional experiments need to be conducted including the *birA* plants under continuous light to fully understand the implications of *birA* expression on *Arabidopsis thaliana*.

Collectively these data demonstrate that expression of *E. coli birA* and *H. thermophilus* TK-6 *fdx* individually or together do not greatly effect plant morphology or growth. However, the expression of *birA* may increase biotinylation while expression of *HyTh-fdx* may increase oxidative stress tolerance under certain conditions. Further analysis and characterization is needed for evaluation of these phenotypes.

References

Allen, R.D., 1995. Dissection of Oxidative Stress Tolerance Using Transgenic Plants. Plant Physiol. 107, 1049–1054.

An, Y.-Q.C., Meagher, R.B., 2010. Strong Expression and Conserved Regulation of ACT2 in *Arabidopsis thaliana* and *Physcomitrella patens*. Plant Mol. Biol. Report. 28, 481–490.

Apel, K., Hirt, H., 2004. REACTIVE OXYGEN SPECIES: Metabolism, Oxidative Stress, and Signal Transduction. Annu. Rev. Plant Biol. 55, 373–399.

Bar-Even, A., Noor, E., Lewis, N.E., Milo, R., 2010. Design and analysis of synthetic carbon fixation pathways. Proc. Natl. Acad. Sci. U. S. A. 107, 8889–8894.

Barker, D.F., Campbell, A.M., 1981. The *birA* gene of *Escherichia coli* encodes a biotin holoenzyme synthetase. J. Mol. Biol. 146, 451–67.

Bevan, M., Barnes, W.M., Chilton, M.D., 1983. Structure and transcription of the nopaline synthase gene region of T-DNA. Nucleic Acids Res. 11, 369–85.

Blanco, N.E., Ceccoli, R.D., Segretin, M.E., Poli, H.O., Voss, I., Melzer, M., Bravo-Almonacid, F.F., Scheibe, R., Hajirezaei, M.-R., Carrillo, N., 2011. Cyanobacterial flavodoxin complements ferredoxin deficiency in knocked-down transgenic tobacco plants. Plant J. 65, 922–935.

Ceccoli, R.D., Blanco, N.E., Medina, M., Carrillo, N., 2011. Stress response of transgenic tobacco plants expressing a cyanobacterial ferredoxin in chloroplasts. Plant Mol. Biol. 76, 535–544.

Chapman-Smith, A., Cronan, J.E., 1999. The enzymatic biotinylation of proteins: a post-translational modification of exceptional specificity. Trends Biochem. Sci. 24, 359–63.

Chen, H., Nelson, R.S., Sherwood, J.L., 1994. Enhanced recovery of transformants of *Agrobacterium tumefaciens* after freeze-thaw transformation and drug selection. Biotechniques 16, 664–8, 670.

Clough, S.J., Bent, A.F., 1998. Floral dip: a simplified method for *Agrobacterium*-mediated transformation of *Arabidopsis thaliana*. Plant J. 16, 735–43.

Dalal, J., Yalamanchili, R., La Hovary, C., Ji, M., Rodriguez-Welsh, M., Aslett, D., Ganapathy, S., Grunden, A., Sederoff, H., Qu, R., 2015. A novel gateway-compatible binary vector series (PC-GW) for flexible cloning of multiple genes for genetic transformation of plants. Plasmid 81, 55–62.

De Greve, H., Dhaese, P., Seurinck, J., Lemmers, M., Van Montagu, M., Schell, J., 1982. Nucleotide sequence and transcript map of the *Agrobacterium tumefaciens* Ti

plasmid-encoded octopine synthase gene. J. Mol. Appl. Genet. 1, 499–511.

Giró, M., Ceccoli, R.D., Poli, H.O., Carrillo, N., Lodeyro, A.F., 2011. An in vivo system involving co-expression of cyanobacterial flavodoxin and ferredoxin-NADP $^{+}$ reductase confers increased tolerance to oxidative stress in plants. FEBS Open Bio 1, 7–13.

Hanke, G., Mulo, P., 2013. Plant type ferredoxins and ferredoxin-dependent metabolism. Plant. Cell Environ. 36, 1071–1084.

Hanke, G.T., Kimata-Ariga, Y., Taniguchi, I., Hase, T., 2004. A post genomic characterization of *Arabidopsis* ferredoxins. Plant Physiol. 134, 255–64.

Hase, T., Schürmann, P., Knaff, D.B., 2006. The Interaction of Ferredoxin with Ferredoxin-Dependent Enzymes, in: Golbeck, J.H. (Ed.), Photosystem I: The Light-Driven Plastocyanin:Ferredoxin Oxidoreductase. Springer Netherlands, Dordrecht, pp. 477–498.

Ikeda, T., Yamamoto, M., Arai, H., Ohmori, D., Ishii, M., Igarashi, Y., 2005. Two tandemly arranged ferredoxin genes in the *Hydrogenobacter thermophilus* genome: comparative characterization of the recombinant [4Fe-4S] ferredoxins. Biosci. Biotechnol. Biochem. 69, 1172–7.

Kuhlgert, S., Austic, G., Zegarac, R., Osei-Bonsu, I., Hoh, D., Chilvers, M.I., Roth, M.G., Bi, K., TerAvest, D., Weebadde, P., Kramer, D.M., 2016. MultispeQ Beta: a tool for large-scale plant phenotyping connected to the open PhotosynQ network. R. Soc. Open Sci. 3, 160592.

Lee, D.W., Kim, J.K., Lee, S., Choi, S., Kim, S., Hwang, I., 2008. *Arabidopsis* Nuclear-Encoded Plastid Transit Peptides Contain Multiple Sequence Subgroups with Distinctive Chloroplast-Targeting Sequence Motifs. Plant Cell Online 20, 1603–1622.

Li, B., Elliott, S.J., 2016. The Catalytic Bias of 2-Oxoacid:ferredoxin Oxidoreductase in CO2: Evolution and reduction through a ferredoxin-mediated electrocatalytic assay. Electrochim. Acta 199, 349–356.

Long, S.P., Marshall-Colon, A., Zhu, X.-G., 2015. Meeting the Global Food Demand of the Future by Engineering Crop Photosynthesis and Yield Potential. Cell 161, 56–66.

Malik, K., Wu, K., Li, X.-Q., Martin-Heller, T., Hu, M., Foster, E., Tian, L., Wang, C., Ward, K., Jordan, M., Brown, D., Gleddie, S., Simmonds, D., Zheng, S., Simmonds, J., Miki, B., 2002. A constitutive gene expression system derived from the tCUP cryptic promoter elements. Theor. Appl. Genet. 105, 505–514.

Meyer, J., 2008. Iron–sulfur protein folds, iron–sulfur chemistry, and evolution. JBIC J. Biol. Inorg. Chem. 13, 157–170.

Polakis, S.E., Guchhait, R.B., Zwergel, E.E., Lane, M.D., Cooper, T.G., 1974. Acetyl

coenzyme A carboxylase system of *Escherichia coli*. Studies on the mechanisms of the biotin carboxylase- and carboxyltransferase-catalyzed reactions. J. Biol. Chem. 249, 6657–67.

Puyaubert, J., Denis, L., Alban, C., 2008. Dual targeting of *Arabidopsis* holocarboxylase synthetase1: a small upstream open reading frame regulates translation initiation and protein targeting. Plant Physiol. 146, 478–91.

Scarpeci, T.E., Zanor, M.I., Carrillo, N., Mueller-Roeber, B., Valle, E.M., 2008. Generation of superoxide anion in chloroplasts of *Arabidopsis thaliana* during active photosynthesis: a focus on rapidly induced genes. Plant Mol. Biol. 66, 361–378.

Suzuki, Y., Takeda, Y., Ikuta, T., 2008. Immunoblotting conditions for human hemoglobin chains. Anal. Biochem. 378, 218–220.

Thelen, J.J., Mekhedov, S., Ohlrogge, J.B., 2001. *Brassicaceae* express multiple isoforms of biotin carboxyl carrier protein in a tissue-specific manner. Plant Physiol. 125, 2016–28.

Tognetti, V.B., Palatnik, J.F., Fillat, M.F., Melzer, M., Hajirezaei, M.-R., Valle, E.M., Carrillo, N., 2006. Functional replacement of ferredoxin by a cyanobacterial flavodoxin in tobacco confers broad-range stress tolerance. Plant Cell 18, 2035–2050.

Tognetti, V.B., Zurbriggen, M.D., Morandi, E.N., Fillat, M.F., Valle, E.M., Hajirezaei, M.-R., Carrillo, N., 2007. Enhanced plant tolerance to iron starvation by functional substitution of chloroplast ferredoxin with a bacterial flavodoxin. Proc. Natl. Acad. Sci. U. S. A. 104, 11495–11500.

Yoon, K.S., Ishii, M., Igarashi, Y., Kodama, T., 1996. Purification and characterization of 2-oxoglutarate:ferredoxin oxidoreductase from a thermophilic, obligately chemolithoautotrophic bacterium, *Hydrogenobacter thermophilus* TK-6. J. Bacteriol. 178, 3365–8.

Zurbriggen, M.D., Tognetti, V.B., Fillat, M.F., Hajirezaei, M.-R., Valle, E.M., Carrillo, N., 2008. Combating stress with flavodoxin: a promising route for crop improvement. Trends Biotechnol. 26, 531–537.

CHAPTER 5

Concluding Remarks

Caroline M. Smith-Moore and Amy Grunden

This work sought to develop a carbon fixation cycle derived from the microbial reverse/reductive TCA (rTCA) cycle to augment carbon fixation in plants. To eliminate some of the oxygen sensitive rTCA cycle enzymes, the proposed cycle was shortened to five enzymatic steps. The shortened cycle was designated the condensed, reverse TCA (crTCA) cycle. Development of the cycle began with the identification of candidate enzymes from microbes preferring mesophilic and aerobic conditions, followed by the expression and characterization of the enzymes in *E. coli*. Candidate enzymes with the best activity were combined and evaluated for full crTCA cycle function using LC-MS. The *in vitro* LC-MS assays demonstrated the carbon fixation capability of the crTCA cycle. Further investigation of the crTCA cycle led to the discovery that the cycle functions primarily with four steps instead of five. To demonstrate the feasibility of this approach in plants, the four crTCA cycle enzymes were individually expressed transiently in tobacco and shown to be active.

Chapter 3 describes the characterization of a candidate 2-oxoglutarate:ferredoxin oxidoreductase (KOR) from *Bacillus* sp. M3-13. KOR is one of the carbon fixing enzymes of the crTCA cycle. The *Bacillus* sp. M3-13 KOR (BaM3-KOR) was demonstrated to have activity at mesophilic temperature, which is beneficial for activity in plants. However, the enzyme was also shown to have high affinity for 2-oxoglutarate and no detectable carboxylation activity under the assay conditions used. While the BaM3-KOR was not utilized in the final composition of the crTCA cycle, further characterization of this enzyme's structure could allow the enzyme to be engineered to prefer carboxylation and make it an ideal candidate for the crTCA cycle.

Additional proteins, other than those performing the crTCA cycle reactions, were required to ensure cycle function in plants. Those proteins included *Hydrogenobacter*

thermophilus TK-6 ferredoxin (FDX), and *E. coli* biotin protein ligase (BirA). Chapter 4 sought to evaluate what effect the expression of these proteins would have in *Arabidopsis thaliana*. This work is vital to ensure that any phenotypes seen in plants expressing the crTCA cycle are not caused by the expression of these accessory proteins. This research led to the creation of homozygous *Arabidopsis* lines expressing FDX, BirA, FDX/BirA, and an empty vector control. The results suggested that the expression of BirA may lead to increased biotinylation. The expression of FDX by western blot was not successful, and the phenotypes of these plants under stress were conflicting. Further research is required to gain an in depth understanding of the phenotypic effect the expression of the proteins may have.

The research presented in this work establishes the first synthetic carbon fixation cycle derived from the rTCA cycle. The crTCA cycle is the shortest carbon fixation cycle demonstrated, and the only one to have its enzymes evaluated *in planta*. Future work should seek to further refine the cycle to optimize its activity. This could include attempting to increase the carboxylation function of the BaM3-KOR through protein engineering driven by structural characterization and analysis. Additionally, the full crTCA cycle is currently being expressed in plants. Analysis of the phenotypes of plants expressing the full cycle will provide information on the ability of this approach to increase plant biomass.